creative commons
COMMONS DEED

저작자표시-비영리-변경금지 2.0 대한민국

이용자는 아래의 조건을 따르는 경우에 한하여 자유롭게

- 이 저작물을 복제, 배포, 전송, 전시, 공연 및 방송할 수 있습니다.

다음과 같은 조건을 따라야 합니다:

저작자표시. 귀하는 원저작자를 표시하여야 합니다.

비영리. 귀하는 이 저작물을 영리 목적으로 이용할 수 없습니다.

변경금지. 귀하는 이 저작물을 개작, 변형 또는 가공할 수 없습니다.

- 귀하는, 이 저작물의 재이용이나 배포의 경우, 이 저작물에 적용된 이용허락조건을 명확하게 나타내어야 합니다.
- 저작권자로부터 별도의 허가를 받으면 이러한 조건들은 적용되지 않습니다.

저작권법에 따른 이용자의 권리는 위의 내용에 의하여 영향을 받지 않습니다.

이것은 이용허락규약(Legal Code)을 이해하기 쉽게 요약한 것입니다.

Disclaimer

dCollection

의학박사 학위논문

Integrative electrophysiological studies of cardiotoxic agents using human stem cell-derived cardiomyocytes

심장독성 약물의 전기생리학적 분석을 위한 줄기세포 이용 통합 연구

2016 년 2 월

서울대학교 대학원

의과학과 의과학전공

이 향 애

A thesis of the Degree of Doctor of Philosophy

심장독성약물의 전기생리학적 분석을 위한 줄기세포 이용 통합 연구

Integrative electrophysiological studies of cardiotoxic agents using human stem cell-derived cardiomyocytes

February 2016

The Department of Biomedical Sciences,
Seoul National University
College of Medicine
Hyang-Ae Lee

ABSTRACT

Even though several *in vitro* and *in vivo* QT screening systems (e.g. hERG assay, telemetry in conscious animals) are currently used as standardized assays for cardiotoxicity, these testing models are deficient. The major reason for their poor predictive powers is that they cannot replicate human cardiac electrophysiology. With the development of stem cell technologies, *in vitro* assays using human pluripotent stem cell-derived cardiomyocytes (hPSC-CMs) is suggested as an effective candidate of drug screening platform. The aims of this study are to explore the necessity of integrative interpretation with multiple types of cardiac ion channels for the cardiotoxicity test, and to evaluate the usefulness of adopting hPSC-CMs for the electrophysiological study.

Chapter 1: Comparison of electrophysiological effects of calcium channel blockers on cardiac repolarization[1]

It is anticipated that Ca^{2+} channel blockers (CCBs) would shorten action potential duration (APD), which could lead to tachycardia. Nevertheless, CCBs are widely prescribed to hypertension without serious problems of cardiac arrhythmia. Here I investigated the electrophysiological effects of dihydropyridine class of CCBs, nicardipine (NIC), isradipine (ISR), and amlodipine (AML). All the three CCBs inhibited the L-type Ca^{2+} currents (I_{Ca}) whereas the shortening of APD was observed only with ISR. In addition, interestingly, NIC and AML also inhibited voltage-gated K^+ channels currents

(I_{Kr} and I_{Ks}) at micromolar ranges while ISR did not. I interpret that the concomitant K^+ channel inhibition by NIC and AML might have compensated the AP shortening effects induced by the I_{Ca} inhibition.

Chapter 2: Integrative analysis of cardiac ion channel modulation by SARI class antidepressants in human stem cell-derived cardiomyocytes[2]

The potential usefulness of human stem cell-derived cardiomyocytes in drug toxicity testing is drawing attention to the pharmaceutical industry recently. Here I evaluated the usefulness of commercialized human induced pluripotent stem cell-derived cardiomyocytes (hiPSC-CMs). The cardiac three types of action potentials, nodal (N)-, atrial (A)-, and ventricular (V)-type, and ion channels related cardiac AP (I_{Kr}, I_{Ks}, I_{K1}, I_f, I_{Na}, I_{Ca}) were recorded in the cells. Additionally, hiPSC-CMs effectively recapitulate the electrophysiological behaviors of the major ion channel blockers, (E-4031 for hERG channel, tetrodotoxin for Na^+ channel, nifedipine for calcium channel), confirming the plausibility of a platform for preclinical drug safety assessment. Then I analyzed the cardiotoxic effects of trazodone and nefazodone, serotonin antagonist and reuptake inhibitor (SARI) class antidepressants, using hiPSC-CMs or HEK293 cells overexpressing cardiac ion channel. Both drugs induced APD prolongation and early afterdepolarizations (EADs) and reduced the upstroke velocity in a dose-dependent manner. Consistent with the changes in the AP parameters, nefazodone and trazodone inhibited I_{Kr}, I_{Ks}, I_{Na}, and I_{Ca}, among them especially I_{Kr} and I_{Na}, but nefazodone had a higher inhibitory potency than trazodone.

Chapter 3: Differentiation period-dependent changes in the electrophysiological properties of human stem cell-derived cardiomyocytes

The assessment of functionality of human embryonic stem cell derived cardiomyocytes (hESC-CMs) at early developmental stages is essential for determining the appropriate differentiation stage for cardiotoxicity screening. In this study, to determine more suitable stage of differentiation required for the reliable pharmacological and toxicological testing, I characterized 2 week (2W) and 4 week (4W) differentiated hESC-CMs and compared their electrophysiological phenotypes and functional maturation using patch-clamp technique. The densities of functional ion channels currents, I_{Na}, I_{Ca}, I_{Kr}, I_{Ks}, and I_{K1}, tended to increase in the 4W hESC-CMs while not significantly. In the AP recordings, the 2W hESC-CMs displayed only A-type (87.5%) and N-type (12.5%) without V-type of APs. However, the 4W hESC-CMs revealed 3 types of AP with the majority of cells revealed V-type APs (69%). The pharmacological responses for anti-arrhythmic drugs revealed that quinidine and amiodarone (Na^+ and K^+ channel blockers, respectively) prolonged APD at 90% (APD_{90}) in the 4W hESC-CMs while not in the 2W hESC-CMs. Nifedipine significantly shortened APD_{90} only in the 4W hESC-CMs.

Taken together, this study demonstrated the drug-induced cardiotoxicity has to be estimated with overall effects on multiple ion channels because of their compensatory effects between depolarizing and repolarizing currents. The hiPSC-CMs could be a valuable testbed for evaluating the proarrhythmic

liability of trazodone and nefazodone; electrophysiological properties of hiPSC-CMs and their responses faithfully reflected the changes of individual ion channel current. The hiPSC-CMs can be an effective model for detection of early drug-induced cardiotoxicity beyond the current standard assay of hERG K^+ channels. However, to use stem cell-derived cardiomyocytes in drug screening, at least 4 weeks of differentiation period is required for the reliable pharmacological and toxicological testing.

[1] This work is published in KJPP Journal (1).

[2] These works are published in HET and TAAP Journals (2, 3).

Keywords: Cardiotoxicity testing, cardiotoxic agents, ion channel, action potential, human stem cell-derived cardiomyocytes, calcium channel blocker, antidepressants

Student number: 2011-30633

CONTENTS

LIST OF TABLES AND FIGURES

General Introduction

Chapter 1

Chapter 2

Chapter 3

LIST OF ABBREVIATIONS

AML	Amlodipine
AP	Action potential
APA	Action potential amplitude
APD	Action potential duration
APD_{50} or **APD_{60}**	Action potential duration at 50% or 60% repolarization
APD_{90}	Action potential duration at 90% repolarization
CCBs	Calcium channel blockers
dV/dt_{max}	Maximum upstroke velocity
EAD	Early afterdepolarization
hERG	Human ether-a-go-go-related gene
hESC-CMs	Human embryonic stem cell-derived cardiomyocytes
hiPSC-CMs	Human induced pluripotent stem cell-derived cardiomyocytes
hPSC-CMs	Human pluripotent stem cell-derived cardiomyocytes
I_{Ca}	Voltage gated Ca^{2+} channel current
I_{Na}	Voltage-gated Na^{+} channel current
I_{Ks}	Slowly-activating voltage-gated K^{+} channel current
I_{K1}	Inward rectifier K^{+} channel current
ISR	Isradipine
MDP	Maximum diastolic membrane potential
NIC	Nicardipine
rVM	Rat ventricular myocytes
SARIs	Serotonin antagonist and reuptake inhibitors
TdP	Torsades de pointes

GENERAL INTRODUCTION

Drug development is an extremely time- and cost-consuming process and suffers from a high failure rate (~90%) due to the two major reasons: lack of efficacy (30% of total fail) and safety issues (another 30%) (4). Especially, serious cardiotoxicity including arrhythmia, hyper/hypotension, coronary artery disorder, and heart failure have led to many drug withdrawals from markets and termination of promising preclinical and clinical drug development of candidates (5, 6). Drug-induced cardiac electrophysiological alterations including QT prolongation and torsadogenic potential, have caused widespread regulatory concern in pharmaceutical industry (7, 8).

In normal cardiac cells, a variety of ion channels expressed on the membrane generate regular action potential (AP) and maintain of the ionic concentrations in the cell. As shown in Figure GI-1, the ventricular AP has 5 phases, numbered 0-4, upstroke (phase 0), early repolarization (phase 1), plateau (phase 2), final repolarization (phase 3), and resting (phase 4). These phases are generated by the movement of ions through the specific ion channels as follows: Phase 0 is the phase of rapid depolarization (upstroke) (9, 10). The membrane potential shifts into positive voltage range because of Na^+ (sodium) influx into the cell resulted in Na^+ currents. Phase 1 is a period of early repolarization. In this phase, the transiently outward K^+ (potassium) current (I_{to}) caused the small downward deflection of the AP. Phase 2, a plateau phase, is the longest phase. During phase 2, the voltage remains relatively constant as Ca^{2+} (calcium) ion enters the cell while K^+ ion exits. Phase 3 is the phase of final repolarization that restores the membrane

potential to its resting value. The primary currents underlying this phase are the rapidly (I_{Kr}) and slowly (I_{Ks}) activating delayed rectifier K^+ channels. Phase 4, a resting phase, is stable in the membrane potential at ≈−90 mV. In this phase the inwardly rectifying K^+ current (I_{K1}) is mainly involved.

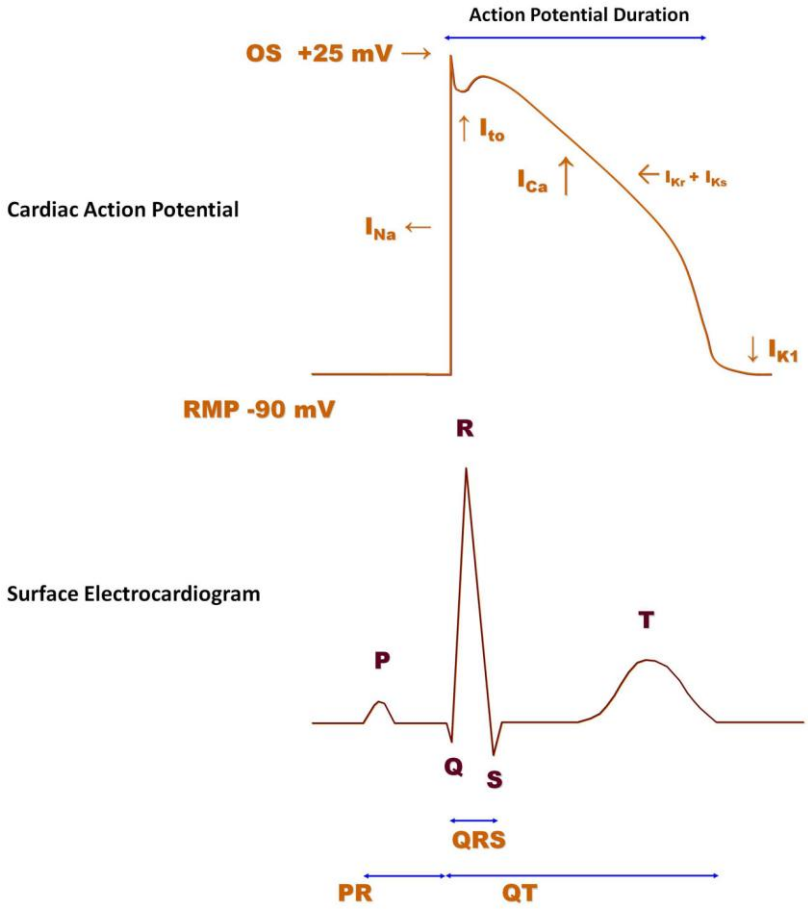

Figure GI-1. Illustrations of cardiac action potential and surface electrocardiogram (ECG) (illustrated by Kaczorowski GJ et al. (10))

OS, overshoot; RMP, resting membrane potential.

The average duration of the ventricular AP is reflected in the QT interval on the electrocardiogram (ECG). Therefore, factors that prolong the AP duration

(APD) (e.g., a decrease in repolarizing K^+ currents or an increase in depolarizing Na^+ current) prolong the APD and also the QT interval on the ECG (9). QT prolongation is a recognized risk factor for pro-arrhythmia associated with torsades de pointes (TdP) and sudden cardiac death (11). Hence many pharmaceutical companies try to quantify drug-induced cardiac electrophysiological alterations using *in vitro* ion channel screening in early stage of drug development.

According to the ICH (International Committee for Harmonization) guideline S7B (guideline on safety pharmacology studies for assessing the potential for delayed ventricular repolarization), most pharmaceutical companies conducted preclinical cardiotoxicity testing with *in vitro* ion channel screening (especially hERG (the human Ether-à-go-go-Related Gene) channel assay) and *in vivo* or *ex vivo* studies with laboratory animals (APD assay, QT or MAP (monophasic AP) assay), but still cannot fully predict the potential arrhythmia induced by drug candidates. Not all drugs which blocked hERG channel cause QT prolongation or TdP (e.g. verapamil) (12, 13) and QT prolongation does not always provoke TdP (e.g. ranolazine, alfuzosin, moxifloxacin) (14-16). Some drugs cause arrhythmias in humans that neither inhibit hERG channels *in vitro* nor cause QT prolongation in animal models (17, 18).

In vitro cell-based drug screening is useful to narrow the large chemical libraries into a list of candidate compounds for further testing. However, for reliable prediction of cardiotoxicity, the cells used in testing need to sufficiently recapitulate the characteristics of the human myocardium. There are many sources for cultured cells that can be used in drug screening assays. Each cell type has certain advantages, but they also have characteristics that

may contribute to the high attrition rate of drug compounds. Arrhythmogenic potentials of drugs are much better assessed with animal-based models (19) because of their higher sensitivity and specificity. However, these models also have limitations of ethical concerns, species differences (20), and cost. Thus, primary adult human cardiomyocytes (CMs) would be ideal for *in vitro* drug screening, however, these cells are scarce, difficult and costly to harvest, and also have limited time in culture (21).

To overcome the limitations of the currently used assays for preclinical safety of pharmaceutical compounds, human pluripotent stem cell-derived cardiomyocytes (hPSC-CMs) are drawing attention. They include human embryonic stem cell (22)- and induced pluripotent stem cell (hiPSC)-derived CMs. The hiPSC-CMs provide a potentially unlimited source of human CMs. In addition, they could also overcome the ethical hurdles that burden hESC-CMs. The noble techniques using hiPSC-CMs have been acknowledged by the pharmaceutical industry, and also by the recent announcement by the US Food and Drug administration of a new paradigm for the evaluation of new molecular entities: the comprehensive in vitro pro-arrhythmia assay (CiPA) (23). The proposed CiPA approach include the following: (i) screening of drug action on multiple human cardiac currents (rather than just hERG) in heterologous expression systems; (ii) integration of ion channel/drug interaction data in in silico models of human ventricular electrophysiology to predict and evaluate changes in the human AP; and (iii) *in vitro* evaluation of compound effects in a myocyte assay such as hiPSC-CMs and comparison to the *in silico* results.

For the reliable safety testing, the in vitro-differentiated cardiomyocytes should sufficiently recapitulate the characteristics of human adult CMs. Several previous studies showed that hESC-CMs have similarities to human CMs in terms of electrophysiology, calcium handling, receptor response, growth, proliferation and survival (22, 24-27). However, other studies also showed some limitations of hPSC-CMs as follows; (i) the expression levels of genes for sarcomeric proteins in hiPSC-CMs more closely resembled those in fetal CMs (28); (ii) they have increased automacity compared with human ventricular CMs due to lack of I_{K1} (29). The hPSC-CMs could be further matured through extended culture period by applying mechanical stretching, pharmacological/neurohormonal agonists, and electric stimulation (30).

Before hiPSC-CMs are adopted for pharmacological screening, they need to be carefully validated for usefulness. They have to be confirmed to display similar electrophysiological properties based on ionic currents and cardiac APs. In addition, their pharmacological sensitivity need to be identified using well-known compounds including specific ion channel blockers (e.g. E-4031 for hERG channel blocker, TTX for Na^+ channel blocker) and cardiotoxic agents.

With these backgrounds, the present study was conducted to explore the necessity of integrative interpretation with multiple types of cardiac ion channels for the cardiotoxicity test. To evaluate the usefulness of adopting hPSC-CMs for the electrophysiological study, I also investigated to determine more suitable stage of differentiation required for the reliable pharmacological and toxicological testing.

CHAPTER 1

Comparison of electrophysiological effects of calcium channel blockers on cardiac repolarization

INTRODUCTION

Calcium channel blockers (CCBs) were developed in the 1970s and are now widely used for cardiovascular diseases such as hypertension and ischemic heart disease (31-34). Since CCBs also potently inhibits Ca^{2+} influx in arterial myocytes, they induce vascular relaxation and lowering the blood pressure. CCBs are divided into several subtypes based on their chemical structures and functional mechanisms: the dihydropyridine, phenylalkylamine and benzothiazepine classes. According to clinical guidelines, dihydropyridine CCBs belong to the recommended first-line antihypertensive drugs to treat essential hypertension (35). Nicardipine (NIC, first-generation), isradipine (ISR, second-generation), and amlodipine (AML, third-generation) belong to the dihydropyridine-derivative group of CCBs (Figure 1-1).

On the cardiac AP, voltage-gated Na^{+} channel current (36) causes initial depolarization of upstroke phase, and thus open the voltage gated Ca^{2+} channel to open, allowing Ca^{2+} into the cell to prolong the AP and onto the sarcoplasmic reticular membrane to stimulate contraction through Ca^{2+}-induced Ca^{2+} release (CICR) (37). CCBs hinder calcium entry to the cardiac myocytes, thereby reducing the amount of Ca^{2+} available to induce CICR (38).

A unique feature of cardiac AP is the plateau phase of sustained depolarization that is due to both delayed activation of voltage-gated K^{+} channels currents (I_{Kv}) and VOCC current (I_{Ca}). Since the balance between I_{Ca} and I_{Kv} determines the amplitude and duration of the plateau phase of cardiac AP, pharmacological inhibition of the associated ion channels has been a

critical issue of cardiac toxicity in terms of electrophysiology. I_{Kv} is composed of rapidly-activating and slowly-activating voltage-gated K^+ channel currents called I_{Kr} and I_{Ks}, respectively. The inhibition of hERG K^+ channel, the major component of I_{Kr} is the most intensively investigated target (39). Along with the decreased hERG activity due to either pharmacological agents or genetic mutations, suppression of slowly-activating voltage-gated K^+ channel current (I_{Ks}) also induce the prolongation of action potential duration (APD) (40). An abnormal APD prolongation predispose to arrhythmia due to early after-depolarization (EAD). EAD was defined as the cells generating oscillatory potentials at depolarized levels. In the heart, drug-induced QT interval prolongation in ECG is recognized as potential risks such as TdP (41, 42). Conversely, however, less is known about short QT syndrome. Nevertheless, genetic disorders or pharmacological side effects may induce abnormally short QT intervals that could potentially increase the risk of sudden death with atrial fibrillation and/or ventricular fibrillation (43-48).

In contrast to the inhibition of K^+ channels, decreased I_{Ca} is expected to shorten APD and/or modify the shape of plateau in the cardiac AP. Therefore, CCBs can theoretically cause APD shortening. However, the above CCBs are widely used without severe side effects. Such results might be due to the low plasma concentrations of CCBs in the patients prescribed with CCBs. Another possibility is a putative compensatory inhibition of K^+ channels such as hERG, which might counterbalance the APD shortening effect of CCBs. However, precise investigations on the latter possibility is lacking yet. The purpose of this study was to examine the effects of NIC, ISR, and AML on the AP in

rabbit Purkinje fibers and on cardiac ion channel currents, especially K^+ channels currents associated with the repolarization process. The integrated analysis of cardiac ion channels might provide a novel insight to understand the pharmacological effects of CCBs without critical side effects in the clinical applications.

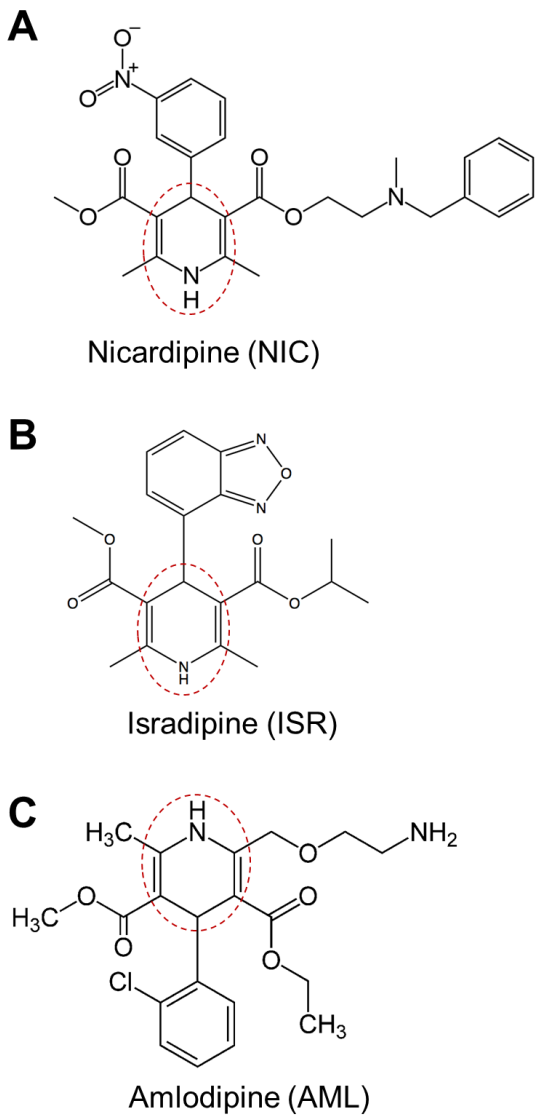

Figure 1-1. Chemical structures of dihydropyridine class-calcium channel blockers, NIC, ISR, and AML

The red dashed circles indicate dihydropyridine molecule which is common structure of the three CCBs, NIC (A), ISR (B), and AML (C).

MATERIALS AND METHODS

1. Animals

The experiments for AP recording and I_{Ca} analysis were performed using New Zealand white rabbit (2.5 – 3.5 kg) and male Sprague-Dawley (SD) rats (250 – 350 g), respectively. The animals were kept in a storage room under the conditions of constant temperature (23 ± 3℃), relative humidity (50 ± 10%), and illumination (12 h light/dark cycles) until the initiation of the experiment. This study was conducted in facilities approved by the Association for Assessment and Accreditation of Laboratory Animal Care (AAALAC) International. All procedures were approved by our Institutional Animal Care and Use Committee (IACUC).

2. Cell preparation

To assess the effects of CCBs on I_{Kr}, I_{Ks}, I_{K1}, and I_{Na}, HEK293 (the human embryonic kidney 293, ATCC, CRL-1573™, USA) cells were transiently transfected with the following genes using Lipofectamin2000 (Gibco BRL, USA) according to the manufacturer's instructions. The *hERG* (human ether-a-go-go-related gene corresponding to I_{Kr}), *KCNQ1/KCNE1* (the gene corresponding to I_{Ks}), *KCNJ2* (the gene corresponding to I_{K1}) or *SCN5A* (the gene corresponding to I_{Na}) cDNA was co-transfected with green fluorescence protein (GFP) to allow assessment of the transfection efficiency. The overexpression system was adopted for the analysis of pharmacological drug effects on the above ionic currents because reliable functional isolation of

respective ion channel current in cardiomyocytes is technically difficult. Although the HEK293 cells endogenously express voltage-gated K^+ currents, the peak amplitudes were less than 10% of the overexpressed I_{Kr} and I_{Ks} amplitudes.

To assess the effects of CCBs on the calcium currents, however, enzymatically isolated rat ventricular myocytes (rVMs) were used because consistent co-expression of multilple subunits (α_1, $\alpha_2\delta$, β, γ) of L-type Ca^{2+} channel proteins were requested. Briefly, the hearts were rapidly excised from anesthetized SD rats and perfused via the aorta on a Langendorff apparatus with an oxygenated normal Tyrode's (NT) solution for 5 min to clear the blood, then perfused with Ca^{2+}-free NT solution for about 3 min. Next the heart was perfused with enzyme solution containing 0.6 mg/ml collagenase (Worthington, type 2, USA) for 30-40 min. Finally, this enzyme-containing solution was washed out for 5 min with a high-K^+ and low-Cl^- Kraft-Bruhe (23) solution. Following the isolation procedure, the left ventricle was dissected out and agitated mechanically with a fire-polished Pasteur pipette in KB solution to obtain single myocytes. The isolated myocytes were stored at 4℃ until use for up to 8 hour.

3. Drugs and Solutions

NIC, ISR and AML were purchased on Sigma-aldrich (MO, USA). These were formulated into stock solution with dimethyl sulfoxide (DMSO). All the drug stock solutions were diluted in NT solution to produce the target exposure concentrations. The concentration of DMSO in NT was always kept

below 0.1%. The external solution for recording the I_{Kr}, I_{Ks} and I_{Na} was NT solution as follows (in mM): 143 NaCl, 5.4 KCl, 1.8 $CaCl_2$, 0.5 $MgCl_2$, 5 HEPES, 0.33 NaH_2PO_4 and 16.6 glucose (pH adjusted to 7.4 with NaOH).

The internal solution for recording I_{Kr} contained the following (in mM): 130 KCl, 5 Ethylene glycol-bis(2-aminoethylether)-N,N,N′,N′-tetraacetic acid (EGTA), 10 4-(2-hydroxyethyl)piperazine-1-ethanesulfonic acid (HEPES), 1 $MgCl_2$, and 5 Mg-ATP (pH adjusted 7.25 with KOH). For recording I_{Ks} the internal solution contained (in mM) 150 KCl, 5 EGTA, 10 HEPES, 2 $MgCl_2$, 1 $CaCl_2$ and 5 Na_2-ATP (pH adjusted 7.25 with KOH). For recording I_{K1}, the internal solution contained (in mM): 130 K-Asp, 15 KCl, 10 HEPES, 1 $MgCl_2$, 5 Na_2-ATP, 5 EGTA (pH adjusted 7.25 with KOH). For recording I_{Na}, the internal solution contained 105 CsF, 35 NaCl, 10 EGTA, 10 HEPES (pH adjusted to 7.25 with NaOH).

For recording I_{Ca}, the fresh isolated rat ventricular myocytes (rVM) were superperfused with an external solution that consisted of (in mM): 137 cholin-Cl, 5 CsCl, 0.5 $MgCl_2$, 2 4-AP, 10 HEPES, 10 glucose and 1.8 $CaCl_2$ (pH adjusted to 7.4 with NaOH). The internal solution for I_{Ca} recording contained (in mM): 20 CsCl, 100 Cs-aspartate, 10 EGTA, 10 HEPES, 20 Tetraethylammonium chloride (TEA-Cl), 5 Mg-ATP (pH adjusted to 7.25 with KOH). KB solution for storage of the freshly isolated rat ventricular myocytes contained (in mM): 70 K-glutamate, 55 KCl, 10 HEPES, 3 $MgCl_2$, 20 taurine, 20 KH_2PO_4, 0.5 EGTA (adjusted to pH 7.2 with KOH).

4. Recording of action potentials

The rabbits were anesthetized with pentobarbitone sodium (30 – 50 mg/kg i.v.) and then their hearts were rapidly removed and placed in oxygenated NT solution to pump the remaining blood out. The left ventricle was opened and Purkinje fibers were carefully dissected out with a small piece of ventricular tissue to be pinned in the experimental chamber. The isolated Purkinje fibers were superfused with oxygenated NT solution (5 ml/min) maintained at 37 ± 0.5℃. The preparations were electrically stimulated at a basal rate (frequency = 1 Hz, duration = 2 ms, voltage = 1.5 – 2 V). Two hours were allowed for each preparation to equilibrate while continuously superfused with NT solution. Action potentials were recorded using the conventional intracellular recording technique involving a glass microelectrode filled with 3 M KCl and connected to a Geneclamp 500B (Axon Instruments, CA, USA). Action potential duration at 50% and 90% repolarization (APD_{50} and APD_{90}) was automatically measured using NOTOCORD-hem™ program (NOTOCORD, France) at a sampling rate of 50 kHz. Before drug treatment, action potential parameters were measured in NT for 1 hour to establish stable control value recording. The vehicle control (0.1% DMSO in NT) and drugs were perfused every 20 min after the stable AP were obtained. Besides AP, resting membrane potential (RMP), AP amplitude (APA), and maximum velocity of initial depolarization (dV/dt_{max}) were analyzed (Table 1-1).

Exclusion criteria:

The PFs were discarded if one of the following parameters during the control recording was out the following ranges: -95 mV < RMP < -75 mV and

200 ms < APD_{90} < 350 ms. All the fibers used in this study were no spontaneous beating without external electric stimulation.

5. Recording of ionic currents

The cells were placed in a recording chamber on the stage of a Nikon inverted microscope, and continuously perfused (5 ± 1 ml/min) with 37 ± 1℃ bath solution. Ionic currents were recorded in a whole-cell configuration with a standard patch clamp technique using a HEKA EPC8 amplifier (Electronik, Lambrecht, Germany). Data were recorded during the approximately 5 minutes following initial application of the bath solution to verify currents stability. Test drug solutions were subsequently superfused for approximately 5 minutes to achieve steady-state blocks. To investigate the effect of these drugs on the ion channel currents, various concentrations (0.01 – 30 μM) of drugs were tested. Voltage-clamp protocol generation and data acquisition were controlled by computers equipped with an A/D converter, Digidata (Axon Inc., USA) and RClamp software developed by Seoul National University (Seoul, Korea). The patch pipettes were made from borosilicate glass capillaries (Clark Electromedical Instruments, UK) using a pipette puller (PP-830, Narishige, Japan). Their resistances were 3-4 MΩ when filled with pipette solution. The current signals were filtered at a sampling rate of 5 kHz, and they were low-pass filtered at 1 kHz and stored on computer. All experimental parameters, such as pulse generation and data acquisition, were controlled using the RClamp software.

6. Statistical Methods

Data analysis and curve fitting of patch clamp experiments were carried out using RClamp, GraphPad InStat (GraphPad Software, San Diego, CA), and SigmaPlot 2000 (SPSS Inc., Chicago, IL). Pooled data are expressed as means ± standard errors of the mean (SEM), and statistical comparisons were made with $p<0.05$, or $p<0.01$ considered significant. Current amplitudes were measured before and after application of the respective drugs. The percent inhibition values were calculated according to the following equation:

$$\%\text{inhibition} = \frac{\text{Initial current amplitude (control) - Current amplitude in the presence of drug}}{\text{Initial current amplitude (control)}} \times 100$$

Effects were calculated from the results of several repeated experiments per concentration of the drugs. Concentration response relations were calculated by a non-linear least squares fit equation [Hill equation; $f = x^H/(IC50^H+x^H)$; H = Hill coefficient, IC50 = IC_{50}, x = concentration, f = inhibition ratio] using the SigmaPlot 2000 program for the half-maximum inhibiting concentration (IC_{50}).

RESULTS

Effects of CCBs on $I_{Ca,L}$ in rVMs

The I_{Ca} of rVMs was activated by a depolarizing step pulse (0 mV, 500 ms) from the holding potential of -80 mV. All three CCBs inhibited the I_{Ca} in a concentration-dependent manner (Figure 1-2). NIC at 0.01, 0.1, 1, and 10 μM reduced the I_{Ca} amplitude by 18.4%, 41.5%, 78.3%, and 99.4%, respectively (n = 3, Figure 1-2A and B). ISR at the same concentrations attenuated the I_{Ca} amplitude by -3.2%, 22.6%, 89.9%, and 99.8%, respectively (n = 3, Figure 1-2C and D). In addition, AML also had potent inhibitory effect on I_{Ca}. AML reduced the I_{Ca} amplitude by 13.8%, 34%, 72.5%, and 100% at 0.01, 0.1, 1, and 10 μM, respectively (n = 3, Figure 1-2E and F). The IC_{50} values were 0.142 ± 0.03 μM for NIC, 0.229 ± 0.02 μM for ISR, and 0.227 ± 0.058 μM for AML (Figure 1-2B, D, and F).

Effect of NIC, ISR, and AML on I_{Na} in SCN5A-transfected HEK293

In the *SCN5A*-overexpressed cells, I_{Na} was generated by a step pulse from -100 mV of holding voltage to -40 mV of 20 ms duration. The CCBs also inhibited I_{Na} at micromolar ranges (Figure 1-3A, C, and E). 30 μM ISR almost completely inhibited I_{Na} while NIC and AML inhibited I_{Na} by about 80% at 30 μM. When fitted to a Hill function, their IC_{50} values were 7.08, 3.05, and 6.38 μM for NIC, ISR, AML, respectively (each n = 4, Figure 1-3B, D, and F).

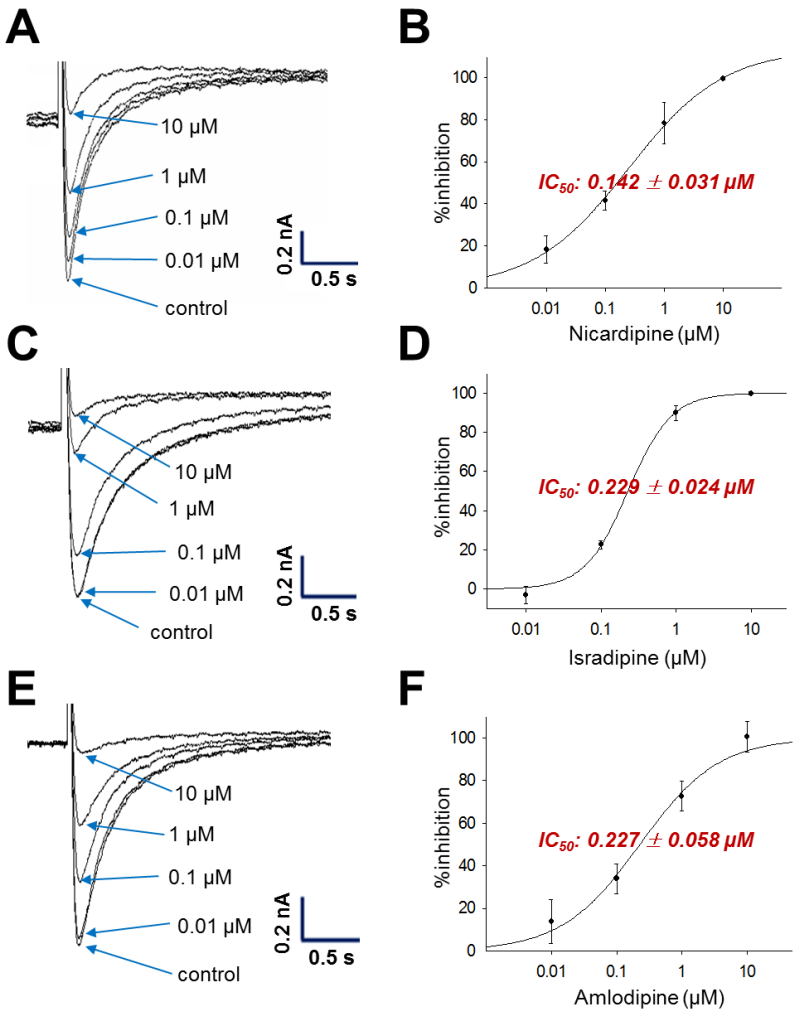

Figure 1-2. Effect of NIC, ISR, and AML on I_{Ca} in rat cardiomyocytes

I_{Ca} traces of rat cardiomyocytes under before and after application of 0.01, 0.1, 1, and 10 μM of NIC (**A**), ISR (**C**), and AML (**E**). Concentration-response relationship for NIC (**B**), ISR (**D**), and AML (**F**) to block of I_{Ca} (each $n = 3$).

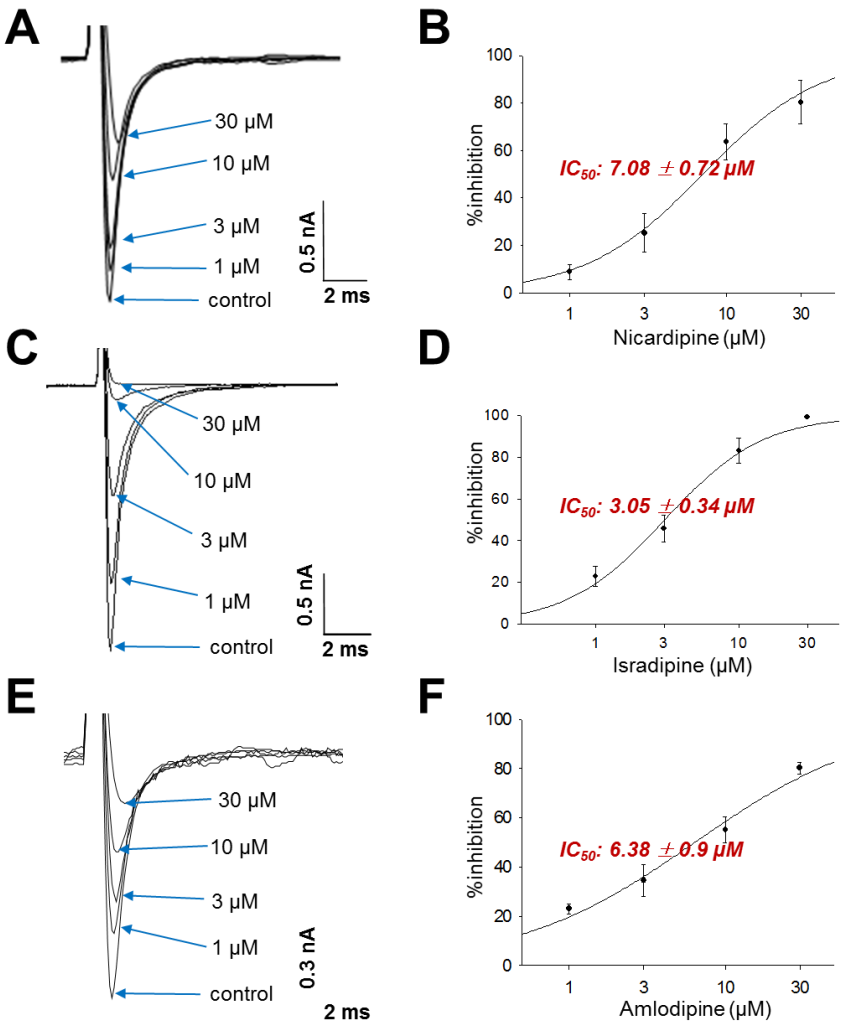

Figure 1-3. Effect of NIC, ISR, and AML on I_{Na} in *SCN5A*-transfected HEK293

Representative I_{Na} traces under control conditions and after application of various test concentrations (1, 3, 10, and 30 μM) of NIC (**A**), ISR (**C**), and AML (**E**). Statistical summary and Hill's fitting of concentration–dependent inhibitions of I_{Na} for NIC (**B**), ISR (**D**), and AML (**F**) (each n = 4).

Effects of CCBs on the cardiac AP

Figure 1-4 shows the concentration-dependent effects of NIC, ISR and AML on the AP configurations in rabbit Purkinje fibers. NIC at a concentration of 30 μM induced a triangulated AP and significantly shortened the APD_{50} compared vehicle control by -65.8 ms ± 9.9 (n = 3, p < 0.05), while not affecting APD_{90} (Figure 1-4A and B). The other AP parameters, including RMP, dV/dt_{max} and APA were not changed (Table 1-1). AML at 30 μM also significantly shortened the APD_{50} by -58.1 ms ± 8.5 (n = 3, p<0.05) while not significantly decreased the APD_{90} (Figure 1-4C and D). AML also decreased the APA by -7.8 mV ± 3.0 compared to vehicle control (Table 1-1). NIC and AML induced a triangulated shape of AP (Figure 1-4A and E). Unlike NIC and AML, ISR at 30 μM significantly shortened both the APD_{50} and APD_{90} by -86.8 ms ± 6.1 and -86.6 ms ± 8.8, respectively (n = 4, p<0.01). In addition, ISR at 30 μM significantly decreased the dV/dt_{max} (-116.4 V/s ± 11.6, p<0.05), but had no significant effect on the RMP and APA (Table 1-1).

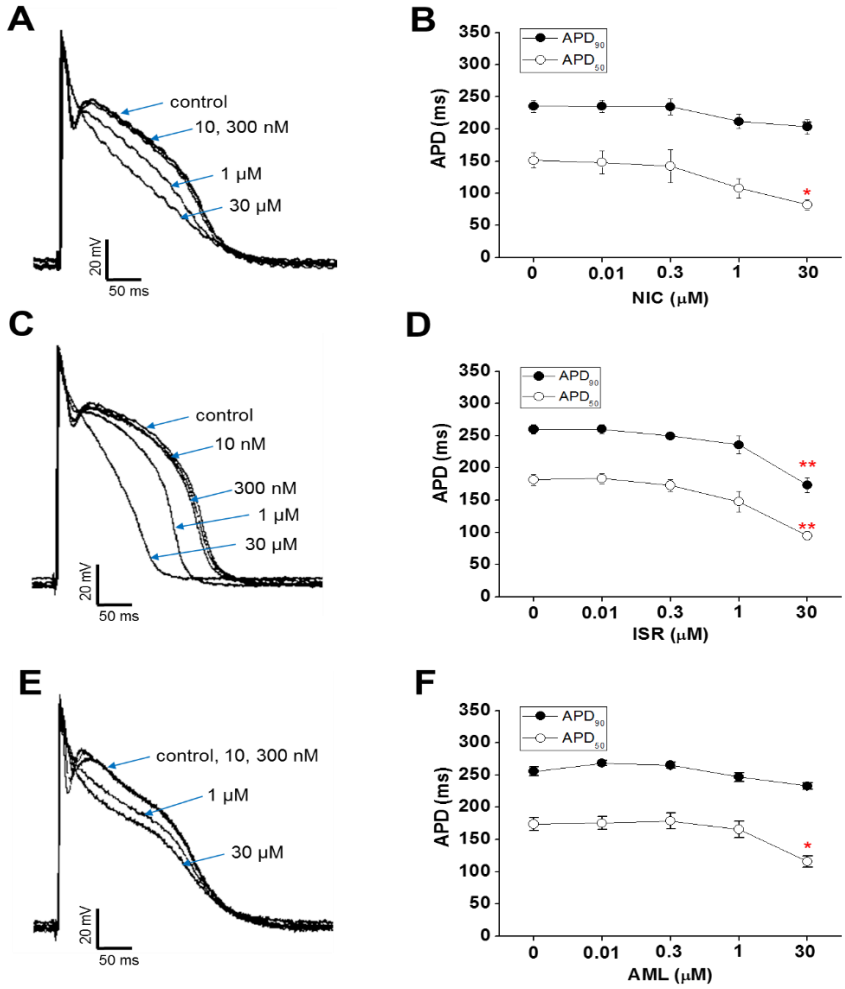

Figure 1-4. Concentration-dependent effects of NIC, ISR and AML on the AP duration in rabbit Purkinje fibers

Representative recordings for the effect of NIC (**A**), ISR (**C**), and AML (**E**) on the cardiac APs in rabbit Purkinje fibers. Effects of NIC (**B**), ISR (**D**), and AML (**F**) on the AP duration at 50% (APD_{50}, opened circles) and 90% repolarization (APD_{90}, closed circles). Data are expressed as mean ± SEM and compared by ANOVA followed by Dunnett's test (n = 3 in NIC and AML, n = 4 in ISR). *p<0.05; **p<0.01, compared with VC (vehicle control, 0.1% DMSO in NT).

Table 1-1 Effects of CCBs on the electrical parameters of rabbit Purkinje fibers

	Concentration	RMP (mV)	dV/dt_{max} (V/s)	APA (mV)
NIC	0 (VC)	-78.5 ± 0.6	407.3 ± 92.1	113.9 ± 4.5
(*n* = 3)	10 nM	-80.4 ± 2.1	395.1 ± 89.4	114.7 ± 3.8
	300 nM	-79.8 ± 2.6	384.9 ± 71.3	115.8 ± 2.1
	1 μM	-80.9 ± 4.0	376.7 ± 67.7	112.8 ± 2.5
	30 μM	-81.7 ± 6.1	337.1 ± 69.4	110.2 ± 3.1
ISR	0 (VC)	-85.4 ± 1.9	259.5 ± 22.6	113.2 ± 2.6
(*n* = 4)	10 nM	-85.7 ± 2.6	250.7 ± 23.0	113.4 ± 2.9
	300 nM	-82.6 ± 1.1	257.3 ± 31.4	112.6 ± 3.4
	1 μM	-82.4 ± 1.5	238.0 ± 41.8	111.1 ± 4.3
	30 μM	-80.6 ± 2.9	143.1 ± 22.7*	103.4 ± 3.4
AML	0 (VC)	-79.3 ± 2.2	329.1 ± 48.0	118.7 ± 0.3
(*n* = 3)	10 nM	-78.3 ± 2.4	323.1 ± 44.2	118.4 ± 1.2
	300 nM	-78.7 ± 2.6	322.8 ± 45.0	119.1 ± 1.7
	1 μM	-77.8 ± 2.3	306.4 ± 47.1	119.2 ± 0.9
	30 μM	-75.3 ± 2.1	250.6 ± 37.2	110.9 ± 3.2*

Data are expressed as mean ± SEM. The data were analyzed for homogeneity of variance using Bartlett's test. Homogeneous data were analyzed using the Analysis of Variance and the significance of inter-group differences between each dose groups and the vehicle-control group were assessed using Dunnett's test. Heterogeneous data were analyzed using Kruskal-Wallis test and the significance of inter-group differences between the control and test article groups were assessed using Dunn's Rank Sum test. Statistical analyses were performed by using Statistical Analysis Systems (SAS/STAT Version 9.2, Cary, USA). RMP, resting membrane potential; dV/dt_{max}, maximal upstroke velocity of phase 0; APA, action potential amplitude. *p<0.05. VC, vehicle control (0.1 % DMSO-contained NT solution)

Effect of NIC, ISR, and AML on I_{Kr} in hERG-transfected HEK293 cells

To examine the tail components of I_{Kr} which reflect the repolarizing K^+ current in the cardiac AP, the cells were depolarized for 2 s to +20 mV from a holding potential of -80 mV followed by a 3s repolarization back to -40 mV. Figure 4A shows the representative cases of the voltage-clamp recording from *hERG*-transfected HEK293 cells. NIC and AML commonly inhibited I_{Kr} in a concentration-dependent manner, and almost complete inhibition was observed at 30 μM (Figure 1-5A, E). NIC at concentrations of 0.1, 0.3, 1, and 3 μM reduced the I_{Kr} amplitude by 5.1 ± 2.9%, 13.0 ± 2.5%, 40.1 ± 5.5%, and 83.0 ± 7.3%, respectively (n = 4). AML at the same concentrations inhibited the I_{Kr} amplitude by 5.2 ± 2.9%, 17.5 ± 3.3%, 67.6 ± 4.0%, and 90.4 ± 5.1%, respectively (n = 4). However, ISR at 1, 3, 10, and 30 μM inhibited the I_{Kr} amplitude by 2.6 ± 1.6%, 15.6 ± 7.7%, 26.0 ± 7.3%, and 42.2 ± 6.6%, respectively (n = 4). The Hill equation fitting function was applied and IC_{50} (half maximal inhibitory concentration) values were measured to examine the relative potency of I_{Kr} inhibition (Figure 1-5B and F). The IC_{50} values were 0.88 ± 0.05 μM for NIC and 6.78 ± 0.36 μM for AML. Since the maximum inhibition rate of ISR was smaller than 50%, we could not obtain the IC_{50} value for ISR.

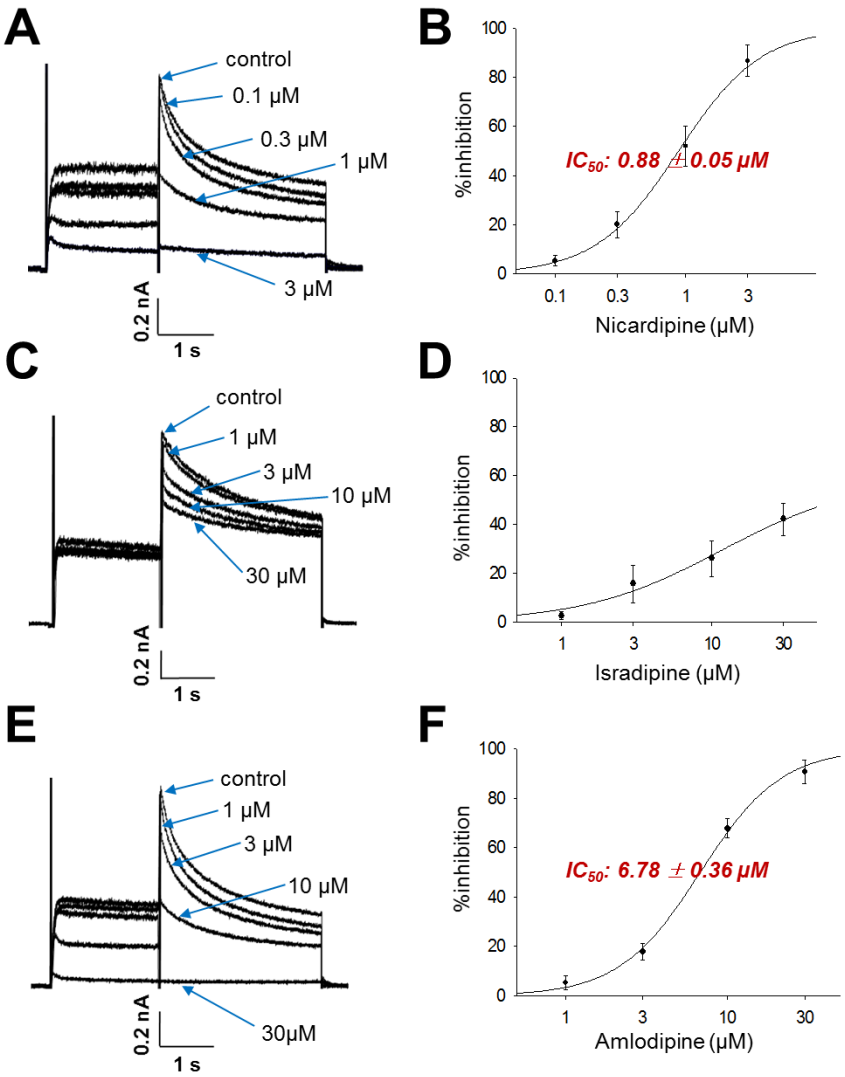

Figure 1-5. Effect of NIC, ISR, and AML on I_{Kr} in *hERG*-transfected HEK293 cells

Representative I_{hERG} traces under control conditions and after application of various test concentrations (0.1 - 30 μM) of NIC (**A**), ISR (**C**), and AML (**E**). Statistical summary and Hill's fitting of concentration–dependent inhibitions of I_{Na} for NIC (**B**), ISR (**D**), and AML (**F**) (each n = 4).

Effect of NIC, ISR, and AML on I_{Ks} in KCNQ1/KCNE1-cotransfected HEK293 cells

For recording I_{Ks}, the *KCNQ1/KCNE1*-coexpressing cells were depolarized for 3 s to +60 mV from a holding potential of -80 mV, followed by a 3s repolarization back to -40 mV. Figure 1-6A, C, and E shows the representative current traces under control conditions and after exposure to 1, 3, 10, and 30 μM NIC, ISR, and AML. Similar to the effects on I_{Kr}, NIC and AML inhibited the I_{Ks} in a concentration-dependent manner while ISR incompletely inhibited I_{Ks} even at 30 μM. Figure 1-6B, D, and F shows the concentration-response curves for these drugs. The IC_{50} values were approximately 9.61 ± 1.01 μM for NIC (Figure 1-6B) and 5.81 ± 0.5 μM for AML (Figure 1-6F). Since the maximum inhibition rate of ISR was smaller than 50%, we could not obtain the IC_{50} value for ISR (Figure 1-6D).

Effect of NIC, ISR, and AML on I_{K1} in KCNJ2-transfected HEK293 cells

Figure 1-7A, C, and E shows the represented currents traces from *KCNJ2*-transfected HEK293 cells and the effects of CCBs. The I_{K1} was elicited by a hyperpolarizing step pulse from -80mV to -120 mV of 1 s duration. All of the three drugs inhibited the I_{K1} in a concentration-dependent manner, however, the maximum inhibition rates of NIC and ISR at 30 μM were below 50 % (45.4 ± 5.3%, and 21.7 ± 2.8%, respectively, each n = 4). The IC_{50} value of AML on the I_{K1} was 9.78 ± 0.18 μM (n = 4, Figure 1-7F).

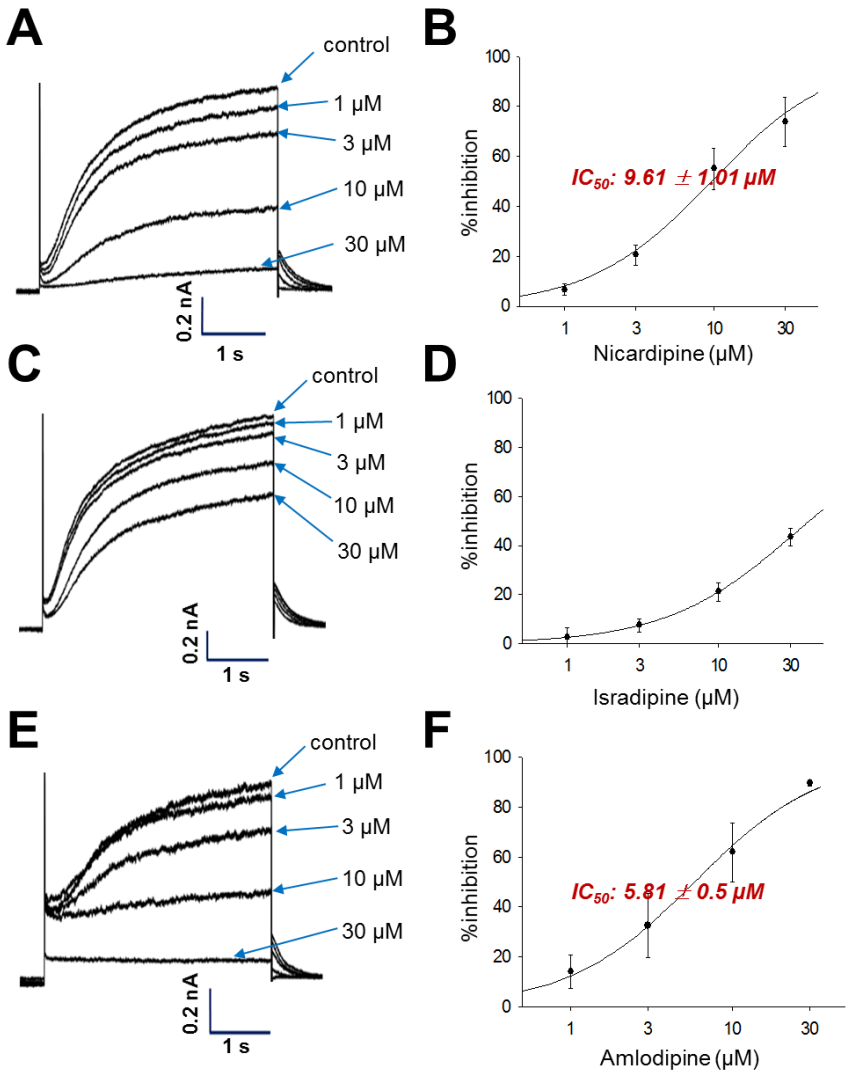

Figure 1-6. Effect of NIC, ISR, and AML on I_{Ks} in *KCNQ1/KCNE1*-cotransfected HEK293 cells

Representative I_{Ks} traces under control conditions and after application of various test concentrations (1, 3, 10, 30 μM) of NIC (**A**), ISR (**C**), and AML (**E**). Statistical summary and Hill's fitting of concentration–dependent inhibitions of I_{Na} for NIC (**B**), ISR (**D**), and AML (**F**) (each n = 4).

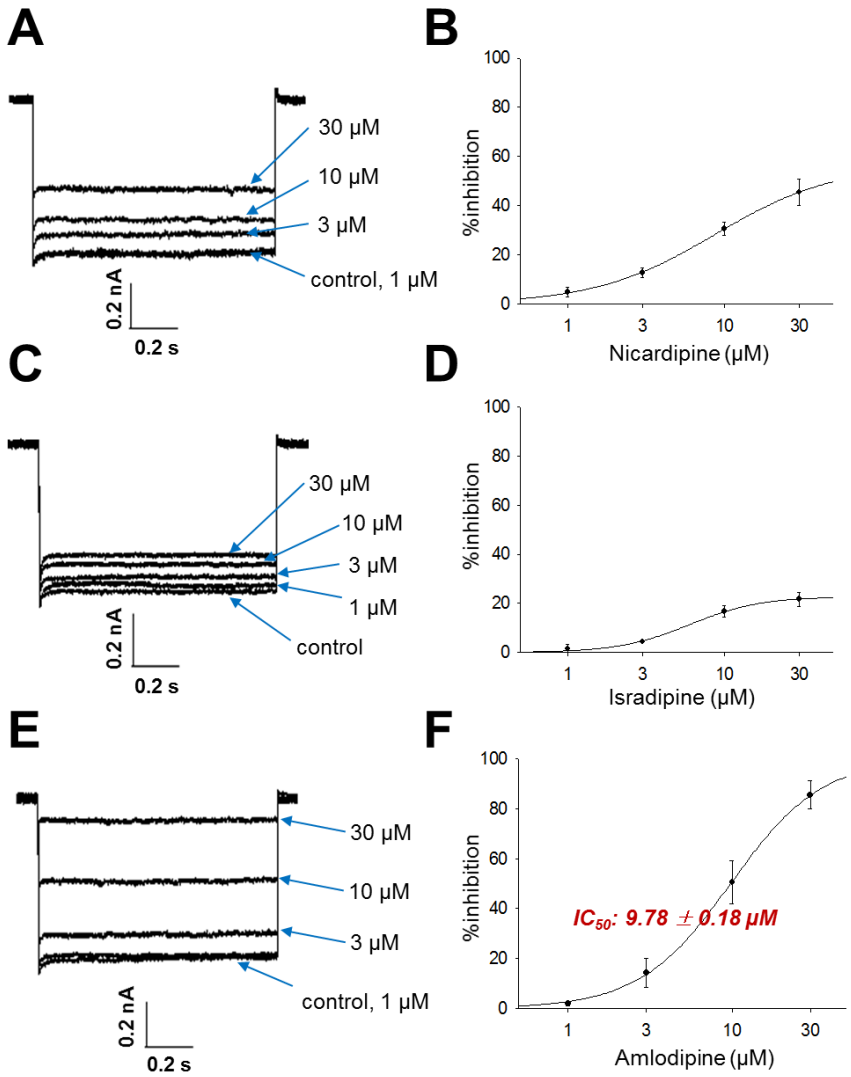

Figure 1-7. Effect of NIC, ISR, and AML on I_{K1} in *KCNJ2*-transfected HEK293 cells

Representative I_{K1} traces under control conditions and after application of various test concentrations (1 - 30 μM) of NIC (**A**), ISR (**C**), and AML (**E**). Statistical summary and Hill's fitting of concentration–dependent inhibitions of I_{Na} for NIC (**B**), ISR (**D**), and AML (**F**) (each n = 4).

Table 1-2 IC_{50} values and Hill coefficients of NIC, ISR, and AML for cardiac major ion channel currents

		NIC	ISR	AML
I_{Kr}	IC_{50} (μM)	0.88 ± 0.05	>30	6.78 ± 0.36
	Hill coefficient	1.37 ± 0.11	-	1.74 ± 0.13
I_{Ks}	IC_{50} (μM)	9.61 ± 1.01	>30	5.81 ± 0.50
	Hill coefficient	1.07 ± 0.12		1.11 ± 0.10
I_{K1}	IC_{50} (μM)	>30	>30	9.78 ± 0.18
	Hill coefficient	-	-	1.57 ± 0.04
I_{Na}	IC_{50} (μM)	7.08 ± 0.72	3.05 ± 0.34	6.38 ± 0.90
	Hill coefficient	1.16 ± 0.13	1.28 ± 0.18	0.76 ± 0.10
I_{Ca}	IC_{50} (μM)	0.142 ± 0.031	0.229 ± 0.024	0.227 ± 0.058
	Hill coefficient	0.67 ± 0.09	2.91 ± 0.33	0.72 ± 0.12

Concentration response relations were calculated by a non-linear least squares fit equation [Hill equation; $f = x^H/(IC50^H+x^H)$; H = Hill coefficient, IC50 = IC_{50}, x = concentration, f = inhibition ratio] using the SigmaPlot 2000 program for the half-maximum inhibiting concentration (IC_{50}). NIC, nicardipine; ISR, isradipine; AML, amlodipine

DISCUSSION

Here I evaluated the electrophysiological safety of the most commonly used dihydropyridine class of CCBs by assessing their effects on the ion channel currents involved in cardiac APD and on repolarization phase in rabbit Purkinje fibers. Despite the common inhibitory effects on I_{Ca}, the APD shortening was not consistent between the three CCBs tested here. APD_{90} was significantly decreased only by ISR from 1 μM whereas APD_{50} was commonly decreased by NIC, ISR and AML at 30 μM. As a result, the AP was generally shortened by ISR whereas showed triangulation in response to NIC and AML. In addition to the above findings, ISR at 30 μM decreased the RMP and dV/dt_{max} while not the APA (Table 1-1). The decrease of dV/dt_{max} might be due to the more potent inhibition of I_{Na} by ISR than by NIC and AML (Figure 1-3).

Except ISR, relatively high concentrations of NIC and AML were required to significantly decrease the APD_{90} of rabbit Purkinje fibers. Indeed, the present ICH S7B guideline does not specifically address the possibility of a drug-induced shortening of the QT interval (49). Although the QT-shortening could potentially increase the ventricular tachycardia and the ventricular fibrillation risk of sudden death (45, 46, 48, 50, 51), Roden (52) and Hondeghem (53, 54) have suggested that simple QT interval change is a poor marker for proarrythmic susceptibility. However, many experiments in isolated rabbit hearts demonstrated that triangulation (prolongation of the fast repolarization phase) is proarrhythmic (54), that was confirmed by other

groups (55-58). Triangulation may be accompanied by either shorting or lengthening of the total action potential duration. In this study, NIC and AML induced the triangulation of AP. However, relatively high concentration (e.g. 30 μM) was required to reveal the triangulation of AP.

Several large clinical trials that have consistently shown that no significant increase in sudden cardiac death with dihydropyridine CCBs even in vulnerable patients (59-62). In fact, the reported plasma concentrations of NIC, ISR and AML ranges below micromolar concentrations (63-68) where no significant changes in APD were observed with NIC and AML in the present study. However, the potent inhibition of I_{Ca} without significant APD shortening by NIC and AML requires further explanation besides the low plasma concentrations.

Despite the concern about the severe shortening or triangulation of cardiac AP, the lack of actual clinical problems might be due, at least partly, to the concomitant changes in other ion channel activities suggested here. In addition to the inhibition of $I_{Ca,L}$, NIC and AML showed concentration-dependent inhibition of I_{Kr} and I_{Ks} (Figure 1-5 and Figure 1-6). The inhibitory effects of ISR on I_{Kr} and I_{Ks} were incomplete (<50 % at 30 μM). Since the voltage-gated K^+ channels would mainly contribute to cardiac repolarization, their inhibition by NIC and AML might compensate for the putative APD shortening effects of CCBs (Table 1-2).

In summary, despite the potent I_{Ca} inhibition, NIC and AML do not induce a significant shortening of APD up to 30 μM of applied concentration. According to ion channel studies, concomitant inhibition of I_{Kr} and I_{Ks} might

differentially counterbalance the influence to cardiac repolarization of CCBs. Further investigation of other classes of CCBs' effects on the cardiac K^+ channel currents are requested for the integrative understanding of cardiac toxicity.

Limitations

On the APD assay, all of tested fibers that escaped the exclusion criteria were randomly allocated to each test agent. However, since the numbers of tested animals are not large (3~4 animals per agent), accidental gathering of Purkinje fibers, there were some variations in control values between agents. (Table 1-1).

To calculate the IC_{50} for each cardiac ion channels of CCBs, only the inhibitory potentials were measured at peak currents for hERG, I_{Ks}, I_{Na}, I_{Ca} and at the end of stable currents for I_{K1} on each maximal activation voltage. In addition to acute inhibition of functional ion channels located in the plasma membrane, some drugs have been revealed to decrease ionic currents chronically through impairment of protein trafficking to the cell surface (69-71). As well as acute current blockade, the disruption of the channel protein trafficking into cell surface membrane has been reported to induce adverse effects (72). Therefore, to better understand the inhibitory mechanisms of the ion channels by the CCBs, the further experiments for ion channel kinetics and channel protein trafficking could be conducted.

CHAPTER 2

Integrative analysis of cardiac ion channel modulation by SARI class antidepressants in human stem cell-derived cardiomyocytes

INTRODUCTION

Several types of *in vitro* (e.g. hERG assay) and *in vivo* QT screening systems (e.g. Telemetry) are currently in use with standardized protocols. However, none of the assay systems reflects the genuine properties of the human cardiac cells yet. The recently established human induced pluripotent stem cell-derived cardiomyocytes (hiPSC-CMs) can be used as an *in vitro* preclinical model to predict cardiotoxicity. Unlike primary culture models of human cardiomyocytes, which lose their ability to beat in the process of proliferation, hiPSC-CMs express cardiac contractile proteins and functional ionic channels to allow the physical contraction of myocytes (28, 73-75). The development of an *in vitro* system based on hiPSC-CMs could provide more relevant human cell lines for drug safety assessment in a reproducible manner (36, 76, 77). Although the endogenous electrophysiological properties of hiPSC-CMs have been well reported (74, 78), there is a paucity of data concerning drug-induced responses that validate hiPSC-CMs as an *in vitro* preclinical model for toxicological evaluation.

Antidepressants for depressive disorders also affect the autonomic nerves innervating the heart and are associated with cardiovascular mortality (79-82). Although a second-generation antidepressant, nefazodone (83-85), has been initially claimed to have significantly less cardiovascular side effects than the first-generation tricyclic antidepressants (86-88), an increasing number of studies on nefazodone have raised concerns regarding its cardiac safety. Trazodone also belong to a class of SARIs. Although SARIs have been shown

to be associated with reduced cardiovascular side effects when compared to their predecessors, an increasing number of studies have raised doubts regarding the safety of SARIs (89-91).

Such concerns were raised by a case of QT prolongation and torsade de pointes (TdP) tachyarrhythmia that occurred in a patient receiving nefazodone (91-94). We have recently found that nefazodone inhibits human ether-a-go-go related gene (hERG, KCNH2 or Kv11.1) channels by interacting with the aromatic binding sites Y652 and F656 within the S6 domain of hERG (95). Although the likely mechanism behind the drug-induced prolongation of the QT interval is the interaction of nefazodone with hERG channels (96, 97), not all hERG blockers cause QT prolongation or TdP, and additional genes associated with the QT interval can cause life-threatening cardiac arrhythmias (98). In addition, mutations in genes that encode cardiac ionic channels, such as KCNQ1/KCNE1-encoded slow component of the delayed rectifier potassium current (I_{Ks}) channels, KCNH2-encoded I_{Kr} channels, and SCN5A-encoded inward voltage-gated sodium current (36) channels, can disrupt the fine balance among ionic currents and lead to life-threatening arrhythmias (99-101).

A new paradigm for cardiac arrhythmic safety assessment in a nonclinical *in vitro* human model relies upon the analysis of effects of drugs on the APs and various types of cardiac ion currents. Thus, to adopt hiPSC-CMs for the assay system, it is necessary to verify the relevance to the pharmacological/toxicological effects on the ionic currents in heterologous expression systems. To understand the mechanisms of arrhythmogenicity of

SARI class antidepressants, nefazodone and trazodone, we investigate the effects of various conventional cardiac ion channels blockers as well as these drugs on hiPSC-CMs and HEK293 cells expressing cardiac ion channels. To elucidate the usefulness of hiPSC-CMs in *in vitro* cardiac safety testing, we examined whether (1) hiPSC-CMs recapitulate appropriate electrical response of cardioactive selective channel blockers; (2) hiPSC-CMs could be used to evaluate cardiotoxicity of nefazodone and trazodone, previously known as a non-cardiac acting drug. These functional evaluation of multiple cardiac ion channels and action potential will provides much information for these SARIs' cardiac risk potential compared to hERG block alone.

MATERIALS AND METHODS

1. Cell culture

The hiPSC-CMs (iCell® Cardiomyocytes; Cellular Dynamics International, Madison, WI, USA) were cultured for single-cell electrophysiological recordings. Frozen vials of hiPSC-CMs were thawed in a water bath maintained at 37℃ and mixed with ice-cold plating medium (iCell Cardiomyocyte Plating Medium). The cells were transferred to four-well culture plates containing 0.1% gelatin-coated glass coverslips and then maintained in a culture incubator at 37℃ in an atmosphere of 93% air and 7% CO_2. After 2 days of culture, the plating medium was replaced with culture medium (iCell Cardiomyocyte Maintenance Medium), which was then changed every 2 days.

2. Isolation of rat ventricular myocytes (rVMs)

To compare the nefazodone sensitivity on I_{Ca} between rat CMs and hiPSC-CMs, we isolated single rVMs using the Langendorff system. Briefly, the hearts were rapidly excised from anesthetized Sprague-Dawley rats (250–350 g) and perfused via the aorta on a Langendorff apparatus with an oxygenated normal Tyrode's (NT) solution for 5 min to clear the blood, then perfused with $Ca2^{+}$-free NT solution for 3 min. Next, the heart was perfused with an enzyme solution containing 0.6 mg/ml collagenase (Worthington, type 2, USA) for 8-10 min. Finally, this enzyme-containing solution was washed out for 5 min with a high-K^{+} and low-Cl^{-} Kraft-Bruhe (23) solution. Following the isolation

procedure, the left ventricle was dissected and agitated mechanically with a fire-polished Pasteur pipette in KB solution to obtain single myocytes. The isolated myocytes were stored at 4℃ for 12 h.

3. Whole-cell patch clamp recordings in hiPSC-CMs

The hiPSC-CMs were cultured for 4 weeks and used at 7 to 28 days post-thaw for electrophysiological analysis. At this time, the amplitudes and intervals of the spontaneous APs are stabilized, and electrically connected syncytial layers are formed. Whole-cell hiPSC-CM recordings were performed at 37℃ using an external solution containing (mM) 145 NaCl, 5.4 KCl, 10 HEPES, 1 $MgCl_2$, 5 glucose, 1.8 $CaCl_2$ (pH 7.4). The internal solution contained (mM) 120 K-Asp, 20 KCl, 5 NaCl, 2 $CaCl_2$, 10 HEPES, 5 EGTA, and 5 Mg-ATP (pH 7.25). We recorded typical APs in hiPSC-CMs in the current-clamp mode. The spontaneous beating activity of single hiPSC-CMs was recorded, and only hiPSC-CMs that could beat stably were included in the analysis. Following stabilization of the AP waveforms, the average of five recorded APs for each test concentration was analyzed. In the voltage-clamp mode, a standardized step protocol was used to elicit the cardiac I_{Kr}, I_{Ks}, I_{Na}, and I_{Ca}. The extracellular solution for recording the I_{Na} contained (mM) 110 CsCl, 50 NaCl, 10 HEPES, 1 $MgCl_2$, 5 glucose, and 1.8 $CaCl_2$ (pH 7.4). The extracellular solution for recording the I_{Ca} contained (mM) 137 Choline-Cl, 5 CsCl, 10 HEPES, 0.5 $MgCl_2$, 10 glucose, and 1.8 $CaCl_2$ (pH 7.4). The internal solution for I_{Na} and I_{Ca} contained (mM) 120 Cs-Asp, 20 CsCl, 5 NaCl, 10 TEA-Cl, 10 EGTA, and 10 HEPES, and 5 Mg-ATP (pH 7.25). A standardized step

protocol was used to elicit the major cardiac ion currents I_{Kr}, I_{Ks}, I_{Na}, and I_{Ca}. The cells were held at −80 mV and depolarized to +20 mV for 2 s, followed by repolarization to −40 mV for 2 s to activate hERG tail currents. The I_{Kr} was isolated by eliminating the calcium currents using 1 μM nifedipine in the external solution. To elicit I_{Ks}, a -80 mV holding potential was used, followed by a 2 s depolarization to +60 mV and a 1 s repolarization to -20 mV. The I_{Ks} was isolated by 100 nM E-4031 and 1 μM nifedipine in the external solution, eliminating the hERG and calcium currents. The cells were held at -100 mV and depolarized to -40 mV for 50 ms to elicit I_{Na}. The I_{Na} was isolated by eliminating the calcium currents using 1 μM nifedipine in the external solution. To elicit I_{Ca} in hiPSC-CMs, the cells were held at -40 mV and depolarized to 0 mV for 300 ms. The I_{Ca} was isolated by eliminating the potassium currents using 2 mM 4-AP in the external solution.

4. Whole-cell voltage clamp recordings in HEK293 cells and isolated rVMs

I_{Na}, I_{Kr} and I_{Ks} currents were recorded in HEK293 cells using NT solution (mM): 143 NaCl, 5.4 KCl, 5 HEPES, 0.33 NaH_2PO_4, 0.5 $MgCl_2$, 10 glucose, and 1.8 $CaCl_2$ (pH 7.4). The internal solution for I_{Na} contained (mM): 105 CsF, 35 NaCl, 10 EGTA, and 10 HEPES (pH 7.25), for I_{Kr} contained (mM): 130 KCl, 5 EGTA, 10 HEPES, 1 $MgCl_2$, and 5 Mg-ATP (pH 7.25), and for I_{Ks} contained (mM): 150 KCl, 5 EGTA, 10 HEPES, 2 $MgCl_2$, 1 $CaCl_2$ and 5 Na_2-ATP (pH 7.25). I_{Ca} currents on rVMs were recorded in the external solution

contained (in mM) Choline-Cl 137, CsCl 5, HEPES 10, $MgCl_2$ 5, Glucose 1.8, $CaCl_2$ 1.8, 4-AP 5, and tetrodotoxin (TTX) 0.003. The internal solution contained (mM) Cs-Asp 120, CsCl 20, NaCl 5, TEA-Cl 10, HEPES 10, EGTA 10, and Mg-ATP 5. In voltage-clamp mode, the standardized step protocols used for hiPSC-CMs study are applied to elicit specific cardiac ion currents.

5. Statistical analysis

pCLAMP (Axon Instruments, Foster City, CA, USA), Origin 8 (OriginLab Corp, Northampton, MA, USA), and Excel (Microsoft, Redmond, WA, USA) software were used for data acquisition and analysis. Ionic current amplitudes normalized to membrane capacitance have been represented as pA/pF to simulate current density values and to compensate for differences in cell size. The concentration–response relationships for drug-induced blockage were calculated using SigmaPlot (Systat Software, San Jose, CA, USA). The IC_{50} value, defined as the drug concentration that reduced the ionic currents by 50%, was obtained using the sigmoidal Hill equation: $f = x^H / (IC_{50}^H + x^H)$, where x is the concentration, H is the Hill coefficient, and f is the inhibition ratio. The data are presented as the means ± SEM, and n represents the number of experimental replicates. Statistical significance was determined using Student's *t*-test and a one-way ANOVA with post hoc testing using Dunnett's method; $p < 0.05$ was considered to indicate statistical significance.

RESULTS

Electrophysiological characterization of hiPSC-CMs

First of all, I measured the APs in spontaneously contracting hiPSC-CMs using the patch clamp technique. The 3 types of representative traces recorded in hiPSC-CMs are shown in Figure 2-1. The majority of the cells (~80%) showed ventricular (V)-type APs, while atrial (A)-, and nodal (N)-type APs were also observed in the 10.7% and 8.9% cells, respectively. The distinction of V-type cells was made on the relatively more negative maximum diastolic membrane potential (MDP) and a rapid upstroke velocity of AP firing with long plateau phase. The absence of a prominent plateau phase was a characteristic of A-type APs, resulting in shorter APD compared to V-type APs. N-type APs showed less negative MDP, slower AP upstroke and a prominent phase 4 depolarization. Table 1 summarizes the AP characteristics of hiPSC-CMs and native human ventricular myocytes (hVMs) in literature. The MDP, dV/dt_{max}, APA, APD_{90}, and APD_{50} were analyzed, and only the V-type of cells with APD_{90} longer than 300 ms were included in the drug test. A-type cells had a control APD_{90} between 200 and 300 ms (n = 6, with a mean APD_{90} of 284 ± 7 ms) and all of these 5 cells classified as N-type cells were discriminated from A-type APs by a significantly lower dV/dt_{max} (< 10 V/s) and a smaller amplitude. None of the cells APD_{90} < 300 ms or dV/dt_{max} < 10 V/s were included in the analysis.

When compared with the parameters of APs in the native hVMs in the literature (102), the MDP of V-type APs is still less negative with values

ranging from -65 to -67 mV. The amplitude of APs in hiPSC-CMs (107-109 mV) was comparable to those of hVMs (104-106 mV) despite the depolarized MDP in hiPSC-CM. The dV/dt_{max} ranged from 41 to 48 V/s, which was slower than those of native hVMs (215-234 V/s). The APDs (e.g., APD_{90}) of ventricular-like hiPSC-CM were longer (477-508 ms) than those of native hVMs (337-365 ms).

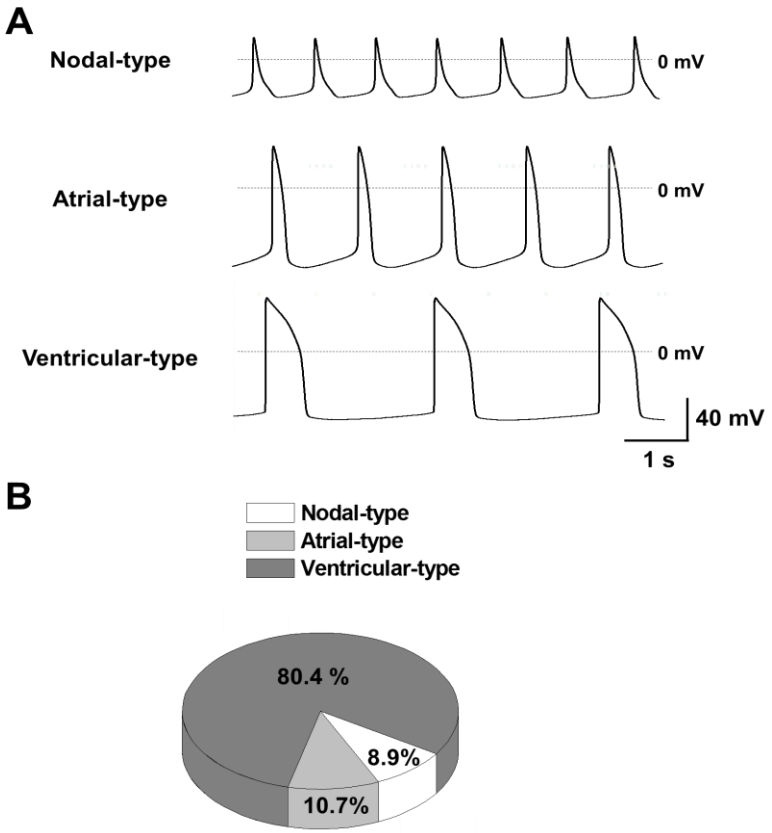

Figure 2-1. Multiple types of action potentials recorded in hiPSC-CMs

A, Representative traces display all three types of APs recorded in hiPSC-CMs. B, Comparison of the relative abundance of different APs subtypes in hiPSC-CMs (n=56).

Table 2-1. Action potential parameters of hiPSC-CMs

Cell type	n	MDP (mV)	dV/dt_{max} (V/s)	APD_{90} (ms)	APA (mV)
N	5	−56.9 ± 1.2	5.7 ± 0.4	244.4 ± 11.9	85.7 ± 1.4
A	6	−66.7 ± 0.9	18.4 ± 2.1	284.2 ± 6.9	106.6 ± 1.2
V	45	−66.0 ± 0.8	44.5 ± 2.8	492.1 ± 15.4	107.9 ± 0.8
hVMs[a]		−81.8 ± 3.3	215 ± 33	351±14	106.7 ± 1.4

The action potential parameters of three different subtypes are summarized (mean ± SEM). MDP, maximal depolarization potential; dV/dt_{max}, maximal upstroke velocity of phase 0; APD_{90}, 90% repolarization of action potential; APA, action potential amplitude. N, nodal; A, atrial; V, ventricular; n, the number of cells; hVMs, human ventricular myocytes. [a] Magyar et al., 2000 (102).

Voltage-gated ion channel currents of hiPSC-CMs were confirmed under whole-cell voltage clamp conditions by using the pulse protocols and pipette solutions specific for each types of ion channels (Figure 2-2, 2-3, and 2-4), and the results are also summarized in Table 2-2. hiPSC-CMs showed a prominent I_{Na} (Figure 2-2A and 2B), which is responsible for the AP upstroke in ventricular CMs. The I_{Na} peak density in hiPSC-CMs is -163 pA/pF, which is much higher than the -20 pA/pF reported in native hVMs (Table 2-2) (103). The hiPSC-CMs also showed an I_{Ca} (Figure 2-2C and 2D) that is an important contributor to the plateau phase of the APs. The maximal peak I_{Ca} density in hiPSC-CM is -6.6 pA/pF, which is slightly lower or comparable to native

hVMs, in which the maximal I_{Ca} shows -10.2 pA/pF (Table 2-2) (102). As for the repolarization of cardiac APs, two types of delayed rectifier potassium currents (I_{Kr} and I_{Ks}) were identified in the hiPSC-CM as E-4031-sensitive currents (I_{Kr}) (Figure 2-3A and 2B) and chromanol 293B-sensitive current (I_{Ks}) (Figure 2-3C and 2D); their current densities were 2.3 pA/pF and 2.9 pA/pF, respectively (Table 2-2). The K^+ current densities were slightly higher or comparable to those in the native hVMs, in which the I_{Kr} and I_{Ks} densities are 0.31 and 0.18 pA/pF, respectively. (102, 104). In ventricular CMs, the inward rectifier K^+ current (I_{K1}) is an important contributor to the maintenance of the RMP and the termination of the final repolarization phase. In hiPSC-CM, the Ba^{2+}- sensitive I_{K1} density was -5.1 pA/pF (Figure 2-4A and 4B), which is slightly lower or comparable to that reported in native hVMs, -10 pA/pF (Table 2-2) (102). The funny current (105) is an inward nonselective cationic current activated by hyperpolarized membrane potentials. The zatebradine-sensitive I_f density in hiPSC-CMs was -0.9 pA/pF (Figure 2-4C and 4D), which is relatively low compared to hVMs, -1.2 pA/pF (Table 2-2) (106).

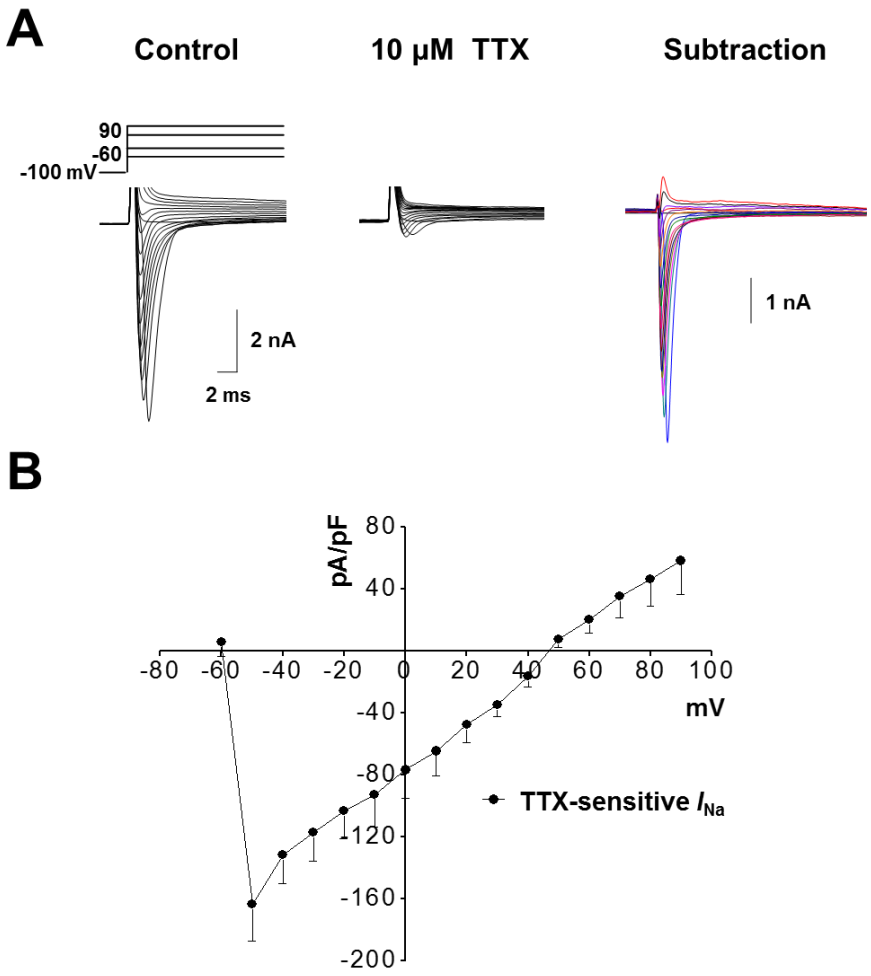

Figure 2-2. TTX-sensitive I_{Na} currents in hiPSC-CMs

(A) Representative trace of the control (left), the presence of TTX (middle), and the TTX -sensitive current of I_{Na} (right) in hiPSC-CMs. (B) I-V relationship of I_{Na} in hiPSC-CMs (means ± SEM).

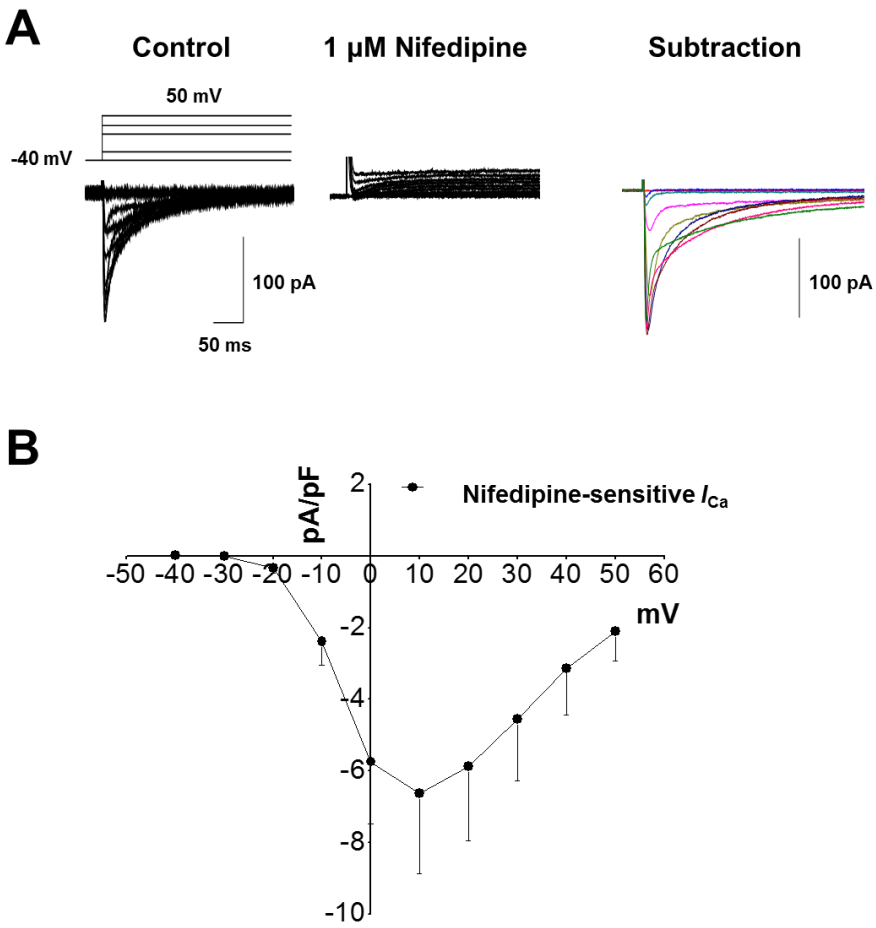

Figure 2-3. Nifedipine-sensitive I_{Ca} currents in hiPSC-CMs

(A) Representative trace of the control (left), the presence of nifedipine (middle), and the nifedipine-sensitive current of I_{Na} (right) in hiPSC-CMs. (B) I-V relationship of I_{Ca} in hiPSC-CMs (means ± SEM).

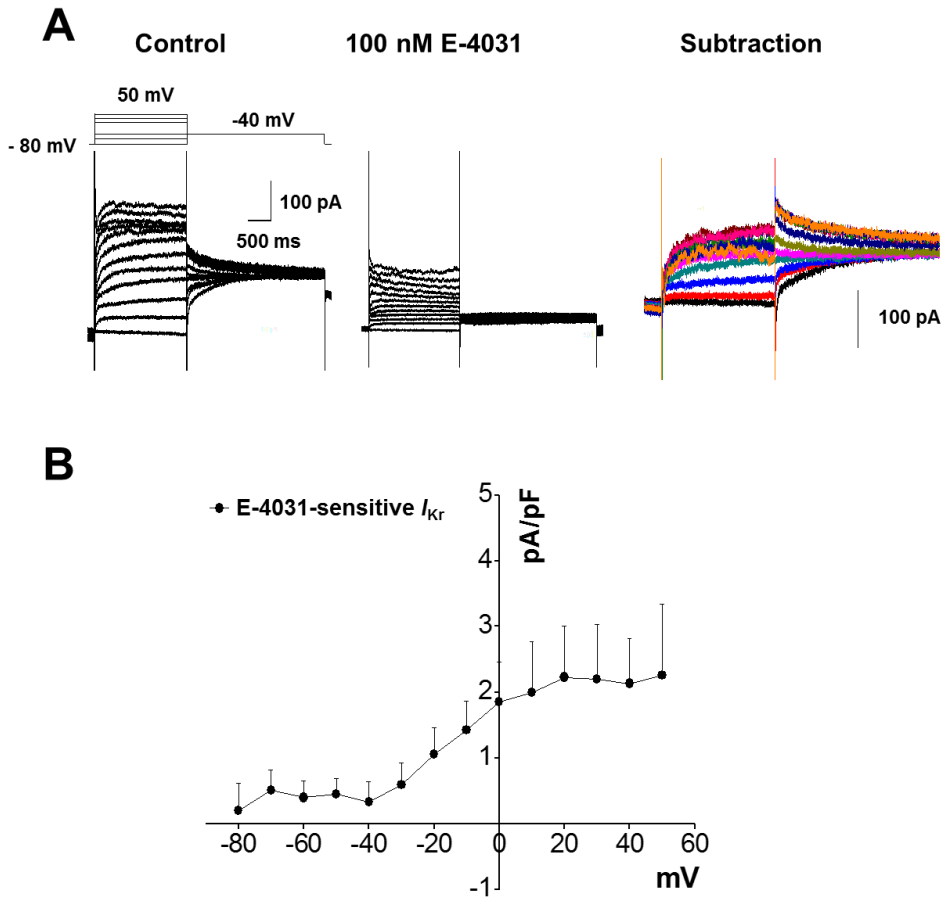

Figure 2-4. E-4031-sensitive hERG (I_{Kr}) currents in hiPSC-CMs

(A) Representative trace of the control (left), the presence of E-4031 (middle), and the E-4031-sensitive current of I_{Kr} (right) in hiPSC-CMs. (B) I-V relationship of I_{Kr} in hiPSC-CMs (means ± SEM).

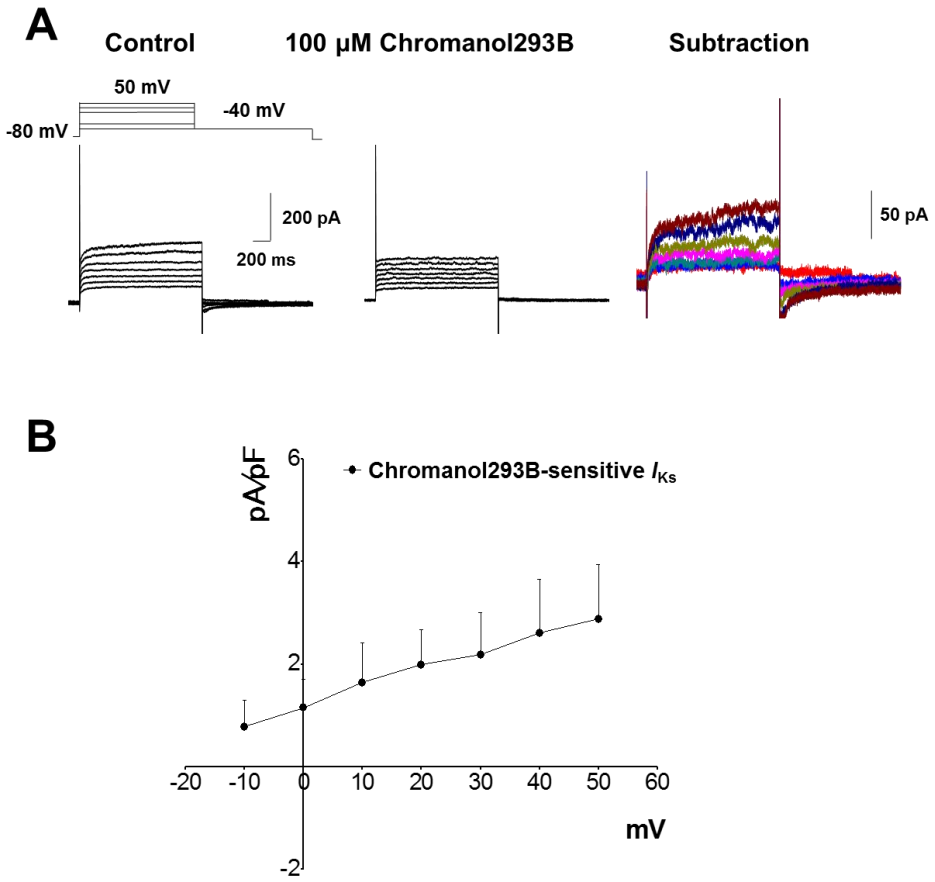

Figure 2-5. Chromanol293B-sensitive I_{Ks} currents in hiPSC-CMs

(A) Representative trace of the control (left), the presence of Chromanol293B (middle), and the Chromanol293B-sensitive current of I_{Ks} (right) in hiPSC-CMs. (B) I-V relationship of I_{Ks} in hiPSC-CMs (means ± SEM).

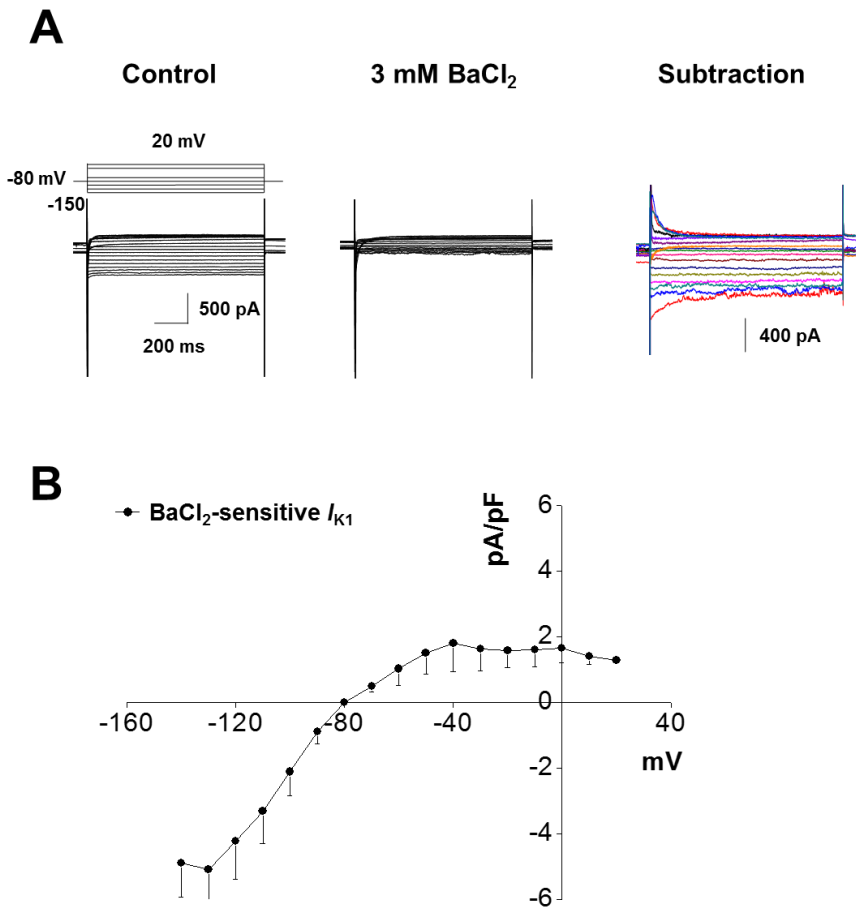

Figure 2-6. Inward rectifier (I_{K1}) currents in hiPSC-CMs

(A) Representative trace of the control (left), the presence of $BaCl_2$ (middle), and the $BaCl_2$-sensitive current of I_{K1} (right) in hiPSC-CMs. (B) I-V relationship of I_{K1} in hiPSC-CMs (means ± SEM).

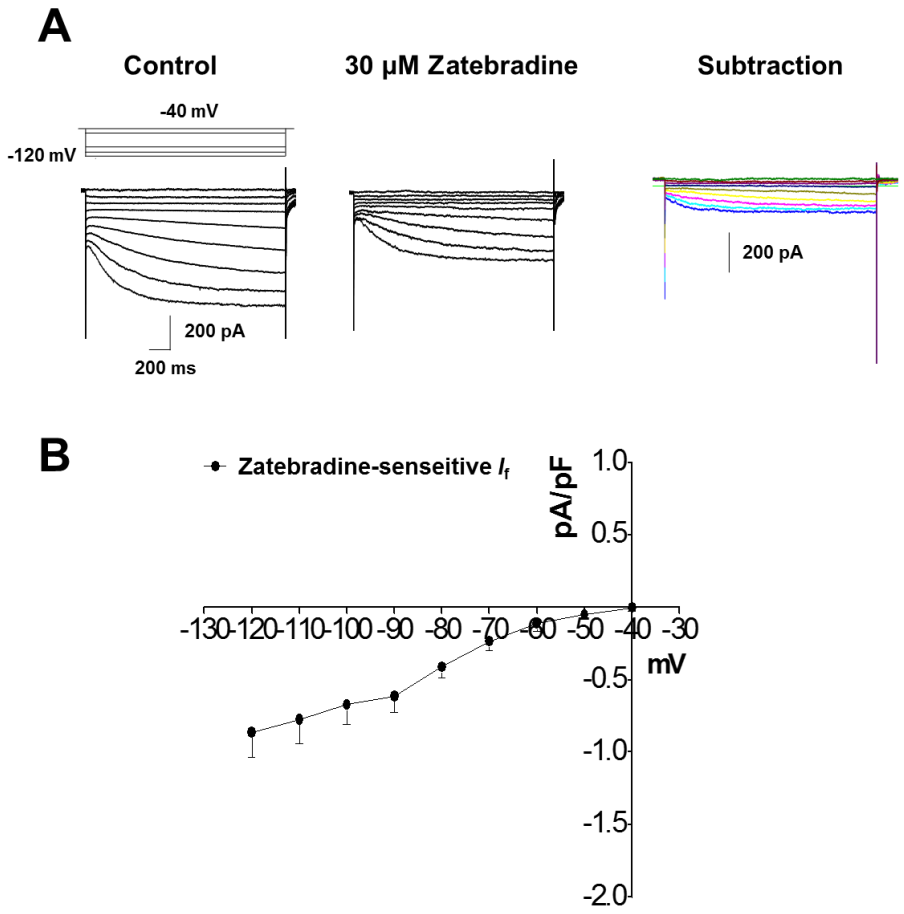

Figure 2-7. Pacemaker currents in hiPSC-CMs

(A) Representative trace of the control (left), the presence of zatebradine (middle), and the zatebradine-sensitive current of I_f (right) in hiPSC-CMs. (B) I-V relationship of I_f in hiPSC-CMs (means ± SEM).

Table 2-2. Ionic currents density in hiPSC-CMs and native hVMs

Current	Cell type	Peak current (pA/pF)
I_{Na}	hVMs[a]	−20.2 ± 2.2
	hiPSC-CMs	−163.2 ± 23.8
I_{Ca}	hVMs[b]	−10.2 ± 0.6
	hiPSC-CMs	−6.6 ± 2.2
I_f	hVMs[b]	−1.2 ± 0.2
	hiPSC-CMs	−0.9 ± 0.2
I_{Kr}	hVMs[b]	0.31 ± 0.02
	hiPSC-CMs	2.3 ± 1.1
I_{Ks}	hVMs[c]	0.18
	hiPSC-CMs	2.9 ± 1.1
I_{K1}	hVMs[d]	~ −10
	hiPSC-CMs	−5.1 ± 1.4

The voltage-dependent current density of hiPSC-CMs and native hVMs are summarized (each n = 3, mean ± SEM). [a] Sakakibara et al., 1993, [b] Magyar et al., 2000, [c] Virag et al., 2001, [d] Hoppe et al. 1998.

Effects of selective ion channel blockers on the APs in hiPSC-CMs

To confirm the utility of hiPSC-CMs as the testbed for drug-induced cardiotoxicity, I tested whether the APs are actually affected by the ion channel blockers specific for I_{Kr}, I_{Ca} and I_{Na}; E-4031, nifedipine, and TTX, respectively (Figure 2-8 and Table 2-3). Application of 100 nM E-4031 induced a significant prolongation of the APs; APD_{50} and APD_{90} were increased by 82 and 150%, respectively. Early afterdepolarization (EAD) was often observed after the exposure to E-4031. There were no significant changes in the MDP, APA, and dV/dt_{max} of the APs after the exposure to E-4031 (n = 4). TTX (100 nM) significantly decreased dV/dt_{max} by 35% at 300 nM whereas it did not induce significant changes in MDP, APA, or APD (n = 4). Nifedipine at 1 μM decreased APD_{90} by 35%, without changing other AP parameters (n = 4). These results indicate that hiPSC-CMs effectively recapitulate the electrophysiological behaviors of native CMs and drug-induced arrhythmias such as EAD.

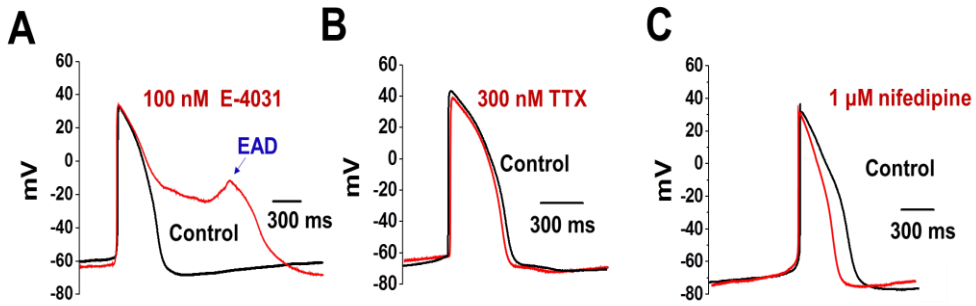

Figure 2-8. Effects of selective ion channel blockers on action potential waveforms in hiPSC-CMs

Representative AP traces in the control and in the presence of 100 nM E-4031 (A), 300 nM TTX (B), and 1 μM nifedipine (C). EAD, early afterdepolarization.

Table 2-3. Effects of selective ion channel blockers on AP parameters in hiPSC-CMs

Drugs	nM	MDP (mV)	dV/dt_{max} (V/s)	APD_{90} (ms)	APD_{50} (ms)	TA (mV)
E-4031	**0**	−71.7 ± 0.4	41.1 ± 6.0	480.1 ± 36.3	339.6 ± 23.8	107.9 ± 1.0
	100	−68.7 ± 1.6	42.8 ± 4.8	1186. 6± 179.3*	620.9 ± 44.7**	106.6 ± 1.7
TTX	**0**	−71.7 ± 1.0	57.9 ± 7.0	332.0 ± 41.0	272.7 ± 35.4	112.9 ± 1.1
	300	−71.7 ± 0.8	42.9 ± 4.7*	332.5 ± 41.4	274.5 ± 31.7	112.4 ± 0.8
Nifedipine	**0**	−69.8 ± 2.2	52.9 ± 6.8	402.7 ± 54.1	288.3 ± 39.5	106.7 ± 2.8
	1000	−70.0 ± 2.9	51.8 ± 6.9	297.9 ± 69.8*	218.6 ± 57.2	105.8 ± 3.3

The effect of ion channel blockers on APs parameters are summarized (each n=4, mean ± SEM). *$p<0.05$, **$p<0.01$ compared to control. MDP, maximum diastolic potential; dV/dt_{max}, maximum upstroke velocity; APD_{90}, action potential duration at 90% repolarization; APD_{50}, action potential duration at 50% repolarization, TA, total amplitude.

Effects of nefazodone on APs and ion channel currents in hiPSC-CMs

The application of 1 μM nefazodone increased APD with EAD and was reversed by washout (Figure 2-9A). Effects on the parameters of APs were normalized to the control value in each cell, and summarized in the bar graphs (Figure 2-9B-F). Prolongation of both APD_{50} and APD_{90} were observed from 0.1 μM of nefazodone in a concentration-dependent manner (Figure 2-9E, F). With 1 μM nefazodone, EAD was induced in all the cells tested (n=6). Also, it was notable that 1 μM nefazodone decreased the dV/dt_{max} of the APs (Figure 2-9D). In three cells, when the concentration of nefazodone was increased to 3 μM, the AP generation was disappeared with depolarization of MDP (data not shown).

Effects of nefazodone on ion channel currents in hiPSC-CMs

To investigate the effects of nefazodone on repolarization-related currents, I_{Kr} and I_{Ks} were recorded; these currents were activated by appropriate step pulse protocols with pharmacological conditions to selectively isolate the currents. Nefazodone inhibited the I_{Kr} in a concentration-dependent manner (Figure 2-10). When the peak amplitudes of repolarizing tail currents were analyzed, the IC_{50} value was 41.4 ± 0.2 nM (Figure 2-10B, n=6). Nefazodone completely blocked the stepwise I_{Kr} current density at 100 nM (Figure 2-10C), but without affecting the voltage sensitivity (Figure 2-10D, n=6). Nefazodone also inhibited I_{Ks} but with low potency ($IC_{50,}$ 10.1 ± 0.5 μM) (Figure 2-11, B, n=5). The inhibition of I_{Ks} by nefazodone was observed at wide range of membrane potentials (Figure 2-11C and D, n=5).

The effects of nefazodone on depolarization-related currents, I_{Na} and I_{Ca}, were analyzed. Nefazodone inhibited the peak amplitude of I_{Na} in concentration-dependent manner (IC_{50}, 1.03 ± 0.01 μM, n = 4) throughout the test voltages (Figure 2-12). Nefazodone also inhibited the nifedipine-sensitive I_{Ca} peak amplitude with an IC_{50} value of 1.03 ± 0.07 μM throughout the test voltages (Figure 2-13A and B, n = 6) without affecting the voltage-sensitivity of I_{Ca} (Figure 2-13C and D, n = 4).

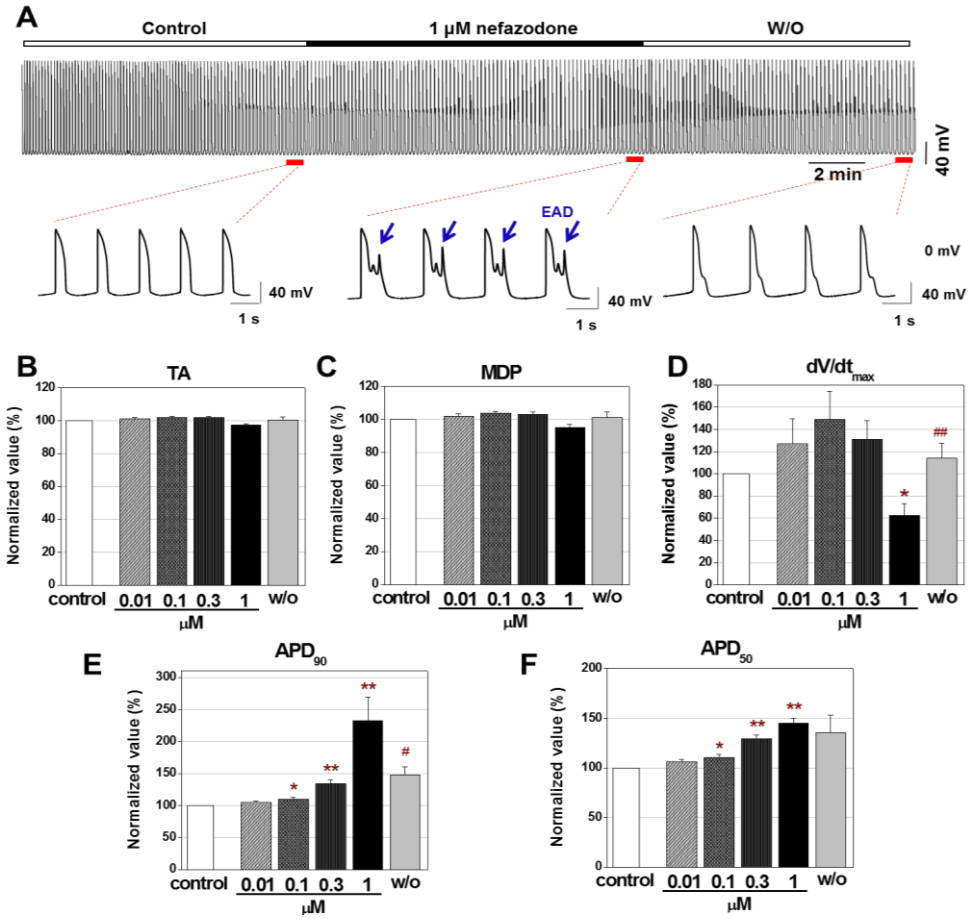

Figure 2-9. Effects of nefazodone on action potential waveforms in hiPSC-CMs

A, Representative traces in the control and in the presence of nefazodone show the typical EAD (arrow) waveform induced by 1 μM nefazodone. B-F, Normalized AP parameters in the control and in the presence of 0.01, 0.1, 0.3, and 1 μM nefazodone. TA, total amplitude; MDP, maximum diastolic potential; dV/dt_{max}, maximum upstroke velocity; APD_{90}, action potential duration at 90% repolarization; APD_{50}, action potential duration at 50% repolarization (mean ± SEM, n=6). *$p<0.05$, **$p<0.01$ compared to control; $^{\#}p<0.05$, $^{\#\#}p<0.01$ compared to 1 μM nefazodone.

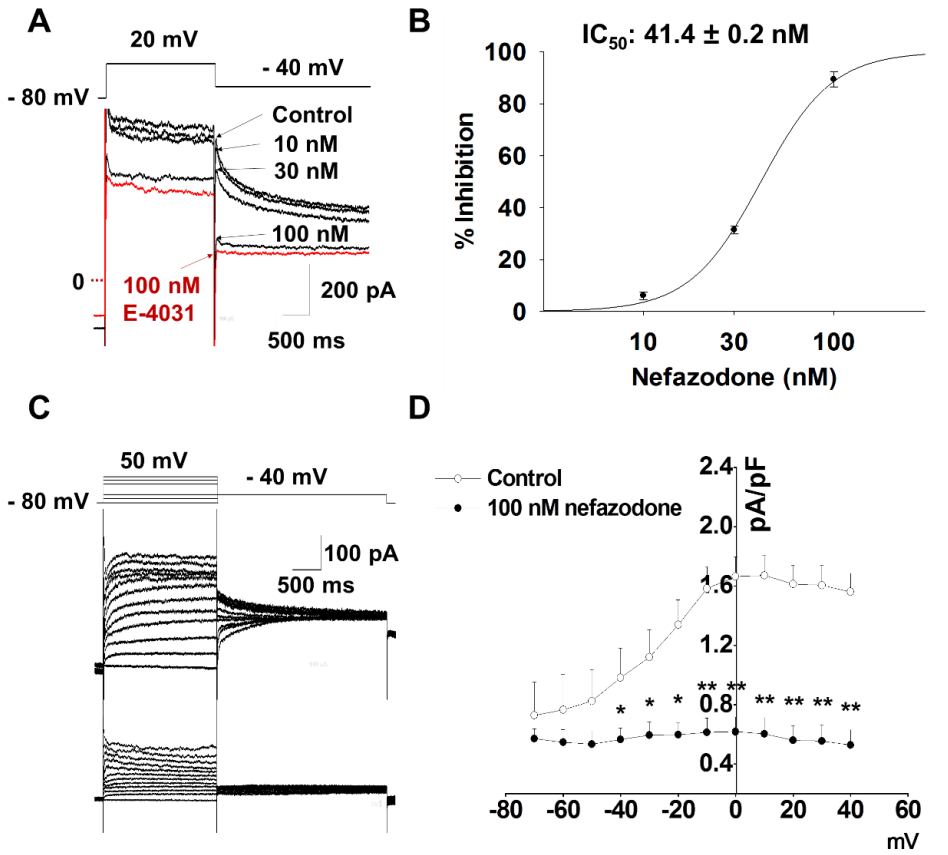

Figure 2-10. Effect of nefazodone on I_{Kr} in hiPSC-CMs

A, Representative traces demonstrating the effect of nefazodone on I_{Kr} at doses of 10, 30, and 100 nM, respectively. B, Dose–response relationship of nefazodone, showing an IC_{50} value for I_{Kr} (mean ± SEM, n=6). C, Pulse protocol (top), representative I-V traces of I_{Kr} in control (middle) and in the presence of 100 nM nefazodone (bottom). D, I-V relationships of I_{Kr} in the control and 100 nM nefazodone (mean ± SEM, n = 6, * p<0.05, ** p<0.01 compared to control).

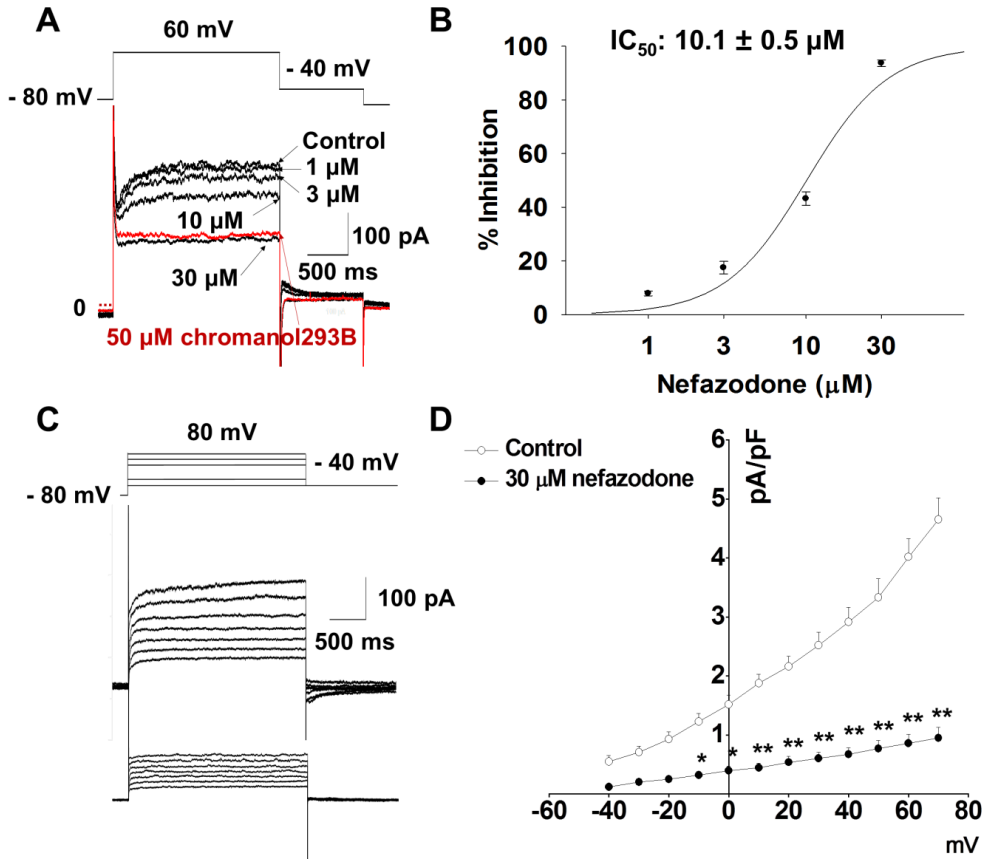

Figure 2-11. Effect of nefazodone on I_{Ks} in hiPSC-CMs

A, Representative traces demonstrating the effect of nefazodone on I_{Ks} at doses of 1, 3, 10 and 30 μM, respectively. B, Dose–response relationship of nefazodone, showing an IC_{50} value for I_{Ks} (mean ± SEM, n=5). C, Pulse protocol (top), representative I-V traces of I_{Ks} in control (middle) and in the presence of 30 μM nefazodone (bottom). D, I-V relationships of I_{Ks} in control and in the presence of 30 μM nefazodone (mean ± SEM, n=5, *p<0.05, **p<0.01).

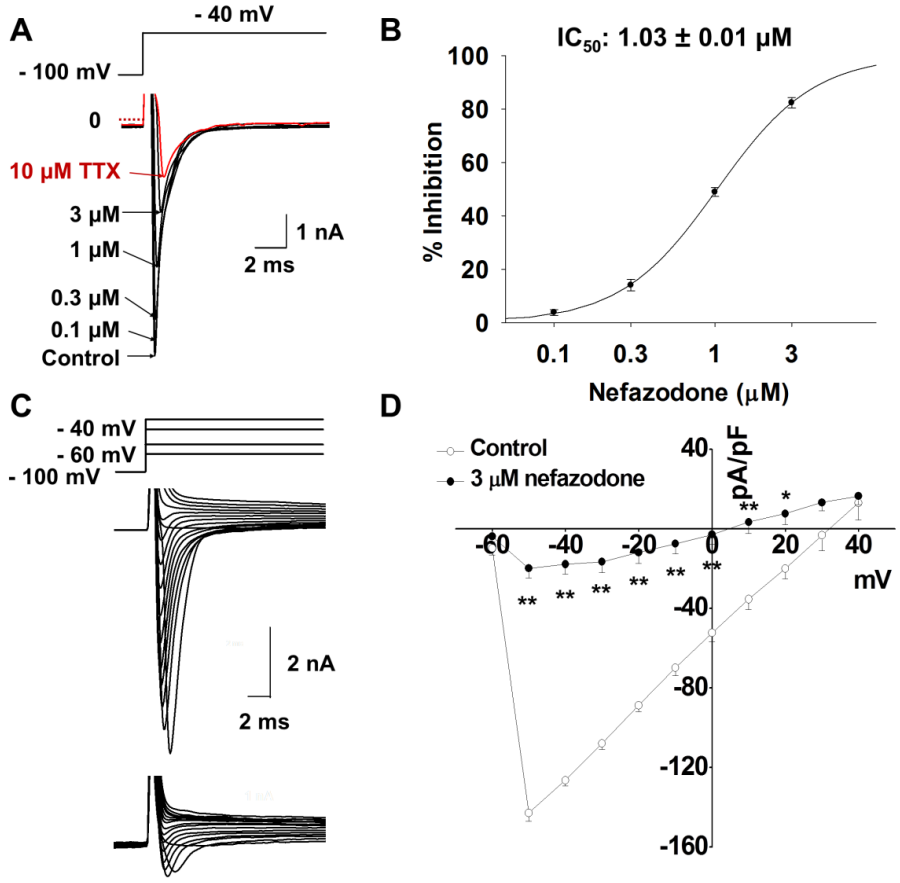

Figure 2-12. Effect of nefazodone on I_{Na} in hiPSC-CMs

A, Representative traces demonstrating the effect of nefazodone on I_{Na} at doses of 0.1, 0.3, 1, and 3 μM, respectively, in hiPSC-CMs. B, Dose–response relationship of nefazodone showing an IC_{50} value for I_{Na} (n=4, mean ± SEM). C, Pulse protocol (top), representative I-V traces of I_{Na} in control (middle) and in the presence of 3 μM nefazodone (bottom). D, I-V relationships of I_{Na} in the control and in the presence of nefazodone (mean ± SEM, n=4, *p<0.05, **p<0.01).

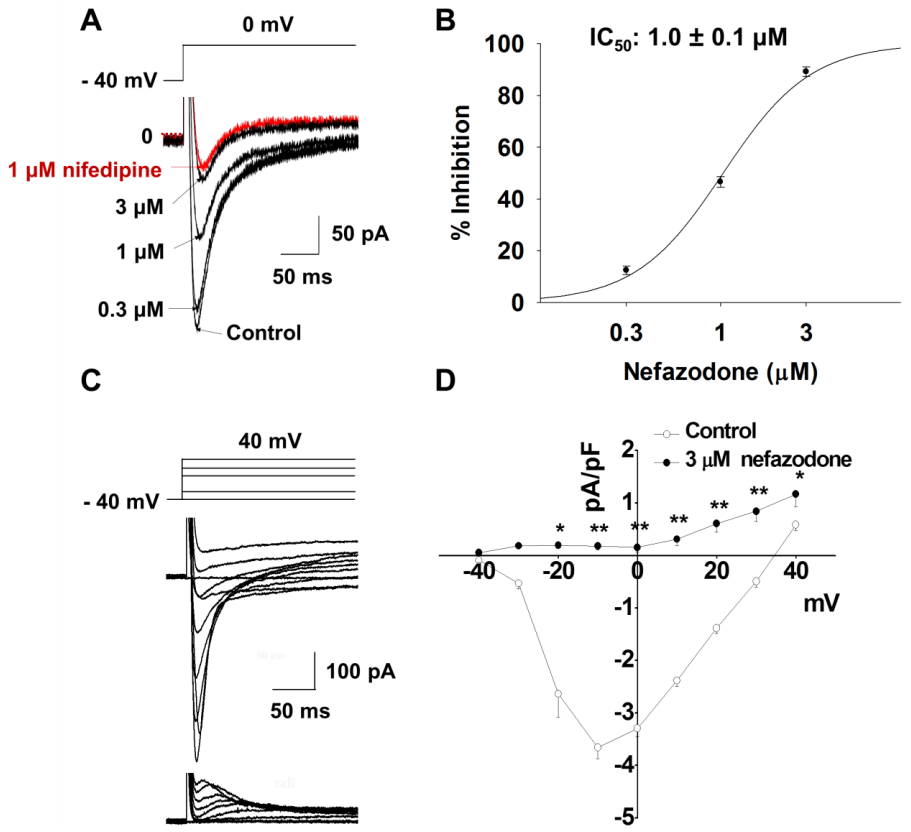

Figure 2-13. Effect of nefazodone on I_{Ca} in hiPSC-CMs

A, Representative traces showing the effect of nefazodone on I_{Ca} at doses of 0.3, 1, and 3 μM, respectively. B, Dose–response relationship of nefazodone showing an IC_{50} value for I_{Ca} (mean ± SEM, n=6). C, Representative I-V traces of I_{Ca} in control cells (top) and in the presence of nefazodone (bottom). D, I-V relationships of I_{Ca} in the control and in the presence of nefazodone (mean ± SEM, n=6, *p<0.05, **p<0.01).

Effects of nefazodone on I_{Kr}, I_{Ks},or I_{Na} expressed in HEK293 and I_{Ca} in rVMs

Even though hiPSC-CMs have been proposed to be more sensitive than other *in vitro* assays (73, 107), it is difficult to correlate these responses with other preclinical assays due to a lack of comparison to other assays in cardiac safety studies. To precisely understand the sensitivity between the various preclinical assays and evaluate the utility of the ion channel assay of hiPSC-CMs for preclinical cardiovascular risk assessment, the depolarization- and repolarization-related currents were compared between the hiPSC-CMs and HEK293 cells.

In HEK293 cells, KCNH2-encoded I_{Kr} and KCNQ1/KCNE1-encoded I_{Ks} were recorded by applying step-like pulses under the voltage-clamp conditions. Nefazodone decreased the I_{Kr} peak amplitude in a concentration-dependent manner with relatively high affinity ($IC_{50,}$ 61.8 ± 0.04 nM, Figure 2-14A and B, n=5). Nefazodone also inhibited the peak amplitude of I_{Ks}, but had a low affinity ($IC_{50,}$ 1.7 ± 0.1 μM, Figure 2-14C and D, n=4). The potency of nefazodone inhibiting I_{Kr} in the heterologous expression system was similar with the one in hiPSC-CMs.

To investigate the effect of nefazodone on the depolarization-related currents, the SCN5A-encoded inward sodium current (36) was recorded in HEK293 and the Ca^{2+}-specific inward current (I_{Ca}) was recorded in isolated rVMs. Nefazodone decreased the I_{Na} peak amplitude with an IC_{50} value of 9.1 ± 0.04 μM (Figure 2-14E and F), which was higher than the IC_{50} value obtained in hiPSC-CMs (1.5 ± 0.1 μM, Figure 2-12B). Nefazodone also inhibited the I_{Ca}

peak amplitude of hiPSC-CMs in a concentration-dependent manner with an IC_{50} value of 1.0 ± 0.1 μM (Figure 2-13A and B, n=3), whereas an IC_{50} value for I_{Ca} blockade produced a low affinity in rVMs with an IC_{50} value of 7.4 ± 0.2 μM (Figure 2-14G and H, n=3).

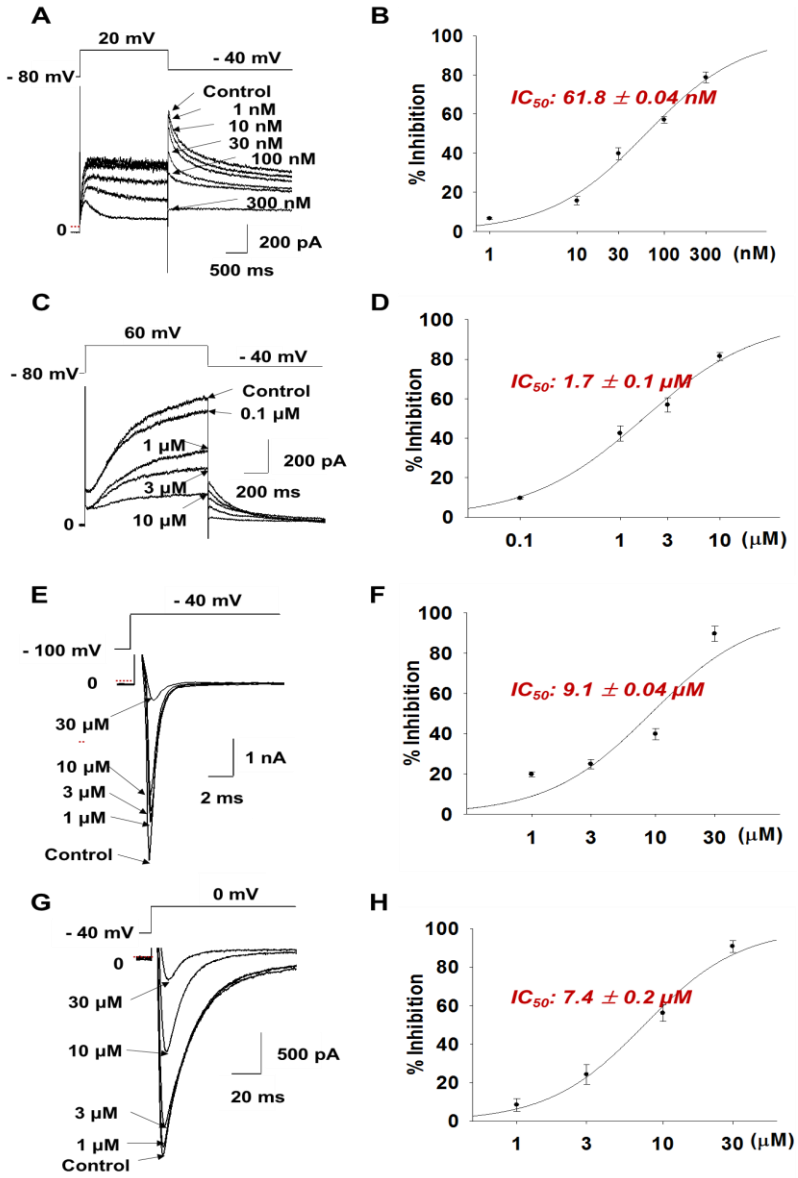

Figure 2-14. Effect of nefazodone on I_{Kr}, I_{Ks} and I_{Na} in HEK293 cells and I_{Ca} in isolated rat VMs

A, Representative traces demonstrating the effect of nefazodone on I_{Kr} at doses of 1, 10, 30, 100 and 300 nM, respectively, in HEK293 cells. B, Dose–response relationship of nefazodone, showing an IC_{50} value for I_{Kr} (mean ± SEM). C, Representative traces showing the effect of nefazodone on I_{Ks} at doses of 0.1, 1, 3 and 10 μM, respectively, in HEK293 cells. D, Dose–response relationship of nefazodone, showing an IC_{50} value for I_{Ks} (mean ± SEM). E, Representative traces presenting the effect of nefazodone on I_{Na} at doses of 1, 3, 10, and 30 μM, respectively, in HEK293 cells. F, Dose–response relationship of nefazodone showing an IC_{50} value for I_{Na} (mean ± SEM). G, Representative traces demonstrating the effect of nefazodone on I_{Ca} at doses of 1, 3, 10 and 30 μM, respectively, in isolated rat VMs. H, Dose–response relationship of nefazodone showing an IC_{50} value for I_{Ca} (mean ± SEM).

Effects of trazodone on AP waveforms in hiPSC-CMs

To assess whether the changes in cardiac AP properties were due to the effect of trazodone, we obtained current clamp recordings in hiPSC-CMs (Figure 2-15). A spontaneous beating activity was recorded and AP-related parameters were quantified as the control condition in hiPSC-CMs (n=21). The MDP, dV/dtmax, TA, APD_{90}, and APD_{60} were analyzed and only ventricular-type cells that had an AP duration longer than 300 ms were included in the analysis. The representative AP traces in control conditions and in the presence of trazodone are shown in Figure 1A. The average from five recorded APs was analyzed at each test concentration and dose-response studies indicated that APs were completely inhibited after treatment with 100 μM trazodone (n=3,

data not shown). Trazodone prolonged APD_{90} and APD_{60} at 3 μM and the EADs were also induced by 10 μM trazodone, suggesting that trazodone affects the AP waveforms of hiPSC-CMs in a concentration-dependent manner (Figure 2-15A). The AP-related parameters showed no significant effect from trazodone on the MDP and TA (n=5, Figure 2-15B); however, a dose-dependent dramatic decrease in dV/dt_{max} was caused by trazodone (n=5, 2-15B). Further, trazodone prolonged the APD and induced EADs in a concentration-dependent manner (n=5). These results demonstrated that trazodone significantly reduced action potentials upstroke velocity prolonging their 90% and 60% durations.

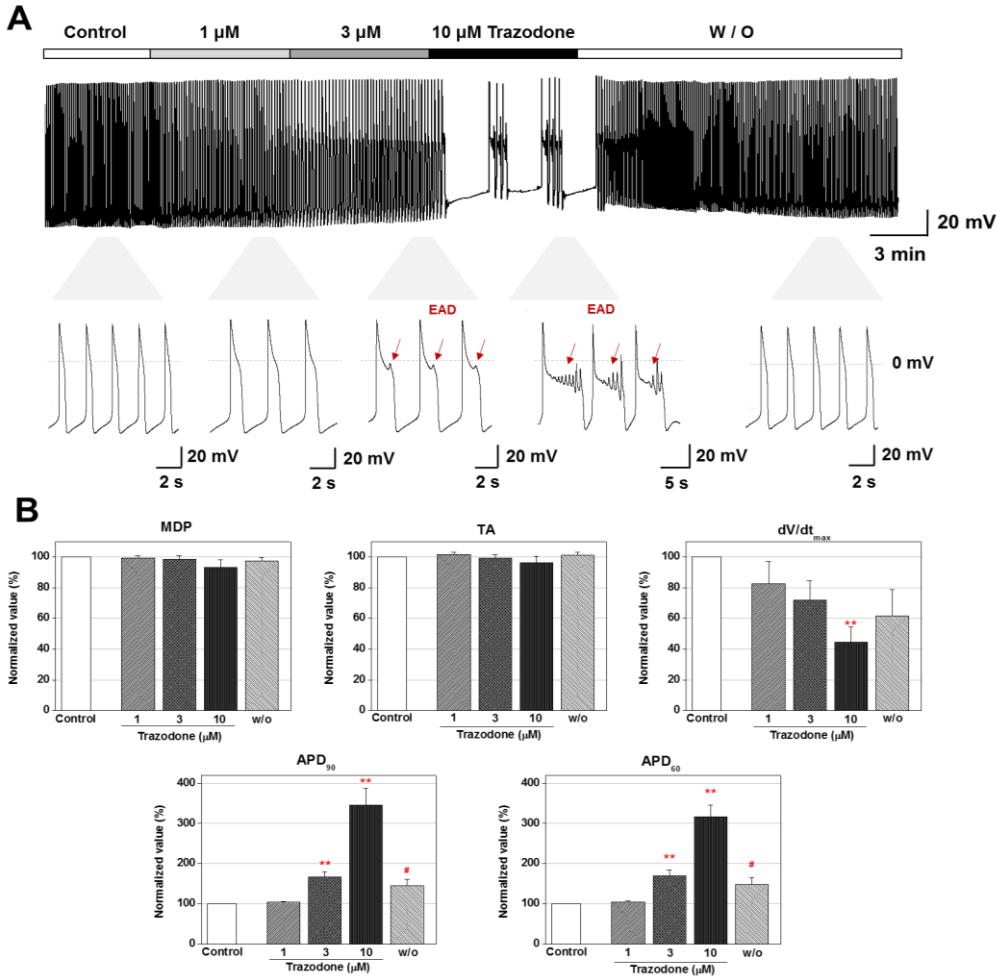

Figure 2-15. Effects of trazodone on action potential waveforms in hiPSC-CMs

A, Representative traces induced by 1 μM trazodone. Representative traces show the typical waveform of EAD induced by 3 μM and 10 μM trazodone. B-F, Normalized AP parameters in control and in the presence of trazodone. MDP: maximum diastolic potential, dV/dtmax: maximum upstroke velocity, TA: total amplitude, APD_{90}: action potential duration at 90% repolarization, APD_{60}: action potential duration at 60% repolarization (mean ± SEM, * $p < 0.05$, ** $p < 0.01$).

Effects of trazodone on cardiac repolarization-related currents: I_{Kr} and I_{Ks} in HEK293

To investigate the cellular mechanism underlying the effects of trazodone on repolarization-related currents, KCNH2-encoded fast components of the delayed rectifier potassium current (I_{Kr}) and KCNQ1/KCNE1-encoded slow components of the delayed rectifier potassium current (I_{Ks}) were recorded using voltage-clamp recordings in HEK293 cells. The fast and slow components of the potassium channel-specific outward currents (I_{Kr} and I_{Ks}, respectively) were activated by each step protocol. Trazodone inhibited the I_{Kr} peak amplitude in a concentration-dependent manner and produced a high affinity for I_{Kr} with an IC_{50} value of 2.83 ± 0.04 μM (Figure 2-16B, n = 3). 10 μM trazodone (Figure 2-16C) completely blocked the peak I_{Kr} current density, but it did not affect the activation- and inactivation-state I-V relationships (Figure 2-16D, E, n = 3). Trazodone also inhibited the peak amplitude of I_{Ks} in a concentration-dependent manner (Figure 2-17A), but had a low affinity for I_{Ks} with an IC_{50} value of 67.5 ± 0.05 μM (Figure 2-17B, n = 3). Trazodone at 300 μM completely blocked the peak I_{Ks} current density, but did not affect the I-V relationships (n = 3, data not shown). These results indicated that trazodone has a higher inhibitory potency on I_{Kr} than I_{Ks} in HEK293.

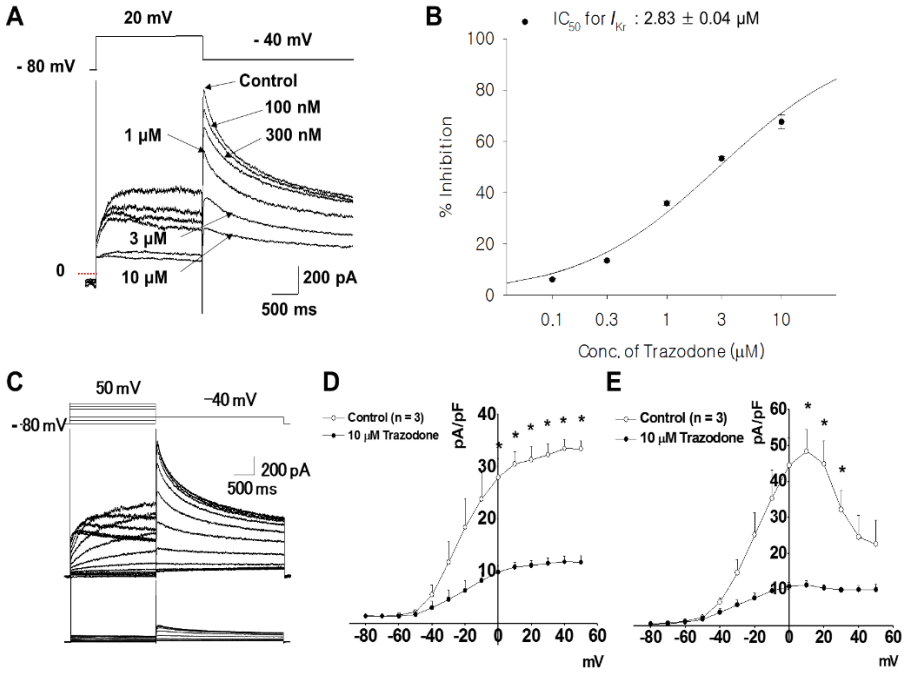

Figure 2-16. Effect of trazodone on I_{Kr} in HEK293 cells

A, Representative traces demonstrating the effect of trazodone on HEK293 I_{Kr} at doses of 0.1, 0.3, 1, 3, and 10 μM, respectively. B, Dose–response relationship of trazodone, providing an IC_{50} value of 2.83 ± 0.04 μM (mean ± SEM). C, Representative I-V traces of I_{Kr} in control cells (top) and in the presence of trazodone (bottom). D, Activation-state I-V relationships of I_{Kr} in control and in the presence of trazodone (mean ± SEM, * $p < 0.05$, ** $p < 0.01$). E, Inactivation-state I-V relationships of I_{Kr} in control and in the presence of trazodone (mean ± SEM, * $p < 0.05$, ** $p < 0.01$).

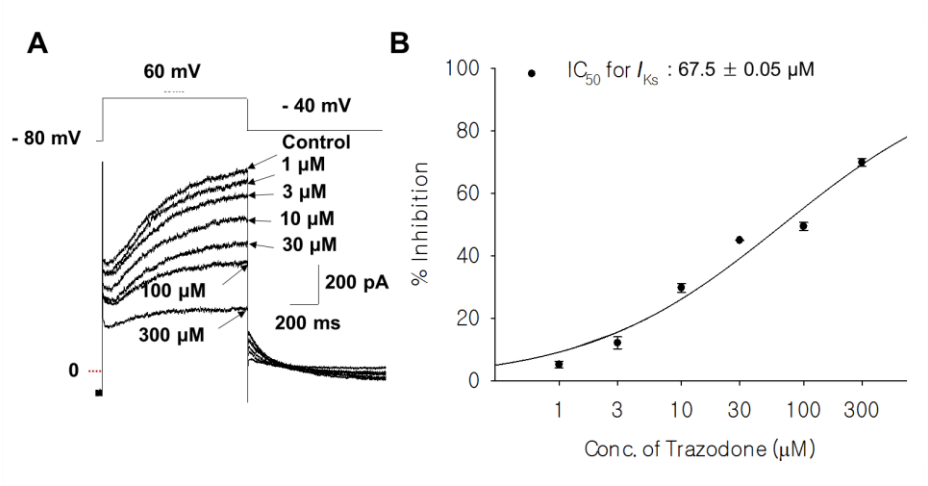

Figure 2-17. Effect of trazodone on I_{Ks} in HEK293 cells

A, Representative traces demonstrating the effect of trazodone on HEK293 I_{Ks} at doses of 1, 3, 10, 30, 100, and 300 μM, respectively. B, Dose–response relationship of trazodone, providing an IC_{50} value of 67.5 ± 0.05 μM (mean ± SEM).

Effects of trazodone on cardiac depolarization-related currents: I_{Na} in HEK293 and I_{Ca} in hiPSC-CMs

To investigate the effect of trazodone on the depolarization-related currents, the SCN5A-encoded inward sodium current (36) was recorded in HEK293 and the Ca^{2+}-specific inward current (I_{Ca}) was recorded in hiPSC-CMs. Trazodone inhibited the peak amplitude of I_{Na} in a concentration-dependent manner (Figure 2-18A), but produced a slightly high affinity for I_{Na} with an IC_{50} value of 11.07 ± 0.09 μM (Figure 2-18B, n = 4). Trazodone at 100 μM completely blocked the peak I_{Na} current density, but did not affect the I-V relationships (n = 3, data not shown). We verified the I_{Ca} of hiPSC-CMs using a selective Ca^{2+} channel antagonist, nifedipine, which inhibited the peak amplitude of I_{Ca} in a concentration-dependent manner with an IC_{50} value of 0.84 μM (n = 4, data not shown). Trazodone inhibited the I_{Ca} peak amplitude in a concentration-dependent manner (Figure 2-18C), but showed a low affinity for I_{Ca} with an IC_{50} value of 19.05 ± 0.13 μM (Figure 2-18D, n = 3). Trazodone at 300 μM completely blocked the peak I_{Ca} current density, but it did not affect the I-V relationships (n = 4, data not shown). These results indicated that trazodone is more effective in inhibiting I_{Na} in HEK293 than I_{Ca} in hiPSC-CMs.

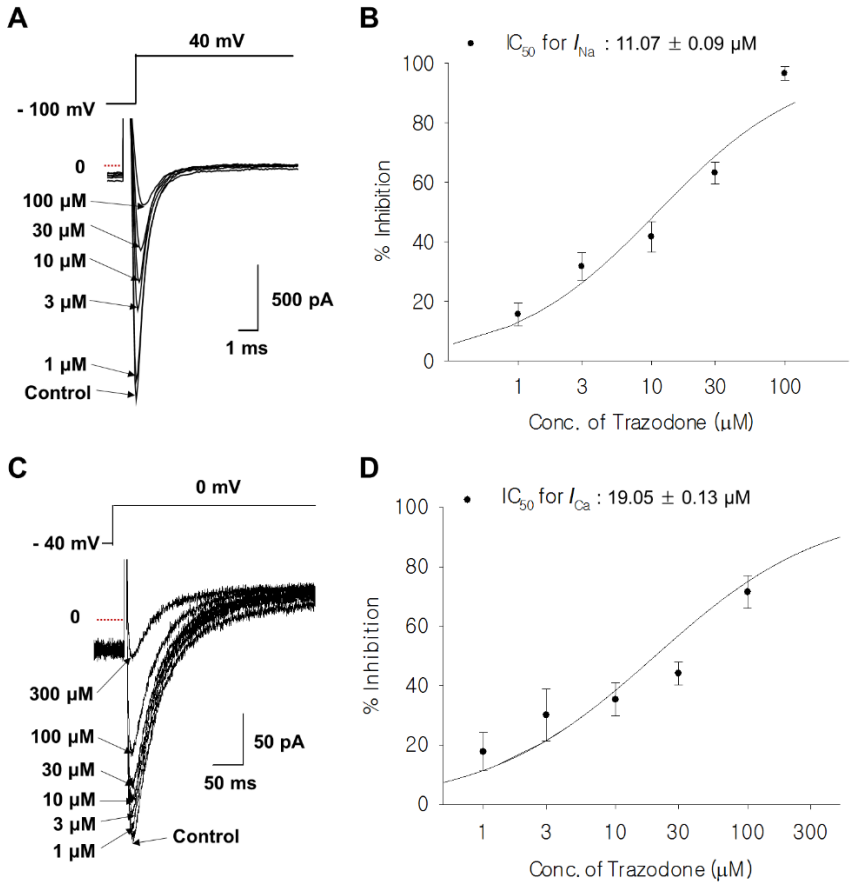

Figure 2-18. Effect of trazodone on I_{Na} in HEK293 cells and I_{Ca} in hiPSC-CMs

A, Representative traces demonstrating the effect of trazodone on HEK293 I_{Na} at doses of 1, 3, 10, 30, and 100 μM, respectively. B, Dose–response relationship of trazodone, providing an IC_{50} value of 11.07 ± 0.09 μM (mean ± SEM). C, Representative traces demonstrating the effect of trazodone on hiPSC-CMs I_{Ca} at doses of 1, 3, 10, 30, 100, and 300 μM, respectively. D, Dose–response relationship of trazodone, providing an IC_{50} value of 19.05 ± 0.13 μM (mean ± SEM).

DISCUSSION

Here, I validated the hiPSC-CMs as a test model for the putative arrhythmogenic agents such as nefazodone and trazodone. The current results show that hiPSC-CMs effectively recapitulate the electrophysiological behaviors of each channel blocker, confirming the plausibility of a platform for preclinical drug safety assessment (Figure 2-8). The comparison with heterologous expression HEK293, the existing preclinical assay system, demonstrated reasonable correlation, thereby justifying the potential use of hiPSC-CMs for electrophysiological cardiac safety screening.

Cardiotoxicity testing, including *in vitro* assays and *in vivo* animal models, is an important part of preclinical drug evaluation prior to first-in-human clinical trials. The previous safety testing paradigm is based primarily on the predictive link between drug-induced *in vitro* hERG blockade and *in vivo*/clinical QT interval prolongation and TdP; however, many drugs that have passed animal tests show unanticipated cardiotoxicity during the clinical phases (108-110).

Our previous studies demonstrated that nefazodone blocks hERG channels that might explain the cardiac toxicity of nefazodone (95). Although it is widely accepted that ventricular arrhythmias are primarily caused by I_{Kr} inhibition (97), the limitations of such a simple interpretation have also been revealed. The QT prolongation is sensitive but not highly specific for predicting which compounds can cause TdP. Additionally, the drug-induced inhibition of I_{Kr} does not show a clear correlation with QT prolongation risk

or the occurrence of arrhythmias (111). Therefore, the combined effects on the non-hERG cardiac membrane currents should be considered. For example, either sodium- or calcium-channel blocks may mitigate the effects of hERG current block. In addition, there are non–hERG-dependent mechanisms responsible for TdP. When assessing pro-arrhythmic liabilities, therefore, new test models as well as an integrative interpretation are needed to understand the effects of agents such as nefazodone, affecting multiple types of ion channels beyond hERG.

hiPSC-CMs could overcome the limitations of the hERG assay, which sometimes does not provide a meaningful indicator of pro-arrhythmic risk. Our present study supports that the hiPSC-CMs are an attractive model for cardiotoxicity testing as they express the major ion channels and recapitulate spontaneous mechanical and electrical activities, similar to adult cardiomyocytes (28, 75). The hiPSC-CM could be comparable with or a more effective system than the comprehensive *in vitro* set of ion current assays using heterologously expressed channels.

AP prolongation; a functional biomarker of hiPSC-CMs

In this study, nefazodone and trazodone modulates the AP waveforms of hiPSC-CMs by prolonging APD_{90} and APD_{50} and decreasing dV/dt_{max}, without affecting the TA or MDP (Figure 2-9 and 2-15). It is most likely that the prolongation of APD_{90} by nefazodone is mediated by hERG inhibition (95). Nefazodone inhibited I_{Kr} with an IC_{50} value of 41.4 ± 0.2 nM (Figure 5B) and blocked hERG completely at a dose of 100 nM (Figure 5D). However,

there is a quite large gap between the sensitivity of hERG current and APD prolongation; nefazodone started to prolong the APD_{90} at 100 nM, at ~90% of the hERG blockade. Although not so potent as to hERG, the depolarizing currents such I_{Ca} and I_{Na} were also inhibited by nefazodone in hiPSC-CMs (Figure 7 and 8), that might attenuated the APD prolongation effects of nefazodone. Nefazodone also inhibited I_{Ks}, but at far lower potency compared to I_{Kr} (IC_{50} of 10.1 ± 0.5 μM, Figure 6A, B).

It has to be noted that nefazodone had a high inhibitory potency on I_{Na} (IC_{50} = 1.0 ± 0.01 μM, Figure 7B) similar to that of TTX, a known blocker of cardiac I_{Na} (IC_{50} = 1.4 ± 0.1 μM, data not shown). These results indicate that nefazodone decreases the dV/dt_{max} of APs in hiPSC-CMs via I_{Na} inhibition (Figure 4D). The abolishment of AP generation with 3 μM nefazodone might be due to the inhibition of I_{Na} as well as the incomplete repolarization by the almost complete hERG inhibition.

The extent of APD prolongation could be determined from the complex interactions with Na^+, Ca^{2+}, and K^+ currents differentially changed by tested agents (7). Thus, the integrative assessment of the multiple ion channels is necessary to identify the risk of SARIs-induced cardiac electrophysiological alterations. In summary, our results demonstrate that the ventricular APs and appearance of EADs of hiPSC-CMs might provide efficient prediction of the arrhythmogenic liability by integrating the ranges of drug actions for blockages of major cardiac ion channels.

In this study, I hypothesized that SARIs modulate the cardiac electrophysiological characteristics and functions through inhibition of

cardiac ion channels. Therefore, I investigated their potential effects on major cardiac ion channels, I_{Na}, I_{Ca}, I_{Kr}, I_{Ks}, and I_{K1} and cardiac action potentials in HEK293 cells or hiPSC-CMs. We evaluated the IC_{50} values of nefazodone and trazodone on cardiac depolarization- or repolarization-related currents (Table 2). These results indicated that nefazodone and trazodone commonly inhibited all of the major cardiac ion channels in a concentration-dependent manner, and had low affinity for I_{Na} and I_{K1} and high affinity for I_{Ca}, I_{Kr}, and I_{Ks}. Nefazodone, however, was a more potent inhibitor of cardiac ion channels than trazodone. In particular, the inhibition of I_{Kr}, I_{Ks} and I_{Ca} was much more potent with nefazodone than trazodone. We emphasize that these experiments were designed not only to measure cardiotoxicity assessment in hiPSC-CMs but also to investigate specific electrophysiologic mechanisms of nefazodone and trazodone actions. Our results demonstrate that hiPSC-CMs can serve as a useful tool in early drug screening and may shed light on the drug safety assessment beyond the current gold standard assay for hERG channels.

Limitations

Including this study, many previous studies have demonstrated the functional expressions of native cardiac ion channels in hiPSC-CMs; I_{Na} (36, 74), I_{Ca} (74, 112, 113), I_{Kr} (74, 105, 114) and I_{Ks} (74). However, a difficulty in the use of hiPSC-CMs as a model system is their immature fetal-like electrophysiological phenotype; less hyperpolarized MDP and slower dV/dt_{max} compared to native adult CMs (115, 116). Since the phenotypes of hiPSC-CMs could vary depending on their maturity; studies addressing the

electrophysiological and pharmacological characteristics of hiPSC-CMs are necessary and the electrophysiological data derived from hiPSC-CMs should be cautiously interpreted. There is potential utility of cardiac stem cells to replace other pro-arrhythmia testing approaches once fully mature stem cells expressing all the currents in the similar densities as human myocytes are developed. Because hiPSC-CMs appeared to be very sensitive to membrane damage during the patch clamp procedure, some of cells lost their beating ability or displayed irregular beating pattern.

Although the SARI concentrations for measuring cardiac APs and ion currents were in the range of therapeutic plasma levels, it is difficult to correlate *in vivo* plasma concentrations and *in vitro* concentrations. Clinical studies reported non-linear pharmacokinetics of SARIs and their plasma concentrations increased proportionally after administration of a single dose or steady-state conditions (117-120). In addition, the delayed onset of action of antidepressants induces cardiac side effects, which remain critical factors (121). Measuring the IC_{50} values for major cardiac ionic channels is important to gain insight into the mechanism of action of SARIs at therapeutic plasma concentrations in humans or other mammalian systems; however, predicting arrhythmogenic concentrations in a clinical setting is slightly difficult.

In Table 2-2, the ion current density of the hESC-CMs were compared to adult hVMs as presented in the literature because the normal hVMs are difficult to obtain and also have limited time in culture.

CHAPTER 3

Differentiation period-dependent changes in the electrophysiological properties of human embryonic stem cell-derived cardiomyocytes

INTRODUCTION

Cardiomyocytes (CMs) derived from hPSCs are considered a promising source for cell-based therapies or screening testbed. Recent several studies showed that hPSC-CMs more closely resembled fetal CMs instead adult CMs (28) and they have increased automacity compared with human ventricular CMs due to lack of inward rectifier K^+ channel (I_{K1}) (29). The shape of APs results from the ordered integration of several functional ionic currents inducing membrane depolarization and repolarization. During cardiac development, ion channels including *hERG* and I_{Ks} undergo fetal and postnatal developmental changes, a complex process leading to the acquisition and maintenance of a mature cardiac electrophysiological phenotype over time (27, 122, 123). In hESC-CMs, the I_{Na} contributed to membrane excitability was present at early stages (20 – 35 days) of differentiation, whereas the I_{K1} related to membrane diastolic potential in mature CMs, was absent (29).

For the reliable safety testing, the in vitro-differentiated cardiomyocytes should sufficiently recapitulate the characteristics of human adult CMs in terms of electophysiological endpoints. Before hiPSC-CMs are adopted for pharmacological screening, they need to be carefully validated for usefulness. They have to be confirmed to display similar electrophysiological properties based on ionic currents and cardiac APs. In addition, their pharmacological sensitivity need to be identified using well-known compounds including specific ion channel blockers and cardiotoxic agents.

The assessment of hESC-CM functionality at early developmental stages is essential for determining the appropriate differentiation stage for cardiotoxicity screening. In this study, to determine more suitable stage of differentiation required for the reliable pharmacological and toxicological testing, I characterized 2 week and 4 week differentiated hESC-CMs and compared their electrophysiological phenotypes and functional maturation using patch-clamp technique. To evaluate their functional response to anti-arrhythmic drugs, I also investigated the effects of quinidine (class IA, Na^+ channel blocker), amiodarone (class III, K^+ channel blocker), and nifedipine (class IV, Ca^{2+} channel blocker) on 2W and 4W hESC-CMs.

MATERIALS AND METHODS

1. Cell preparation

The hESC (SNUhES3 cell line)-derived CMs were obtained from Seoul National University Bundang Hospital. The cells were differentiated for 2 weeks or 4 weeks in culture dishes, after then frozen and stored in LN_2. After delivered, the frozen vials of hESC-CMs were thawed in a 37℃ water bath and mixed with in RPMI medium (Gibco) supplemented with B27 supplement (Gibco). For patch clamp recordings, the cells were plated on four-well culture plates containing 0.1% gelatin-coated glass coverslips and then maintained in a 37℃ culture incubator in an atmosphere of 95% air and 5% CO_2. The media were changed every 2~3 days.

2. Antiarrhythmic drugs

The quinidine (class IA, Na^+ channel blocker), amiodarone (class III, K^+ channel blocker), and nifedipine (class IV, Ca^{2+} channel blocker) were used to evaluate the functional response of 2W and 4W hESC-CMs. These drugs were purchased from Sigma-Aldrich (St. Louis, MO, USA). Drugs were formulated into stock solution with dimethyl sulfoxide (DMSO). The stock solutions were further diluted in the bath solution to yield final perfusion solutions with 0.1% DMSO and appropriate drug concentrations.

3. Recordings of spontaneous AP and ionic currents in hESC-CMs

The hESC-CMs were cultured for up to 4 weeks and used for patch clamp

recordings. Whole-cell hESC-CMs recordings were performed at 37℃ using an external solution containing (mM) 145 NaCl, 5.4 KCl, 10 HEPES, 1 $MgCl_2$, 5 glucose, 1.8 $CaCl_2$ (pH 7.4). The internal solution contained (mM) 120 K-Asp, 20 KCl, 5 NaCl, 2 $CaCl_2$, 10 HEPES, 5 EGTA, and 5 Mg-ATP (pH 7.25). We recorded typical APs in hESC-CMs in the current-clamp mode. The spontaneous beating activity of single hESC-CMs was recorded, and only hESC-CMs that could beat stably were included in the analysis. Following stabilization of the AP waveforms, the average of five recorded APs for each test concentration was analyzed. In the voltage-clamp mode, a standardized step protocol was used to elicit the current density of I_{Kr}, I_{Ks}, I_{Na}, I_{Ca}. $I_{K1,}$ I_f. The extracellular solution for recording the I_{Na} contained (mM) 110 CsCl, 50 NaCl, 10 HEPES, 1 $MgCl_2$, 5 glucose, and 1.8 $CaCl_2$ (pH 7.4). The extracellular solution for recording the I_{Ca} contained (mM) 137 Choline-Cl, 5 CsCl, 10 HEPES, 0.5 $MgCl_2$, 10 glucose, and 1.8 $CaCl_2$ (pH 7.4). The internal solution for I_{Na} and I_{Ca} contained (mM) 120 Cs-Asp, 20 CsCl, 5 NaCl, 10 TEA-Cl, 10 EGTA, and 10 HEPES, and 5 Mg-ATP (pH 7.25). A standardized step protocol was used to elicit the major cardiac ion currents I_{Kr}, I_{Ks}, I_{Na}, and I_{Ca}. The cells were held at −80 mV and depolarized to +20 mV for 2 s, followed by repolarization to −40 mV for 2 s to activate hERG tail currents. The I_{Kr} was isolated by eliminating the calcium currents using 1 μM nifedipine in the external solution. To elicit I_{Ks}, a -80 mV holding potential was used, followed by a 2 s depolarization to +60 mV and a 1 s repolarization to -20 mV. The I_{Ks} was isolated by 100 nM E-4031 and 1 μM nifedipine in the external solution, eliminating the hERG and calcium currents. The cells were

held at -100 mV and depolarized to -40 mV for 50 ms to elicit I_{Na}. The I_{Na} was isolated by eliminating the calcium currents using 1 μM nifedipine in the external solution. To elicit I_{Ca} in hESC-CMs, the cells were held at -40 mV and depolarized to 0 mV for 300 ms. The I_{Ca} was isolated by eliminating the potassium currents using 2 mM 4-AP in the external solution.

RESULTS

AP recordings of 2W hESC-CMs and 4W hESC-CMs

SNUhES3 cells were differentiated into cardiomyocytes, and their electrophysiological properties were analyzed and compared between two- and four-weeks of periods. In the AP recordings, the 2W hESC-CMs displayed only two types of APs with the majority of cells revealed A-type APs (A-type 87.5%, N-type 12.5%). However, in the 4W hESC-CMs, the percentage of cells with V-type APs was 46.7% (V-type 46.7%, A-type 33.3%, N-type 20%) (Figure 3-1 and Table 3-1). The distinction of V-type cells was made on the relatively long APD (APD_{90} > 300 ms) with more negative MDP and a rapid upstroke velocity of AP firing with distinguished plateau phase. The absence of a prominent plateau phase was a characteristic of A-type APs, resulting in shorter APD compared to V-type APs. N-type APs showed less negative MDP, short APD (APD_{90} < 100 ms) slower AP upstroke and a prominent phase 4 depolarization. When compared AP parameters, the 4W hESC-CMs have faster upstroke velocities, increased AP amplitudes, prolonged AP duration, and greater hyperpolarized MPD than 2W hESC-CMs (Table 3-1).

The densities of functional ion channels currents were different; all of tested voltage-gated I_{Na} (Figure 3-2), I_{Ca} (Figure 3-3), I_{Kr} (Figure 3-4), I_{Ks} (Figure 3-5), and I_{K1} (Figure 3-6) tended to increase in the 4W hESC-CMs while not significantly. Otherwise, the I_f tended to decrease in the 4W hESC-CMs but not significantly (Figure 3-7).

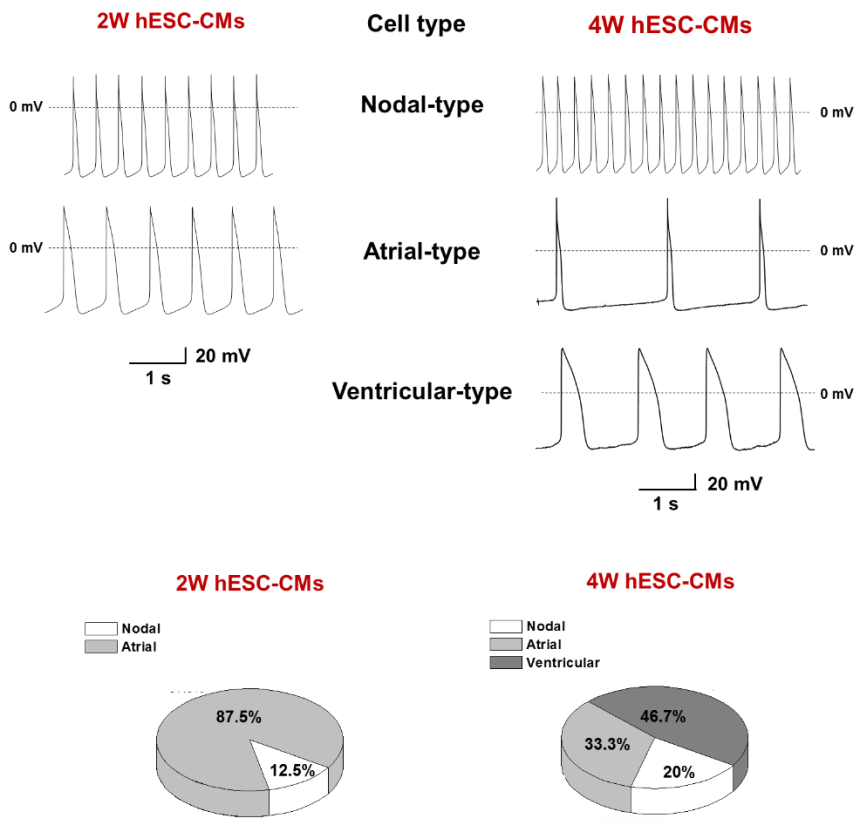

Figure 3-1. AP morphologies recorded in 2W and 4W hESC-CMs

A, Representative traces display only two types, nodal- and atrial-type of APs recorded in 2W hESC-CMs. B, Three types of APs recorded in 4W hESC-CMs. B, Comparison of the relative abundance of different APs subtypes in 2W and 4W hESC-CMs.

Table 3-1. Action potential parameters of 2W and 4W hESC-CMs

period	Cell type	APD_{90} (ms)	dV/dt_{max} (V/s)	APA (mV)	MDP (mV)	n
2W	N	75.0 ± 0.8	25.8 ± 2.5	72.9 ± 3.3	-58.1 ± 0.9	2
	A	136.4 ± 6.7	48.2 ± 3.7	103.8 ± 2.7	-71.5 ± 1.0	14
4W	N	72.9 ± 8.4	23.4 ± 1.8	83.2 ± 3.7	-62.6 ± 1.9	3
	A	133.0 ± 11.0	38.8 ± 3.0	106.7 ± 2.1	-70.3 ± 3.3	5
	V	406.0 ± 38.8	52.0 ± 7.8	113.0 ± 4.7	-72.5 ± 2.8	7

N, nodal-type; A, atrial-type; V, ventricular-type; APD_{90}, action potential duration at 90% repolarization; dV/dt_{max}, maximum upstroke velocity; APA, action potential amplitude; MDP, maximum diastolic potential; n, number of cells

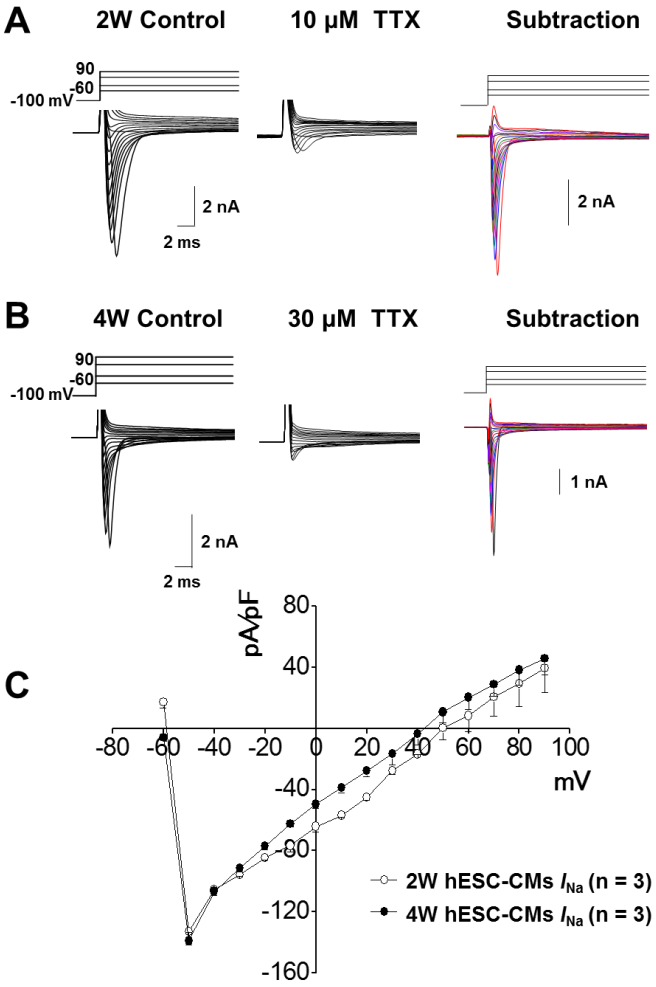

Figure 3-2. TTX-sensitive I_{Na} currents in 2W and 4W hESC-CMs

(A) Representative trace of the control (left), the presence of TTX (middle), and the TTX-sensitive current of I_{Na} (right) in 2W hESC-CMs. (B) Representative trace of the control (left), the presence of TTX (middle), and the TTX-sensitive current of I_{Na} (right) in 4W hESC-CMs. (C) I-V relationship of I_{Na} in 2W (open circle) and 4W (closed circle) hESC-CMs (means ± SEM) (each n = 3).

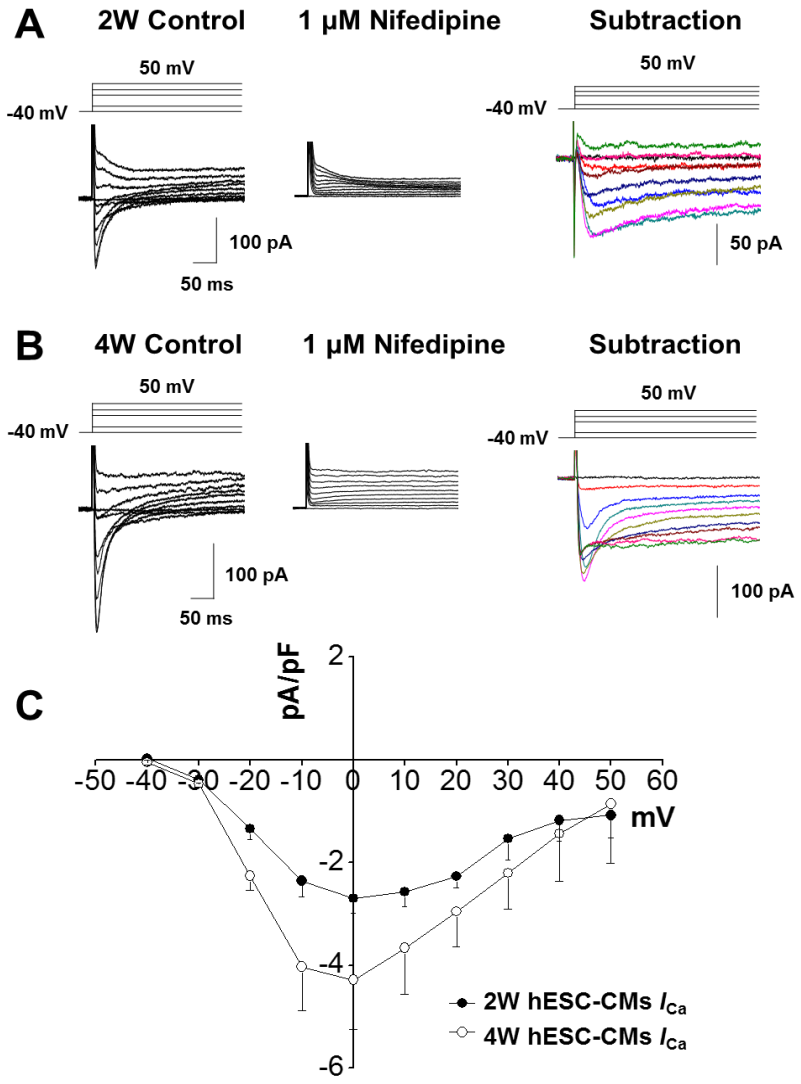

Figure 3-3. Nifedipine-sensitive I_{Ca} currents in 2W and 4W hESC-CMs

(A) Representative trace of the control (left), the presence of nifedipine (middle), and the nifedipine-sensitive current of I_{Ca} (right) in 2W hESC-CMs. (B) Representative trace of the control (left), the presence of nifedipine (middle), and the nifedipine-sensitive current of I_{Ca} (right) in 4W hESC-CMs. (C) I-V relationship of I_{Cs} in 2W (open circle) and 4W (closed circle) hESC-CMs (means ± SEM) (n = 4 for 2W, n = 3 for 4W).

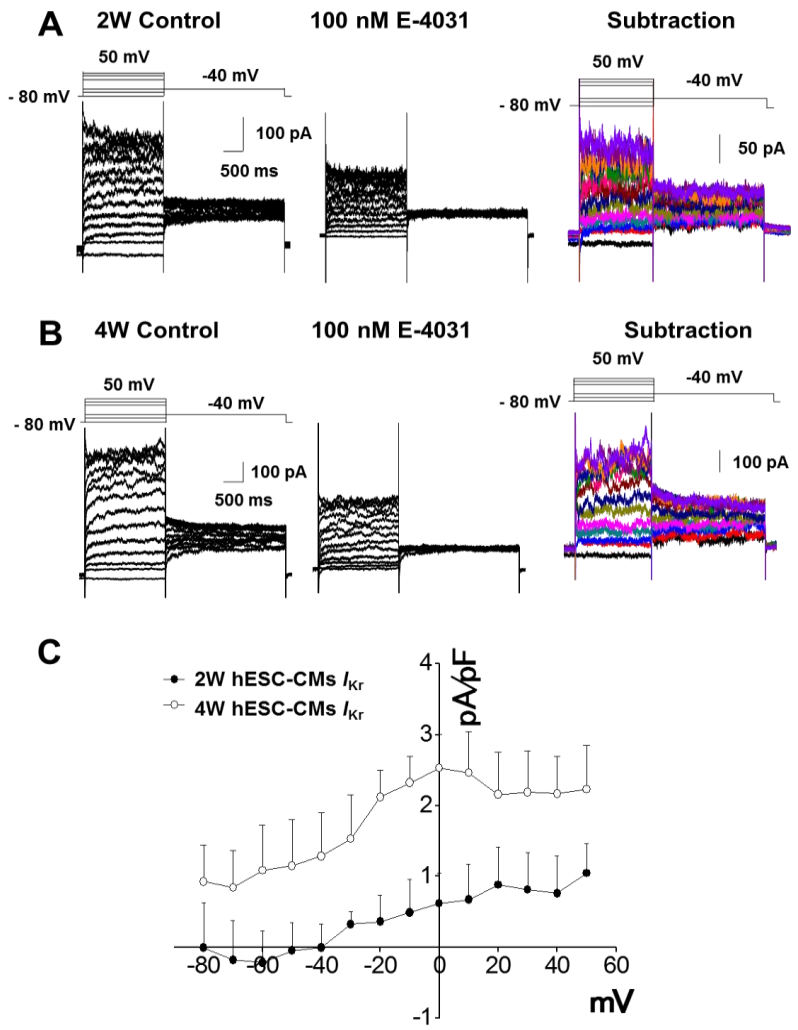

Figure 3-4. E-4031-sensitive hERG (I_{Kr}) currents in 2W and 4W hESC-CMs

(A) Representative trace of the control (left), the presence of E-4031 (middle), and the E-4031-sensitive current of I_{Kr} (right) in 2W hESC-CMs. (B) Representative trace of the control (left), the presence of E-4031 (middle), and the E-4031-sensitive current of I_{Kr} (right) in 4W hESC-CMs. (C) I-V relationship of I_{Kr} in 2W (open circle) and 4W (closed circle) hESC-CMs (each n = 3).

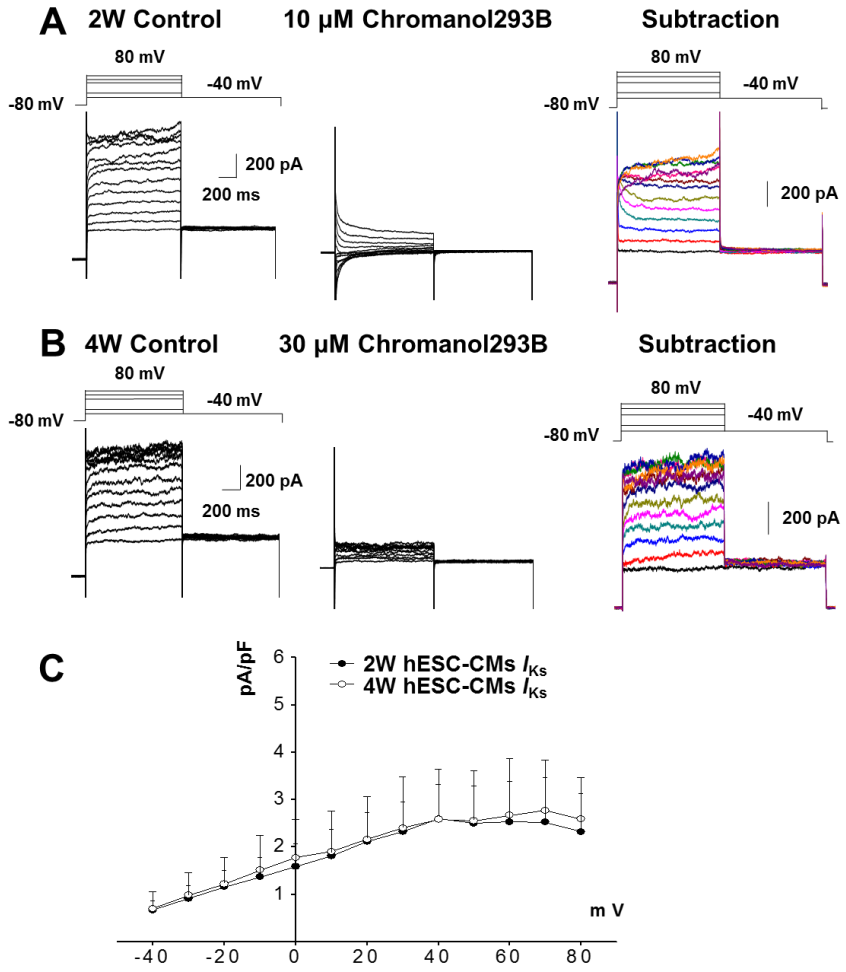

Figure 3-5. Chromanol293B-sensitive I_{Ks} currents in 2W and 4W hESC-CMs

(A) Representative trace of the control (left), the presence of Chromanol293B (middle), and the Chromanol293B-sensitive current of I_{Ks} (right) in 2W hESC-CMs. (B) Representative trace of the control (left), the presence of Chromanol293B (middle), and the Chromanol293B-sensitive current of I_{Ks} (right) in 4W hESC-CMs. (C) I-V relationship of I_{Ks} in 2W (open circle) and 4W (closed circle) hESC-CMs (each n = 3).

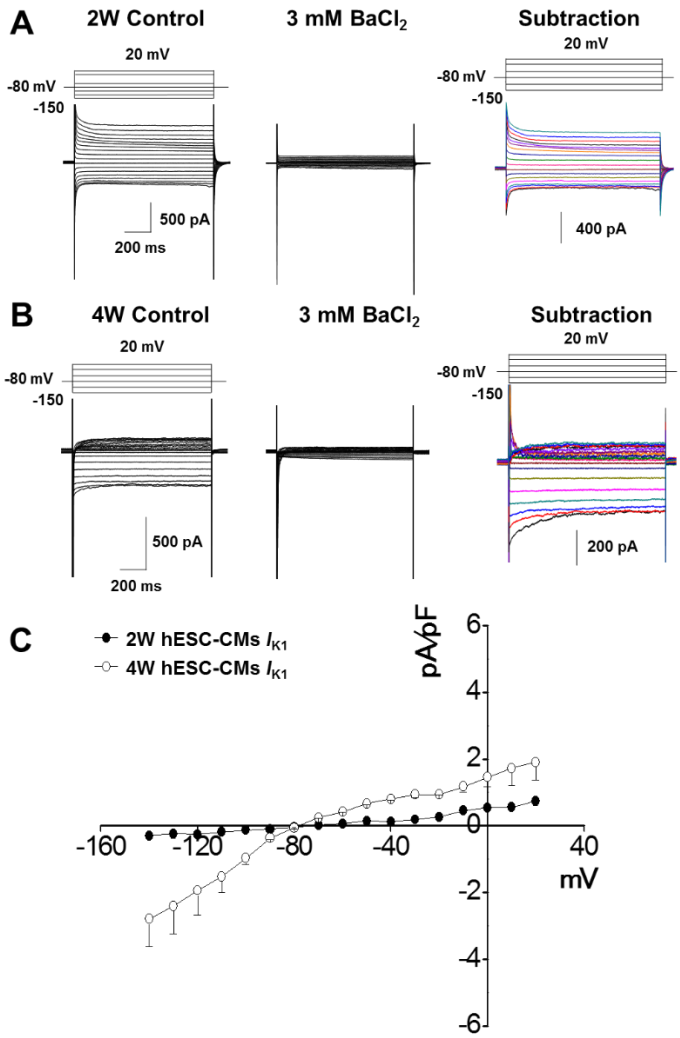

Figure 3-6. $BaCl_2$-sensitive I_{K1} currents in 2W and 4W hESC-CMs

(A) Representative trace of the control (left), the presence of $BaCl_2$ (middle), and the $BaCl_2$-sensitive current of I_{K1} (right) in 2W hESC-CMs. (B) Representative trace of the control (left), the presence of $BaCl_2$ (middle), and the $BaCl_2$-sensitive current of I_{K1} (right) in 4W hESC-CMs. (C) I-V relationship of I_{K1} in 2W (open circle) and 4W (closed circle) hESC-CMs (each n = 3).

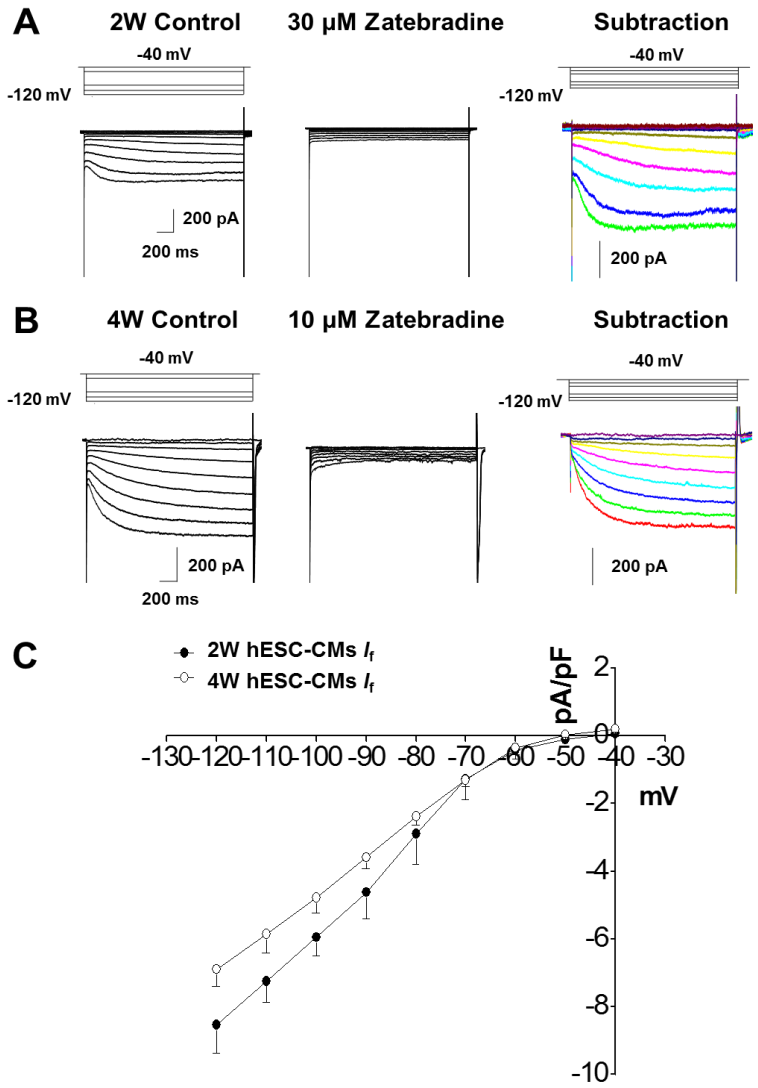

Figure 3-7. Zatebradine-sensitive I_f currents in 2W and 4W hESC-CMs

(A) Representative trace of the control (left), the presence of zatebradine (middle), and the zatebradine-sensitive current of I_f (right) in 2W hESC-CMs. (B) Representative trace of the control (left), the presence of zatebradine (middle), and the zatebradine-sensitive current of I_f (right) in 4W hESC-CMs. (C) I-V relationship of I_{K1} in 2W (open circle) and 4W (closed circle) hESC-CMs (n = 4 for 2W, n = 3 for 4W).

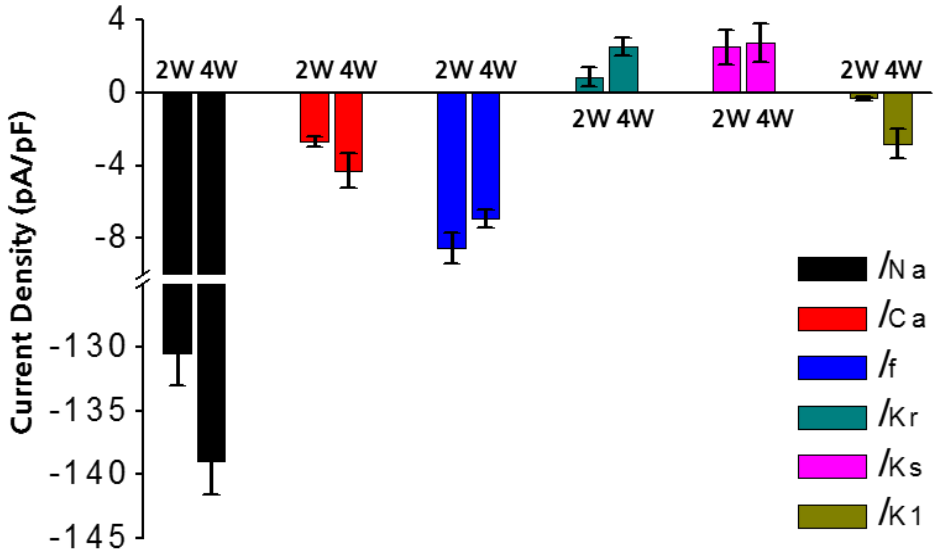

Figure 3-8. Summary of ionic currents density of 2W and 4W hESC-CMs

Cardiac major ion currents density in 2W and 4W hESC-CMs.

2. Pharmacological responses for anti-arrhythmic drugs

The majority of cells in 2W hESC-CMs were displayed atrial-type AP shape. Among them, I selected the cells with APD_{90} longer than 150 ms and with relatively more negative MDP and a rapid upstroke velocity of AP firing for drug test. In 4W hESC-CMs, only the ventricular type of cells with APD_{90} longer than 300 ms were included in the analysis. Quinidine and amiodarone (Na^+ and K^+ channel blockers, respectively) prolonged APD_{90} in the 4W hESC-CMs while not in the 2W hESC-CMs (Figure 3-9 and 3-10). In addition, nifedipine significantly shortened APD_{90} only in the 4W hESC-CMs (Figure 3-11).

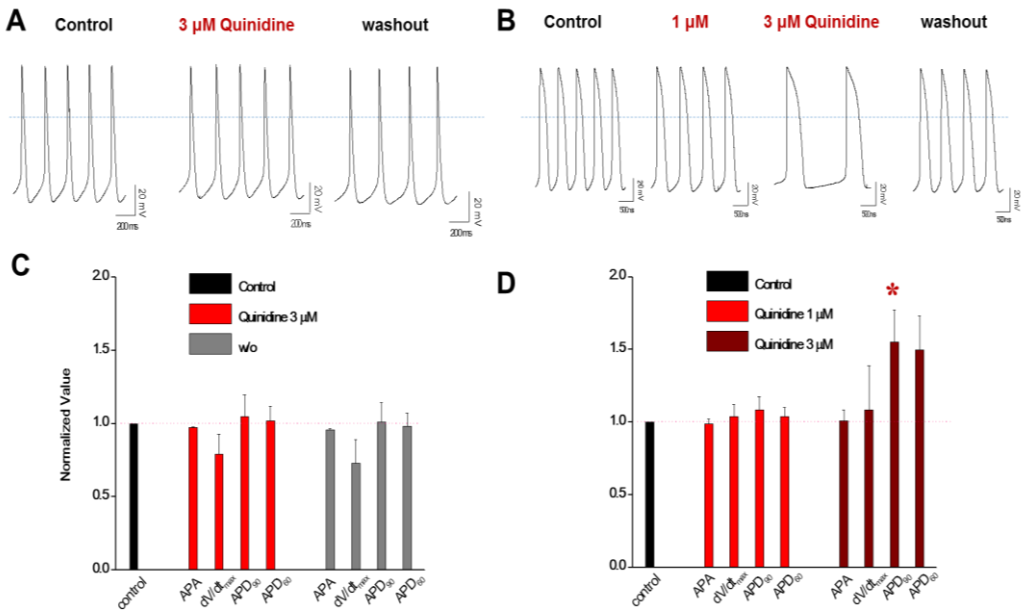

Figure 3-9. Effect of class IA antiarrhythmic drug quinidine on APs in 2W and 4W hESC-CMs

(A) Representative AP traces in the control (left) and in the presence of 3 μM quinidine (middle) and after washout (right) in 2W hESC-CMs. (B) Representative AP traces in the control (left) and in the presence of 1 and 3 μM quinidine (middle) and after washout (right) in 4W hESC-CMs. Dotted lines indicated 0 mV. (C) and (D), Normalized AP parameters in control and in the presence of quinidine in 2W hESC-CMs (C) and 4W hESC-CMs (D) (mean ± SEM, * p<0.05).

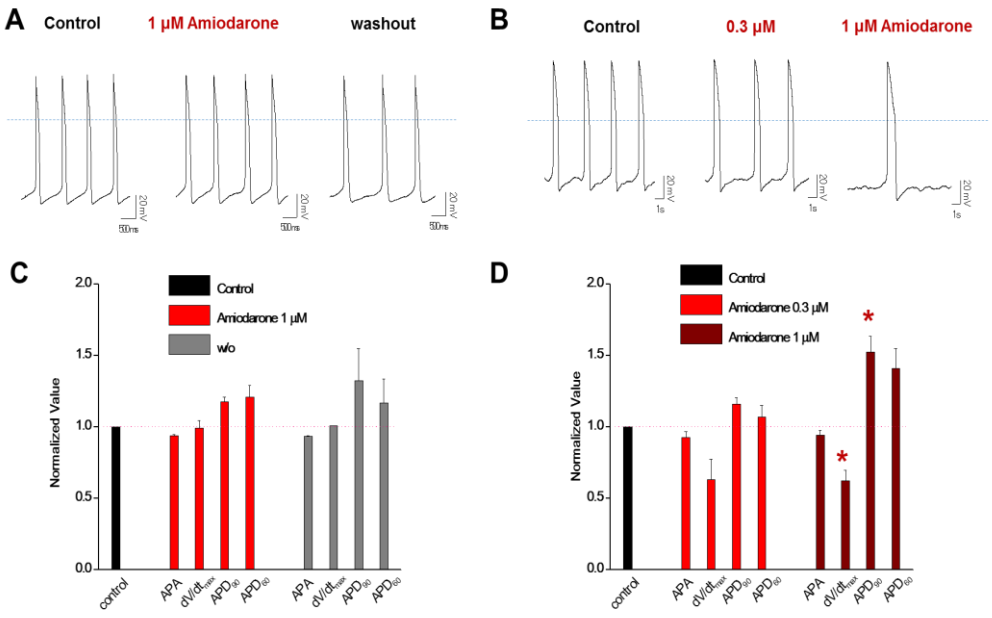

Figure 3-10. Effect of class III antiarrhythmic drug amiodarone on APs in 2W and 4W hESC-CMs

(A) Representative AP traces in the control (left) and in the presence of 1 μM amiodarone (middle) and after washout (right) in 2W hESC-CMs. (B) Representative AP traces in the control (left) and in the presence of 0.3 and 1 μM quinidine (middle) and after washout (right) in 4W hESC-CMs. Dotted lines indicated 0 mV. (C) and (D), Normalized AP parameters in control and in the presence of amiodarone in 2W hESC-CMs (C) and 4W hESC-CMs (D) (mean ± SEM, * p<0.05).

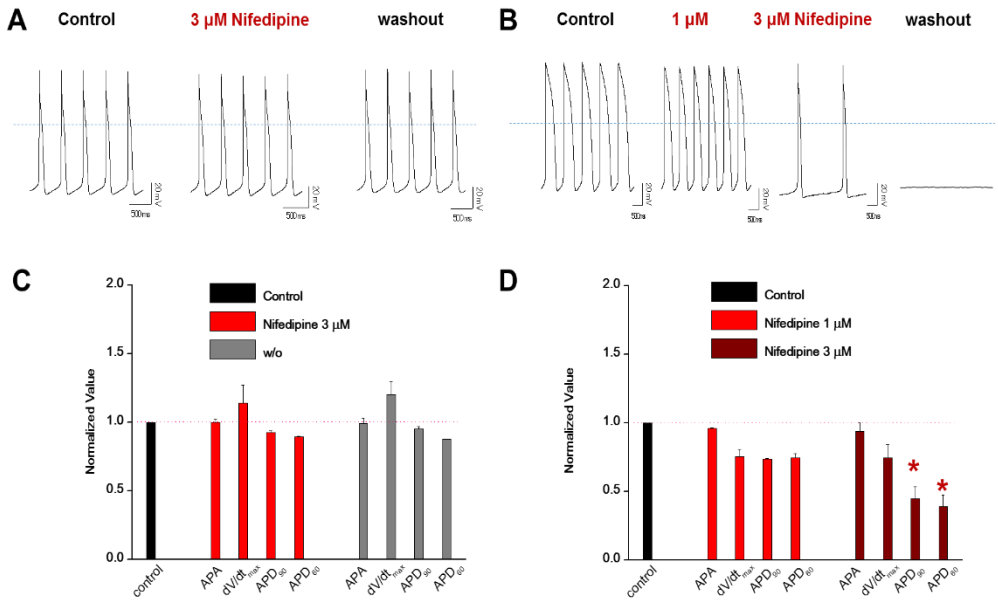

Figure 3-11. Effect of class IV antiarrhythmic drug nifedipine on APs in 2W and 4W hESC-CMs

(A) Representative AP traces in the control (left) and in the presence of 3 μM nifedipine (middle) and after washout (right) in 2W hESC-CMs. (B) Representative AP traces in the control (left) and in the presence of 1 and 3 μM nifedipine (middle) and after washout (right) in 4W hESC-CMs. Dotted lines indicated 0 mV. (C) and (D), Normalized AP parameters in control and in the presence of nifedipine in 2W hESC-CMs (C) and 4W hESC-CMs (D) (mean ± SEM, * p<0.05).

DISCUSSION

hESC-CMs can be used to predict arrhythmia risks of candidate drugs; however, the specific stage for these immature cells to develop a mature cardiac characteristics remains uncertain. Therefore, the assessment of hESC-CM functionality at early developmental stages is essential for determining the appropriate differentiation stage for cardiotoxicity screening. In this study, I characterized 2 weeks (2W) and 4 weeks (4W) differentiated hESC-CMs and compared their electrophysiological phenotypes and functional maturation using whole-cell patch-clamp recordings.

To identify whether early-stage hESC-CMs exhibit phenotypic maturation, I compared the current density of the major cardiac ion channels in both 2W and 4W hESC-CMs. The functional current densities tested in this study, the depolarization-related I_{Na} and I_{Ca}, and the repolarization-related I_{Kr}, I_{Ks}, and I_{K1}, tended to increase slightly in 4W hESC-CMs than in 2W hESC-CMs. Otherwise, the I_f tended to decrease in the 4W hESC-CMs but not significantly.

To characterize the AP subtypes in hESC-CMs and to evaluate their functional response to anti-arrhythmic drugs, we recorded AP properties in both 2W and 4W hESC-CMs. We found that the 4W hESC-CMs have faster upstroke velocities, increased APA, prolonged APD, and greater hyperpolarized MDP than 2W hESC-CMs. These findings suggest that hESC-CMs differentiate into V-type CMs depending on the developmental period in the culture system. The electrophysiological analyses revealed that quinidine

and amiodarone, sodium and potassium channel blockers, prolonged APD_{90} in the 4W hESC-CMs but not in the 2W hESC-CMs. Nifedipine, a calcium channel blocker, shortened APD_{90} only in the 4W hESC-CMs. These results demonstrated that only 4W hESC-CMs have electrophysiological responses to anti-arrhythmic drugs.

Overall, compared to the 2W hESC-CMs, the 4W differentiated hESC-CMs exhibited an increased functional maturation over time. Although the AP shapes demonstrate characteristic cardiac phenotypes from the 2 weeks of differentiation in the hESC-CMs, at least 4 weeks of differentiation is required for the reliable pharmacological and toxicological testing. Moreover, this study aims to highlight the potential use of 4W early-stage hESC-CMs for cardiotoxicity screening, and the need for a long-term differentiation approach to develop hESC-CMs that mimic the functional properties of adult CMs. These results might contribute to development of improved models that possess adult phenotypes for the assessment of drug safety.

Limitations

Although functional maturation of stem cell-derived cardiomyocytes proceeds during long-term culture over several months (27, 124), in this study, I characterized 2 groups of “early-stage” cells (2 week and 4 week differentiated hESC-CMs) to determine more suitable stage of differentiation required for the reliable pharmacological and toxicological testing. In common with previous studies, the differentiating hESC-CMs are highly heterogeneous and show a variety of AP phenotypes.

GENERAL DISCUSSION

The heart is one of the most important organs which acts as pump suppling blood and oxygen to all parts of the body. Cardiac function depends on the appropriate timing of excitation-contraction coupling induced by cardiac APs in various regions. The APs are the membrane potential waveform that is generated by the movement of ions through the transmembrane ion channels. The APs induce the propagation of excitation information from cell to cell and allows the heart to function as an electrical and mechanical syncytium. Therefore, some dysfunctions of ionic currents associated with disorganization of electrical activity leading to abnormal APs can cause lethal heart problem with abnormal heart rhythms called arrhythmias.

New drug and candidates may cause perturbations in cardiac electrical signals by modulation of cardiac ion channels which can be fatal (e.g. drug-induced long QT syndrome). To evaluate and predict of these effects is critical in selecting or discarding new drug candidates. Toxicity induced by ion channel perturbations in cardiac tissue is one of the most common causes of late-stage failure in drug development. Although rare than the drug–induced long QT syndrome, the QT-shortening could potentially increase the ventricular tachycardia and the ventricular fibrillation risk of sudden death (45, 46, 48, 50, 51). Hence many pharmaceutical companies try to quantify drug-induced cardiac electrophysiological alterations related to QT interval or APD using *in vitro* ion channel screening in early stage of drug development.

K^+ channel has been known as a major reason of cardiac arrhythmia and sudden death. In contrast to the inhibition of K^+ channels, decreased I_{Ca} is

expected to shorten APD and/or modify the shape of plateau in the cardiac AP. Therefore, the drugs which blocked Ca^{2+} channel including nicardipine, amlodipine, and isradipine can theoretically cause APD shortening. However, many CCBs are widely used without severe side effects. Such results might be due to the low plasma concentrations of CCBs in the patients prescribed with CCBs. Contrary to theoretical guess that the CCBs tested in this study will cause the AP shortening, indeed, NIC and ISR did not affect APD_{90}.

In the chapter 1 of these studies, I demonstrated another possibility that is a putative compensatory inhibition of K^+ channels such as hERG, which might counterbalance the APD shortening effect of CCBs. This study showed the limitation of simple interpretation based on the representative effects of known ion channel modulators. The drug-induced cardiotoxicity has to be estimated with overall effects on multi ion channels.

In the chapter 2, I validated the hiPSC-CMs as a test model for the putative arrhythmogenic agents such as nefazodone and trazodone. The current results show that hiPSC-CMs effectively recapitulate the electrophysiological behaviors of each channel blocker, confirming the plausibility of a platform for preclinical drug safety assessment. The comparison with heterologous expression HEK293, the existing preclinical assay system, demonstrated reasonable correlation, thereby justifying the potential use of hiPSC-CMs for electrophysiological cardiac safety screening. These results demonstrate that hiPSC-CMs can serve as a useful tool in early drug screening and may shed light on the drug safety assessment beyond the current gold standard assay for hERG channels.

In chapter 3 of these study, I characterized 2 weeks (2W) and 4 weeks (4W) differentiated hESC-CMs and compared their electrophysiological phenotypes and functional maturation using whole-cell patch-clamp recordings. Compared to the 2W hESC-CMs, the 4W differentiated hESC-CMs exhibited an increased functional maturation over time in current density of cardiac major ion channels and pharmacological responses. Although the AP shapes demonstrate characteristic cardiac phenotypes from the 2 weeks of differentiation in the hESC-CMs, at least 4 weeks of differentiation is required for the reliable pharmacological and toxicological testing.

REFERENCES

1. Lee HA, Hyun SA, Park SG, Kim KS, Kim SJ. Comparison of electrophysiological effects of calcium channel blockers on cardiac repolarization. Korean J Physiol Pharmacol. 2016;20(1):119-27.

2. Lee S, Lee HA, Choi SW, Kim SJ, Kim KS. Evaluation of nefazodone-induced cardiotoxicity in human induced pluripotent stem cell-derived cardiomyocytes. Toxicol Appl Pharmacol. 2016.

3. Lee S, Lee HA, Kim SJ, Kim KS. Cellular mechanisms for trazodone-induced cardiotoxicity. Human & experimental toxicology. 2015.

4. Kola I, Landis J. Can the pharmaceutical industry reduce attrition rates? Nature reviews Drug discovery. 2004;3(8):711-5.

5. Valentin JP, Hammond T. Safety and secondary pharmacology: successes, threats, challenges and opportunities. Journal of pharmacological and toxicological methods. 2008;58(2):77-87.

6. Laverty H, Benson C, Cartwright E, Cross M, Garland C, Hammond T, et al. How can we improve our understanding of cardiovascular safety liabilities to develop safer medicines? British journal of pharmacology. 2011;163(4):675-93.

7. Redfern WS, Carlsson L, Davis AS, Lynch WG, MacKenzie I, Palethorpe S, et al. Relationships between preclinical cardiac electrophysiology, clinical QT interval prolongation and torsade de pointes for a broad range of drugs: evidence for a provisional safety margin in drug development. Cardiovascular research. 2003;58(1):32-45.

8. Ewart L, Gallacher DJ, Gintant G, Guillon JM, Leishman D, Levesque P, et al. How do the top 12 pharmaceutical companies operate safety pharmacology? Journal of pharmacological and toxicological methods. 2012;66(2):66-70.

9. Grant AO. Cardiac ion channels. Circulation Arrhythmia and electrophysiology. 2009;2(2):185-94.

10. Kaczorowski GJ, Garcia ML, Bode J, Hess SD, Patel UA. The importance of being profiled: improving drug candidate safety and efficacy using ion channel profiling. Frontiers in pharmacology. 2011;2:78.

11. Yap YG, Camm AJ. Drug induced QT prolongation and torsades de pointes. Heart (British Cardiac Society). 2003;89(11):1363-72.

12. De Ponti F, Poluzzi E, Cavalli A, Recanatini M, Montanaro N. Safety of non-antiarrhythmic drugs that prolong the QT interval or induce torsade de pointes: an overview. Drug safety. 2002;25(4):263-86.

13. Meyer T, Leisgen C, Gonser B, Gunther E. QT-screen: high-throughput cardiac safety pharmacology by extracellular electrophysiology on primary cardiac myocytes. Assay and drug development technologies. 2004;2(5):507-14.

14. Frothingham R. Rates of torsades de pointes associated with ciprofloxacin, ofloxacin, levofloxacin, gatifloxacin, and moxifloxacin. Pharmacotherapy. 2001;21(12):1468-72.

15. Thomsen MB, Beekman JD, Attevelt NJ, Takahara A, Sugiyama A, Chiba K, et al. No proarrhythmic properties of the antibiotics Moxifloxacin or Azithromycin in anaesthetized dogs with chronic-AV block. British journal of pharmacology. 2006;149(8):1039-48.

16. Extramiana F, Maison-Blanche P, Cabanis MJ, Ortemann-Renon C, Beaufils P, Leenhardt A. Clinical assessment of drug-induced QT prolongation in association with heart rate changes. Clinical pharmacology and therapeutics. 2005;77(4):247-58.

17. Demiryurek AT, Demiryurek S. Cardiotoxicity of digitalis glycosides: roles of autonomic pathways, autacoids and ion channels. Autonomic & autacoid pharmacology. 2005;25(2):35-52.

18. Chan TY. Aconite poisoning. Clinical toxicology (Philadelphia, Pa). 2009;47(4):279-85.

19. Carlsson L. In vitro and in vivo models for testing arrhythmogenesis in drugs. Journal of internal medicine. 2006;259(1):70-80.

20. Lu HR, Marien R, Saels A, De Clerck F. Species plays an important role in drug-induced prolongation of action potential duration and early afterdepolarizations in isolated Purkinje fibers. Journal of cardiovascular electrophysiology. 2001;12(1):93-102.

21. Khan JM, Lyon AR, Harding SE. The case for induced pluripotent stem cell-derived cardiomyocytes in pharmacological screening. British journal of pharmacology. 2013;169(2):304-17.

22. Reppel M, Boettinger C, Hescheler J. Beta-adrenergic and muscarinic modulation of human embryonic stem cell-derived cardiomyocytes. Cellular physiology and biochemistry : international journal of experimental cellular physiology, biochemistry, and pharmacology. 2004;14(4-6):187-96.

23. Sager PT, Gintant G, Turner JR, Pettit S, Stockbridge N. Rechanneling the cardiac proarrhythmia safety paradigm: a meeting report from the Cardiac Safety Research Consortium. American heart journal. 2014;167(3):292-300.

24. Pekkanen-Mattila M, Chapman H, Kerkela E, Suuronen R, Skottman H, Koivisto AP, et al. Human embryonic stem cell-derived cardiomyocytes: demonstration of a portion of cardiac cells with fairly mature electrical phenotype. Experimental biology and medicine (Maywood, NJ). 2010;235(4):522-30.

25. Harding SE, Ali NN, Brito-Martins M, Gorelik J. The human embryonic stem cell-derived cardiomyocyte as a pharmacological model. Pharmacology & therapeutics. 2007;113(2):341-53.

26. Liu J, Fu JD, Siu CW, Li RA. Functional sarcoplasmic reticulum for calcium handling of human embryonic stem cell-derived cardiomyocytes: insights for driven maturation. Stem cells (Dayton, Ohio). 2007;25(12):3038-44.

27. Sartiani L, Bettiol E, Stillitano F, Mugelli A, Cerbai E, Jaconi ME. Developmental changes in cardiomyocytes differentiated from human embryonic stem cells: a molecular and electrophysiological approach. Stem cells (Dayton, Ohio). 2007;25(5):1136-44.

28. Guo L, Abrams RM, Babiarz JE, Cohen JD, Kameoka S, Sanders MJ, et al. Estimating the risk of drug-induced proarrhythmia using human induced pluripotent stem cell-derived cardiomyocytes. Toxicological sciences : an official journal of the Society of Toxicology. 2011;123(1):281-9.

29. Satin J, Kehat I, Caspi O, Huber I, Arbel G, Itzhaki I, et al. Mechanism of spontaneous excitability in human embryonic stem cell derived cardiomyocytes. The Journal of physiology. 2004;559(Pt 2):479-96.

30. Zhu R, Blazeski A, Poon E, Costa KD, Tung L, Boheler KR. Physical developmental cues for the maturation of human pluripotent stem cell-derived cardiomyocytes. Stem cell research & therapy. 2014;5(5):117.

31. Pepine CJ, Handberg EM, Cooper-DeHoff RM, Marks RG, Kowey P, Messerli FH, et al. A calcium antagonist vs a non-calcium antagonist hypertension treatment strategy for patients with coronary artery disease. The International Verapamil-Trandolapril Study (INVEST): a randomized controlled trial. Jama. 2003;290(21):2805-16.

32. Major outcomes in high-risk hypertensive patients randomized to angiotensin-converting enzyme inhibitor or calcium channel blocker vs diuretic: The Antihypertensive and Lipid-Lowering Treatment to Prevent Heart Attack Trial (ALLHAT). Jama. 2002;288(23):2981-97.

33. Dahlof B, Sever PS, Poulter NR, Wedel H, Beevers DG, Caulfield M, et al. Prevention of cardiovascular events with an antihypertensive regimen of amlodipine adding perindopril as required versus atenolol adding bendroflumethiazide as required, in the Anglo-Scandinavian Cardiac Outcomes Trial-Blood Pressure Lowering Arm (ASCOT-BPLA): a multicentre randomised controlled trial. Lancet (London, England). 2005;366(9489):895-906.

34. Black HR, Elliott WJ, Grandits G, Grambsch P, Lucente T, White WB, et al. Principal results of the Controlled Onset Verapamil Investigation of Cardiovascular End Points (CONVINCE) trial. Jama. 2003;289(16):2073-82.

35. Burnier M, Pruijm M, Wuerzner G. Treatment of essential hypertension with calcium channel blockers: what is the place of lercanidipine? Expert opinion on

drug metabolism & toxicology. 2009;5(8):981-7.

36. Davis RP, Casini S, van den Berg CW, Hoekstra M, Remme CA, Dambrot C, et al. Cardiomyocytes derived from pluripotent stem cells recapitulate electrophysiological characteristics of an overlap syndrome of cardiac sodium channel disease. Circulation. 2012;125(25):3079-91.

37. Hirano Y, Hiraoka M. [Electrophysiology of cardiac ion channels]. Nihon rinsho Japanese journal of clinical medicine. 1996;54(8):2050-5.

38. DeWitt CR, Waksman JC. Pharmacology, pathophysiology and management of calcium channel blocker and beta-blocker toxicity. Toxicological reviews. 2004;23(4):223-38.

39. Priest BT, Bell IM, Garcia ML. Role of hERG potassium channel assays in drug development. Channels (Austin, Tex). 2008;2(2):87-93.

40. Barhanin J, Attali B, Lazdunski M. IKs, a slow and intriguing cardiac K+ channel and its associated long QT diseases. Trends in cardiovascular medicine. 1998;8(5):207-14.

41. Haverkamp W, Breithardt G, Camm AJ, Janse MJ, Rosen MR, Antzelevitch C, et al. The potential for QT prolongation and proarrhythmia by non-antiarrhythmic drugs: clinical and regulatory implications. Report on a policy conference of the European Society of Cardiology. European heart journal. 2000;21(15):1216-31.

42. Cubeddu LX. QT prolongation and fatal arrhythmias: a review of clinical implications and effects of drugs. American journal of therapeutics. 2003;10(6):452-7.

43. Giustetto C, Di Monte F, Wolpert C, Borggrefe M, Schimpf R, Sbragia P, et al. Short QT syndrome: clinical findings and diagnostic-therapeutic implications. European heart journal. 2006;27(20):2440-7.

44. Gaita F, Giustetto C, Bianchi F, Wolpert C, Schimpf R, Riccardi R, et al. Short QT Syndrome: a familial cause of sudden death. Circulation. 2003;108(8):965-70.

45. Extramiana F, Antzelevitch C. Amplified transmural dispersion of repolarization as the basis for arrhythmogenesis in a canine ventricular-wedge model of short-QT syndrome. Circulation. 2004;110(24):3661-6.

46. Hondeghem LM. Thorough QT/QTc not so thorough: removes torsadogenic predictors from the T-wave, incriminates safe drugs, and misses profibrillatory drugs. Journal of cardiovascular electrophysiology. 2006;17(3):337-40.

47. Lu HR, Vlaminckx E, Hermans AN, Rohrbacher J, Van Ammel K, Towart R, et al. Predicting drug-induced changes in QT interval and arrhythmias: QT-shortening drugs point to gaps in the ICHS7B Guidelines. British journal of pharmacology. 2008;154(7):1427-38.

48. Garberoglio L, Giustetto C, Wolpert C, Gaita F. Is acquired short QT due to digitalis intoxication responsible for malignant ventricular arrhythmias? Journal of electrocardiology. 2007;40(1):43-6.

49. International Conference on Harmonisation; guidance on S7B Nonclinical Evaluation of the Potential for Delayed Ventricular Repolarization (QT Interval Prolongation) by Human Pharmaceuticals; availability. Notice. Federal register. 2005;70(202):61133-4.

50. D'Alonzo AJ, Zhu JL, Darbenzio RB, Dorso CR, Grover GJ. Proarrhythmic effects of pinacidil are partially mediated through enhancement of catecholamine release in isolated perfused guinea-pig hearts. Journal of molecular and cellular cardiology. 1998;30(2):415-23.

51. D'Alonzo AJ, Hess TA, Darbenzio RB, Sewter JC, Conder ML, McCullough JR. Effects of cromakalim or pinacidil on pacing- and ischemia-induced ventricular fibrillation in the anesthetized pig. Basic research in cardiology. 1994;89(2):163-76.

52. Roden DM. Drug-induced prolongation of the QT interval. The New England journal of medicine. 2004;350(10):1013-22.

53. Hondeghem LM. QT and TdP. QT: an unreliable predictor of proarrhythmia. Acta cardiologica. 2008;63(1):1-7.

54. Hondeghem LM, Carlsson L, Duker G. Instability and triangulation of the action potential predict serious proarrhythmia, but action potential duration prolongation is antiarrhythmic. Circulation. 2001;103(15):2004-13.

55. Milberg P, Eckardt L, Bruns HJ, Biertz J, Ramtin S, Reinsch N, et al. Divergent proarrhythmic potential of macrolide antibiotics despite similar QT prolongation: fast phase 3 repolarization prevents early afterdepolarizations and torsade de pointes. The Journal of pharmacology and experimental therapeutics. 2002;303(1):218-25.

56. Lu HR, Vlaminckx E, Van Ammel K, De Clerck F. Drug-induced long QT in isolated rabbit Purkinje fibers: importance of action potential duration, triangulation and early afterdepolarizations. European journal of pharmacology. 2002;452(2):183-92.

57. Guo D, Zhao X, Wu Y, Liu T, Kowey PR, Yan GX. L-type calcium current reactivation contributes to arrhythmogenesis associated with action potential triangulation. Journal of cardiovascular electrophysiology. 2007;18(2):196-203.

58.Champeroux P, Viaud K, El Amrani AI, Fowler JS, Martel E, Le Guennec JY, et al. Prediction of the risk of Torsade de Pointes using the model of isolated canine Purkinje fibres. British journal of pharmacology. 2005;144(3):376-85.

59. O'Connor CM, Carson PE, Miller AB, Pressler ML, Belkin RN, Neuberg GW, et al. Effect of amlodipine on mode of death among patients with advanced heart

failure in the PRAISE trial. Prospective Randomized Amlodipine Survival Evaluation. The American journal of cardiology. 1998;82(7):881-7.

60. Packer M, O'Connor CM, Ghali JK, Pressler ML, Carson PE, Belkin RN, et al. Effect of amlodipine on morbidity and mortality in severe chronic heart failure. Prospective Randomized Amlodipine Survival Evaluation Study Group. The New England journal of medicine. 1996;335(15):1107-14.

61. Udelson JE, DeAbate CA, Berk M, Neuberg G, Packer M, Vijay NK, et al. Effects of amlodipine on exercise tolerance, quality of life, and left ventricular function in patients with heart failure from left ventricular systolic dysfunction. American heart journal. 2000;139(3):503-10.

62. Littler WA, Sheridan DJ. Placebo controlled trial of felodipine in patients with mild to moderate heart failure. UK Study Group. British heart journal. 1995;73(5):428-33.

63. Williams DM, Cubeddu LX. Amlodipine pharmacokinetics in healthy volunteers. Journal of clinical pharmacology. 1988;28(11):990-4.

64. Christensen HR, Antonsen K, Simonsen K, Lindekaer A, Bonde J, Angelo HR, et al. Bioavailability and pharmacokinetics of isradipine after oral and intravenous administration: half-life shorter than expected? Pharmacology & toxicology. 2000;86(4):178-82.

65. Elliott HL, Meredith PA, Reid JL, Faulkner JK. A comparison of the disposition of single oral doses of amlodipine in young and elderly subjects. Journal of cardiovascular pharmacology. 1988;12 Suppl 7:S64-6.

66. Li K, Zhang X, Yuan YS, Zhao FL. A high-performance liquid chromatographic method for the determination of nicardipine in plasma and its application to pharmacokinetics in humans. Biomedical chromatography : BMC. 1998;12(6):326-9.

67. Fitton A, Benfield P. Isradipine. A review of its pharmacodynamic and pharmacokinetic properties, and therapeutic use in cardiovascular disease. Drugs. 1990;40(1):31-74.

68. Faulkner JK, McGibney D, Chasseaud LF, Perry JL, Taylor IW. The pharmacokinetics of amlodipine in healthy volunteers after single intravenous and oral doses and after 14 repeated oral doses given once daily. British journal of clinical pharmacology. 1986;22(1):21-5.

69. Ficker E, Kuryshev YA, Dennis AT, Obejero-Paz C, Wang L, Hawryluk P, et al. Mechanisms of arsenic-induced prolongation of cardiac repolarization. Molecular pharmacology. 2004;66(1):33-44.

70. Rajamani S, Eckhardt LL, Valdivia CR, Klemens CA, Gillman BM, Anderson CL, et al. Drug-induced long QT syndrome: hERG K+ channel block and disruption of protein trafficking by fluoxetine and norfluoxetine. British journal of

pharmacology. 2006;149(5):481-9.

71. Takemasa H, Nagatomo T, Abe H, Kawakami K, Igarashi T, Tsurugi T, et al. Coexistence of hERG current block and disruption of protein trafficking in ketoconazole-induced long QT syndrome. British journal of pharmacology. 2008;153(3):439-47.

72. Staudacher I, Schweizer PA, Katus HA, Thomas D. hERG: protein trafficking and potential for therapy and drug side effects. Current opinion in drug discovery & development. 2010;13(1):23-30.

73. Anson BD, Kolaja KL, Kamp TJ. Opportunities for use of human iPS cells in predictive toxicology. Clinical pharmacology and therapeutics. 2011;89(5):754-8.

74. Ma J, Guo L, Fiene SJ, Anson BD, Thomson JA, Kamp TJ, et al. High purity human-induced pluripotent stem cell-derived cardiomyocytes: electrophysiological properties of action potentials and ionic currents. American journal of physiology Heart and circulatory physiology. 2011;301(5):H2006-17.

75. Cohen JD, Babiarz JE, Abrams RM, Guo L, Kameoka S, Chiao E, et al. Use of human stem cell derived cardiomyocytes to examine sunitinib mediated cardiotoxicity and electrophysiological alterations. Toxicol Appl Pharmacol. 2011;257(1):74-83.

76. Pugsley MK, Towart R, Authier S, Gallacher DJ, Curtis MJ. Innovation in safety pharmacology testing. Journal of pharmacological and toxicological methods. 2011;64(1):1-6.

77. Redfern WS, Valentin JP. Trends in safety pharmacology: posters presented at the annual meetings of the Safety Pharmacology Society 2001-2010. Journal of pharmacological and toxicological methods. 2011;64(1):102-10.

78. Peng S, Lacerda AE, Kirsch GE, Brown AM, Bruening-Wright A. The action potential and comparative pharmacology of stem cell-derived human cardiomyocytes. Journal of pharmacological and toxicological methods. 2010;61(3):277-86.

79. Nicholson A, Kuper H, Hemingway H. Depression as an aetiologic and prognostic factor in coronary heart disease: a meta-analysis of 6362 events among 146 538 participants in 54 observational studies. European heart journal. 2006;27(23):2763-74.

80. Roose SP, Miyazaki M. Pharmacologic treatment of depression in patients with heart disease. Psychosomatic medicine. 2005;67 Suppl 1:S54-7.

81. Jiang W, Davidson JR. Antidepressant therapy in patients with ischemic heart disease. American heart journal. 2005;150(5):871-81.

82. Whooley MA, de Jonge P, Vittinghoff E, Otte C, Moos R, Carney RM, et al.

Depressive symptoms, health behaviors, and risk of cardiovascular events in patients with coronary heart disease. Jama. 2008;300(20):2379-88.

83. Owens MJ, Ieni JR, Knight DL, Winders K, Nemeroff CB. The serotonergic antidepressant nefazodone inhibits the serotonin transporter: in vivo and ex vivo studies. Life sciences. 1995;57(24):Pl373-80.

84. Schatzberg AF. New indications for antidepressants. The Journal of clinical psychiatry. 2000;61 Suppl 11:9-17.

85. Eison AS, Eison MS, Torrente JR, Wright RN, Yocca FD. Nefazodone: preclinical pharmacology of a new antidepressant. Psychopharmacology bulletin. 1990;26(3):311-5.

86. Miura N, Saito T, Taira T, Umebachi R, Inokuchi S. Risk factors for QT prolongation associated with acute psychotropic drug overdose. The American journal of emergency medicine. 2014.

87. DeVane CL, Grothe DR, Smith SL. Pharmacology of antidepressants: focus on nefazodone. The Journal of clinical psychiatry. 2002;63 Suppl 1:10-7.

88. Greene DS, Barbhaiya RH. Clinical pharmacokinetics of nefazodone. Clinical pharmacokinetics. 1997;33(4):260-75.

89. Ciraulo DA, Shader RI, Greenblatt DJ. Clinical Pharmacology and Therapeuticsof Antidepressants. 2011:33-124.

90. Coupland N, Wilson S, Nutt D. Antidepressant drugs and the cardiovascular system: a comparison of tricylics and selective serotonin reuptake inhibitors and their relevance for the treatment of psychiatric patients with cardiovascular problems. Journal of psychopharmacology. 1997;11(1):83-92.

91. Fernandez A, Bang SE, Srivathsan K, Vieweg WV. Cardiovascular side effects of newer antidepressants. Anadolu kardiyoloji dergisi : AKD = the Anatolian journal of cardiology. 2007;7(3):305-9.

92. Isbister GK, Hackett LP. Nefazodone poisoning: toxicokinetics and toxicodynamics using continuous data collection. Journal of toxicology Clinical toxicology. 2003;41(2):167-73.

93. Rasimas JJ, Burkhart KK. Cardiac conduction disturbances after an overdose of nefazodone and gabapentin. The American journal of emergency medicine. 2006;24(7):886-8.

94. Siddiqui MA, Khan IA. Nefazodone-associated torsade de pointes. International journal of cardiology. 2004;93(1):85-6.

95. Shin DS, Park MJ, Lee HA, Lee JY, Chung HC, Yoo DS, et al. A novel assessment of nefazodone-induced hERG inhibition by electrophysiological and

stereochemical method. Toxicol Appl Pharmacol. 2014;274(3):361-71.

96. Sanguinetti MC, Tristani-Firouzi M. hERG potassium channels and cardiac arrhythmia. Nature. 2006;440(7083):463-9.

97. Katchman AN, Koerner J, Tosaka T, Woosley RL, Ebert SN. Comparative evaluation of HERG currents and QT intervals following challenge with suspected torsadogenic and nontorsadogenic drugs. The Journal of pharmacology and experimental therapeutics. 2006;316(3):1098-106.

98. Goldenberg I, Moss AJ. Long QT syndrome. Journal of the American College of Cardiology. 2008;51(24):2291-300.

99. Curran ME, Splawski I, Timothy KW, Vincent GM, Green ED, Keating MT. A molecular basis for cardiac arrhythmia: HERG mutations cause long QT syndrome. Cell. 1995;80(5):795-803.

100. Wang Q, Curran ME, Splawski I, Burn TC, Millholland JM, VanRaay TJ, et al. Positional cloning of a novel potassium channel gene: KVLQT1 mutations cause cardiac arrhythmias. Nature genetics. 1996;12(1):17-23.

101. Wang Q, Shen J, Splawski I, Atkinson D, Li Z, Robinson JL, et al. SCN5A mutations associated with an inherited cardiac arrhythmia, long QT syndrome. Cell. 1995;80(5):805-11.

102. Magyar J, Iost N, Kortvely A, Banyasz T, Virag L, Szigligeti P, et al. Effects of endothelin-1 on calcium and potassium currents in undiseased human ventricular myocytes. Pflugers Archiv : European journal of physiology. 2000;441(1):144-9.

103. Sakakibara Y, Furukawa T, Singer DH, Jia H, Backer CL, Arentzen CE, et al. Sodium current in isolated human ventricular myocytes. The American journal of physiology. 1993;265(4 Pt 2):H1301-9.

104. Virag L, Iost N, Opincariu M, Szolnoky J, Szecsi J, Bogats G, et al. The slow component of the delayed rectifier potassium current in undiseased human ventricular myocytes. Cardiovascular research. 2001;49(4):790-7.

105. Matsa E, Rajamohan D, Dick E, Young L, Mellor I, Staniforth A, et al. Drug evaluation in cardiomyocytes derived from human induced pluripotent stem cells carrying a long QT syndrome type 2 mutation. European heart journal. 2011;32(8):952-62.

106. Hoppe UC, Jansen E, Sudkamp M, Beuckelmann DJ. Hyperpolarization-activated inward current in ventricular myocytes from normal and failing human hearts. Circulation. 1998;97(1):55-65.

107. Kamp TJ, Lyons GE. On the road to iPS cell cardiovascular applications. Circulation research. 2009;105(7):617-9.

108. Fermini B, Fossa AA. The impact of drug-induced QT interval prolongation on drug discovery and development. Nature reviews Drug discovery. 2003;2(6):439-47.

109. Haverkamp W, Breithardt G, Camm AJ, Janse MJ, Rosen MR, Antzelevitch C, et al. The potential for QT prolongation and pro-arrhythmia by non-anti-arrhythmic drugs: clinical and regulatory implications. Report on a Policy Conference of the European Society of Cardiology. Cardiovascular research. 2000;47(2):219-33.

110. Giorgi MA, Bolanos R, Gonzalez CD, Di Girolamo G. QT interval prolongation: preclinical and clinical testing arrhythmogenesis in drugs and regulatory implications. Current drug safety. 2010;5(1):54-7.

111. Fenichel RR, Malik M, Antzelevitch C, Sanguinetti M, Roden DM, Priori SG, et al. Drug-induced torsades de pointes and implications for drug development. Journal of cardiovascular electrophysiology. 2004;15(4):475-95.

112. Yazawa M, Hsueh B, Jia X, Pasca AM, Bernstein JA, Hallmayer J, et al. Using induced pluripotent stem cells to investigate cardiac phenotypes in Timothy syndrome. Nature. 2011;471(7337):230-4.

113. Itzhaki I, Maizels L, Huber I, Zwi-Dantsis L, Caspi O, Winterstern A, et al. Modelling the long QT syndrome with induced pluripotent stem cells. Nature. 2011;471(7337):225-9.

114. Itzhaki I, Maizels L, Huber I, Zwi-Dantsis L, Caspi O, Winterstern A, et al. Modelling the long QT syndrome with induced pluripotent stem cells. Nature. 2011;471(7337):225-9.

115. Davis RP, van den Berg CW, Casini S, Braam SR, Mummery CL. Pluripotent stem cell models of cardiac disease and their implication for drug discovery and development. Trends in molecular medicine. 2011;17(9):475-84.

116. Mummery C, Ward-van Oostwaard D, Doevendans P, Spijker R, van den Brink S, Hassink R, et al. Differentiation of human embryonic stem cells to cardiomyocytes: role of coculture with visceral endoderm-like cells. Circulation. 2003;107(21):2733-40.

117. Barbhaiya RH, Marathe PH, Greene DS, Mayol RF, Shukla UA, Gammans RR, et al. Safety, tolerance, and preliminary pharmacokinetics of nefazodone after administration of single and multiple oral doses to healthy adult male volunteers: a double-blind, phase I study. Journal of clinical pharmacology. 1995;35(10):974-84.

118.Barbhaiya RH, Brady ME, Shukla UA, Greene DS. Steady-state pharmacokinetics of nefazodone in subjects with normal and impaired renal function. European journal of clinical pharmacology. 1995;49(3):229-35.

119. DeVane CL, Boulton DW, Miller LF, Miller RL. Pharmacokinetics of trazodone and its major metabolite m-chlorophenylpiperazine in plasma and brain of rats.

The international journal of neuropsychopharmacology / official scientific journal of the Collegium Internationale Neuropsychopharmacologicum (CINP). 1999;2(1):17-23.

120. Otani K, Mihara K, Yasui N, Ishida M, Kondo T, Tokinaga N, et al. Plasma concentrations of trazodone and m-chlorophenylpiperazine at steady state can be predicted from those after an initial dose of trazodone. Progress in neuro-psychopharmacology & biological psychiatry. 1997;21(1):239-44.

121. Sicouri S, Antzelevitch C. Sudden cardiac death secondary to antidepressant and antipsychotic drugs. Expert opinion on drug safety. 2008;7(2):181-94.

122. Guo W, Kamiya K, Toyama J. Modulated expression of transient outward current in cultured neonatal rat ventricular myocytes: comparison with development in situ. Cardiovascular research. 1996;32(3):524-33.

123. Obreztchikova MN, Sosunov EA, Plotnikov A, Anyukhovsky EP, Gainullin RZ, Danilo P, et al. Developmental changes in IKr and IKs contribute to age-related expression of dofetilide effects on repolarization and proarrhythmia. Cardiovascular research. 2003;59(2):339-50.

124. Lundy SD, Zhu WZ, Regnier M, Laflamme MA. Structural and functional maturation of cardiomyocytes derived from human pluripotent stem cells. Stem cells and development. 2013;22(14):1991-2002.

총괄 국문 초록

심장독성은 신약개발단계에서 의약후보물질이 탈락하는 주원인 중 하나이다. 심실재분극 지연에 관여하는 hERG K^+ 채널의 억제효과 여부는 심전도 QT 파의 연장에 따르는 부정맥 발생에 중요하기에 필수 점검 사항이다. 하지만 hERG 채널 뿐 아니라 심장에 존재하는 다른 이온채널전류들 (I_{Ks}, I_{Na}, I_{Ca}, I_{K1})의 비정상적 변화도 심부정맥을 일으킬 수 있어서 hERG 시험만으로는 실험실 수준 (*in vitro*) 독성스크리닝에 한계가 있다. 실제 동물에 적용하는 원격 심전도측정법 (Telemetry)은 종간 상이성으로 인해 인체의 독성예측에는 한계점이 있다. 이러한 배경에서, 인간 줄기세포 유래 심근세포를 이용하여 약물의 심장독성 잠재성을 스크리닝하는 것이 주목받고 있다. 본 연구에서는 3 가지 소주제를 통해 심장 이온채널들의 통합적인 분석이 필요한 이유와 인간 줄기세포 유래 심근세포를 이용한 통합적인 전기생리학적 영향평가의 유효성을 살펴보고자 하였다.

제 1 장: 칼슘채널 억제제들의 심장 활동전위의 재분극에 대한 효과 비교

일반적으로 칼슘채널의 억제는 활동전위기간을 줄이고, 빈맥을 일으켜 심부정맥으로 이어질 수 있다. 하지만, 칼슘채널억제제는 오늘날 가장

널리 처방되는 항고혈압제 중 하나이다. 칼슘채널 억제제의 심장에 대한 안전성을 평가하기 위해 dihydropyridine 계열의 칼슘억제제 중 제 1 세대의 nicardipine, 제 2 세대의 amlodipine, 그리고 3 세대인 isradipine 을 선택하여 전기생리학적 영향을 살펴보았다. 이 3 가지 약물은 모두 백서 심근세포의 칼슘채널을 민감하게 억제하였으나, 토끼 심장의 퍼킨제섬유에서 기록한 활동전위 재분극에 대한 영향은 isradipine 만 민감하게 활동전위기간을 줄였다. 심실재분극에 관여하는 칼륨 채널들에 대한 영향을 비교해본 결과, 막전압의존성 칼륨 채널에 대한 민감도 차이로 활동전위기간 감소에 대한 보상 효과가 차이 남을 확인할 수 있었다. 이러한 결과는 약물의 심장독성을 평가하기 위해서는 다양한 이온채널에 대한 영향을 종합적으로 판단해야 함을 시사한다.

제 2 장: 상용화된 줄기세포 유래 심근세포의 유효성 확인 및 항우울제의 심장독성 평가

최근 제약산업계에서는 약물독성평가에 대한 인간 줄기세포 유래 심근세포의 유용성에 대해 주목하고 있으며, 실제로 몇몇 세포들은 이미 상용화되어 판매 중이다. 상용화된 분화 심근세포 (iCell® Cardiomyocytes, Cellular Dynamics International, 미국)의 심장독성

평가에 대한 유용성을 확인하기 위해 전기생리학적 특성분석과 이온채널억제제에 대한 활동전위의 반응성을 확인하였다. 역분화 줄기세포 유래 심근세포에서 3 가지 타입의 활동전위와, 활동전위에 관계된 이온채널전류-I_{Kr}, I_{Ks}, I_{K1}, I_f, I_{Na}, I_{Ca}-를 기록할 수 있었고, hERG 채널 억제제인 E-4031 에 의해 활동전위 재분극이 지연되고 EAD (early after depolarization)가 발생되는 것을 확인하였다. 또한, Na^+ 채널 억제제에 의해 활동전위의 최대속도(dV/dt_{max})가 감소되고, Ca^{2+} 채널 억제제인 nifedipine 에 의해서 활동전위기간이 짧아짐을 확인하였다. 이러한 결과는 줄기세포 유래 심근세포에 정상적인 기능성을 가진 심장 이온채널들이 존재하고 있음을 보여준다. 이 세포를 이용하여 최근 심장독성에 대한 우려가 증가되고 있는 선택적 세로토닌 재흡수억제제 (SARI) 계열의 항우울제 중 nefazodone 과 trazodone 에 대한 in vitro 심장독성평가를 수행하였다. 두 약물은 모두 분화줄기세포나 HEK293 세포에 발현된 이온채널의 활성을 억제하였고, 이러한 효과는 활동전위의 형태변화로 나타났다. 이 결과들은 nefazodone 과 trazodone 의 심장 이온채널들과의 복잡한 상호작용을 분화심근세포에서 통합적으로 평가할 수 있음을 보여주었다. 그러므로,

줄기세포 유래 심근세포는 hERG assay 를 넘어서 심장활동전압 변화를 직접 평가하는 약물 스크리닝에 유용할 것이다.

제 3 장: 줄기세포 분화 심근세포에서 분화시기에 따른 심독성 약물분석의 유효성 차이

비임상 심장독성평가 모델로 줄기세포 유래 심근세포를 활용하기 위해서는 표준화된 심근세포의 확보가 중요하다. 또한, 초기 발달단계에서 심장독성 스크리닝을 위해 줄기세포 유래 심근세포의 기능성을 평가하는 것은 적절한 분화시기를 결정하는데 필수적이다. 이러한 배경에서, SNUhES3(서울대학교에서 확립한 인간 배아줄기세포주)를 이용하여 2 주와 4 주 동안 심근으로 분화시킨 후 전기생리학적 특성을 분석하였고, 약물에 대한 민감도를 확인하였다. 4 주 분화 심근세포에서 2 주 분화 심근세포보다 심장 이온채널의 활성이 더 높게 나타났다. 분화 2 주차 세포들의 활동전위는 87.5%가 심방근 유형임에 비해 4 주차에서는 69%가 심실근 유형이었다. 즉, 분화기간이 늘어날수록 활동전위기간이 늘어나고, 심실근 유형의 세포가 늘어남을 알 수 있었다. 항부정맥제로서 각각 Na^+과 K^+ 채널 억제제인 quinidine 과 amiodarone 은 2 주 분화 심근세포에서와는 달리

4 주 분화세포에서 APD_{90} 을 연장시켰다. Ca^{2+}채널 억제제인 nifedipine 역시 4 주 분화세포에서만 유의하게 APD_{90}을 감소시켰다.

종합하자면, 인간 배아줄기세포 유래 심근세포는 분화기간에 따라 심실근 유형의 심근세포로 분화되고, 약물의 독성평가를 위한 성숙된 분화세포를 얻기 위해서는 최소 1 달간의 분화기간이 필요함을 보여준다. 이러한 연구들을 통해 저자는 4 주 분화 심근세포가 in vitro 심장독성 스크리닝과 약물 안전성 평가에 활용 될 수 있음을 보여주었다. 이러한 결과들은 약물 안전성평가를 위해 전기생리학적으로 성숙된 표현형을 가진 개선된 모델을 개발하는데 기여할 것이다.

주요어 : 심장독성평가, 심장독성 약물, 이온채널, 활동전위, 인간줄기세포 유래 심근세포, 칼슘채널억제제, 항우울제

학 번 : 2011-30633